QA: QA

ANL-EBS-MD-000015 REV 02

August 2004

NOTICE OF OPEN CHANGED DOCUMENTS - THIS DOCUMENT IS IMPACTED BY THE LISTED CHANGE DOCUMENT AND CANNOT BE USED WITHOUT IT.
----
1) ACN-001 IS CANCELLED, EFFECTIVE 05/04/2005

CSNF Waste Form Degradation: Summary Abstraction

Prepared for:
U.S. Department of Energy
Office of Civilian Radioactive Waste Management
Office of Repository Development
1551 Hillshire Drive
Las Vegas, Nevada 89134-6321

Prepared by:
Bechtel SAIC Company, LLC
1180 Town Center Drive
Las Vegas, Nevada 89144

Under Contract Number
DE-AC28-01RW12101

DISCLAIMER

This report was prepared as an account of work sponsored by an agency of the United States Government. Neither the United States Government nor any agency thereof, nor any of their employees, nor any of their contractors, subcontractors or their employees, makes any warranty, express or implied, or assumes any legal liability or responsibility for the accuracy, completeness, or any third party's use or the results of such use of any information, apparatus, product, or process disclosed, or represents that its use would not infringe privately owned rights. Reference herein to any specific commercial product, process, or service by trade name, trademark, manufacturer, or otherwise, does not necessarily constitute or imply its endorsement, recommendation, or favoring by the United States Government or any agency thereof or its contractors or subcontractors. The views and opinions of authors expressed herein do not necessarily state or reflect those of the United States Government or any agency thereof.

QA: QA

CSNF Waste Form Degradation: Summary Abstraction

ANL-EBS-MD-000015 REV 02

August 2004

INTENTIONALLY LEFT BLANK

OCRWM	MODEL SIGNATURE PAGE/CHANGE HISTORY	Page iii 1. Total Pages: 160

2. Type of Mathematical Model

☐ Process Model ☒ Abstraction Model ☐ System Model

Describe Intended Use of Model

Calculate the release rate of radionuclides from commercial spent nuclear fuel (CSNF) following breach of the cladding in the repository.

3. Title

CSNF Waste Form Degradation: Summary Abstraction

4. DI (including Rev. No., if applicable):

ANL-EBS-MD-000015 REV 02

5. Total Appendices	6. No. of Pages in Each Appendix
Five (5)	I-2, plus 1 CD-ROM; II-8; III-4; IV-4; V-6

	Printed Name	Signature	Date
7. Originator	James C. Cunnane	SIGNATURE ON FILE	8/31/04
8. Independent Technical Reviewer	Bob Andrews	SIGNATURE ON FILE	8/31/04
9. Checker	Patricia Bernot	SIGNATURE ON FILE	8/31/04
10. QER	Charlie Warren	SIGNATURE ON FILE	8/31/04
11. Responsible Manager/Lead	Dennis Thomas	SIGNATURE ON FILE	8/31/04
12. Responsible Manager	Neil Brown	SIGNATURE ON FILE	8/31/04

13. Remarks

- The errata are addressed, as applicable, in the appropriate sections of the document and each is addressed in block 13 of the Model Signature Page/Change History as follows:
- CR 785 - This CR is not applicable to the current revision (i.e. REV 02E); DTN:MO0306ANLSF001.001 has been superseded by DTN:MO0404ANLSF001.001. The subject data are in Table 8-3 of the current revision i.e. REV02E.
- CR1468 – Section 2. Of the current revision i.e. REV02E references the TWP (BSC 2004 [DIRS 169944], Appendix A) for control of the electronic management of data.
- CR1495 – The basis for not using portions of the data sets for DTN:MO0302PNLDUFTD.000 and DTN:MO0304PNLLPHDDD.000 is provided in the last paragraph of Section 4.1.2.
- CR1496 – The source DTN for the data in Appendix I, Excel Spreadsheet file: CSNF MR REV2.XLS, Spreadsheet A6, has been changed from MO0301ANLSF001.451 to MO0301ANLSF001.450.

Change History

14. Revision No.	15. Description of Change
REV 00	Initial Issue
REV 01	Major revision for the Total System Performance Assessment for the License Application. The changes from REV00 are extensive and represent an almost complete rewrite of the document. The changes are too extensive to track using change bars or other change tracking notation.

3. Title
CSNF Waste Form Degradation: Summary Abstraction
4. DI (including Rev. No., if applicable):
ANL-EBS-MD-000015 REV 02

Change History

14. Revision No.	15. Description of Change
REV 01 (Continued)	In addition to the document outline and content changes mandated by the governing procedure (AP-SIII.10Q) this revision includes extensive technical changes. The technical changes include: 1. changing the dependent variable from the specific dissolution rate of the matrix to the fractional release rate of the matrix radionuclides, 2. changing the input data, 3. changing the modeling section to update the model for the instantaneous fractional release of the gap and grain-boundary inventories, to update the model for the specific dissolution rate of the matrix under acidic and alkaline conditions, and to include an estimate of the effective specific area parameter for corroding fuel, 4. an extensive validation section, and 5. a description of the modeling output and associated uncertainties.
REV 02	This is a complete revision addressing specific issues identified with REV 01. Change bars are not used because the changes were too extensive to track. This revision also includes changes made to address CR numbers 1439, 1468, 1469, 1495, and 1496. The changes address the NRC comments documented in "NRC Staff Evaluation of DOE Model Reports" dated April 10, 2004 that apply to this model report. In addition, this revision incorporates changes resulting from the Regulatory Integration review in preparation for licensing. Transparency and traceability are improved, TBVs and RIT Action Items are closed, and the most up-to-date versions of supporting documents are cited.

CONTENTS

Page

1. PURPOSE 1-1

2. QUALITY ASSURANCE 2-1

3. USE OF SOFTWARE 3-1

4. INPUTS 4-1
   4.1 DIRECT INPUT 4-1
      4.1.1 Instantaneous Fractional Release Data 4-1
      4.1.2 Matrix Dissolution Rate Data: Flow-Through Tests 4-2
      4.1.3 CSNF Surface Area Data 4-8
      4.1.4 Input Data Summary 4-10
   4.2 CRITERIA 4-11
   4.3 CODES AND STANDARDS 4-12

5. ASSUMPTIONS 5-1
   5.1 FRACTIONAL DEGRADATION RATE BOUNDS RADIONUCLIDE RELEASE 5-1
   5.2 FUEL FRAGMENTS AND SHORT FUEL ROD SEGMENTS CONSERVATIVELY REPRESENT DEGRADED CSNF 5-1
   5.3 SIMILARITY BETWEEN OXYGEN AND TEMPERATURE DEPENDENCE FOR ACIDIC AND ALKALINE CONDITIONS 5-2

6. MODEL DISCUSSION 6-1
   6.1 MODELING OBJECTIVES 6-1
   6.2 BASIS FOR MODELING RADIONUCLIDE RELEASE 6-1
      6.2.1 State of CSNF When Cladding is Breached 6-1
      6.2.2 Processes Influencing CSNF State and Radionuclide Release after Cladding Breach 6-4
      6.2.3 FEPs Included in the Model 6-16
   6.3 MODELING THE INSTANTANEOUS RELEASE FRACTIONS 6-17
      6.3.1 The Gap and Grain-Boundary Inventory Data Input and Uncertainties 6-17
      6.3.2 The Instantaneous Release Fraction Model 6-22
   6.4 MODELING THE CSNF MATRIX FRACTIONAL RELEASE RATES 6-23
      6.4.1 The CSNF Matrix Degradation Models 6-23
      6.4.2 Alternative Conceptual Models 6-39
      6.4.3 Description of Barrier Capability 6-46

7. VALIDATION 7-1
   7.1 COMPARISON OF BASE-CASE MODEL TO EXPERIMENTAL DATA 7-4
      7.1.1 Comparison of the Instantaneous Release Model to CSNF Instantaneous Release Data 7-4
      7.1.2 Validation of CSNF Matrix Radionuclide Release Models for Alkaline and Acidic Conditions 7-6

CONTENTS (Continued)

Page

7.1.3 Comparison with UO_{2+x} Data 7-18
7.2 COMPARISON OF THE DEVELOPED MODEL TO ALTERNATIVE MODELS 7-19
7.3 NATURAL ANALOGUES 7-22
7.3.1 Studies of Natural Analogue Sites 7-22
7.3.2 Comparison of Laboratory Corrosion Products to Nopal Minerals 7-23
7.4 VALIDATION SUMMARY 7-26

8. CONCLUSIONS 8-1
8.1 DEVELOPED OUTPUT - THE MODEL PARAMETER VALUES 8-1
8.2 UNCERTAINTY IN THE DEVELOPED PARAMETER VALUES 8-4
8.3 YUCCA MOUNTAIN REVIEW PLAN ACCEPTANCE CRITERIA 8-6
8.3.1 System Description and Demonstration of Multiple Barriers 8-7
8.3.2 Degradation of Engineered Barriers 8-8
8.3.3 Radionuclide Release Rates and Solubility Limits 8-12

9. INPUTS AND REFERENCES 9-1
9.1 DOCUMENTS CITED 9-1
9.2 CODES, STANDARDS, REGULATIONS, AND PROCEDURES 9-8
9.3 SOURCE DATA, LISTED BY DATA TRACKING NUMBER 9-8
9.4 OUTPUT DATA, LISTED BY DATA TRACKING NUMBER 9-9

APPENDIX I MICROSOFT EXCEL SPREADSHEETS AND SIGMA PLOT REGRESSION ANALYSES (WITH CD-ROM) I-1

APPENDIX II MATHCAD REGRESSION ANALYSIS OF ALKALINE AND ACID DATA II-1

APPENDIX III FILE INFORMATION FOR ATTACHED CD-ROM III-1

APPENDIX IV DATA QUALIFICATION PLAN IV-1

APPENDIX V DATA QUALIFICATION REPORT V-1

FIGURES

Page

6-1. Cladding Fuel-Side Corrosion Observed in Tests Conducted in Humid Air at 175°C ... 6-6
6-2. Scanning Electron Microscopy Images of Corroded CSNF 6-14
6-3. Comparison of the Base-Case Model (pCO_3 = 2.7) to the Input CSNF and UO_2 Data. 6-30
6-4. Comparison of Models (pCO_3 = 2.7) Obtained when the CSNF Data (Red) and the UO_2 Data (Blue) are Regressed Separately 6-31

INTENTIONALLY LEFT BLANK

TABLES

Page

4-1. Light Water Reactor SNF Gap and Grain-Boundary Inventories 4-3
4-2. CSNF Flow-Through Test Dissolution Data (Alkaline Conditions) 4-5
4-3. Unirradiated UO_2 Flow-Through Test Dissolution Data (Alkaline Conditions) 4-7
4-4. CSNF Flow-Through Test Dissolution Data - Acidic Conditions 4-7
4-5. Estimated Geometric-Specific Surface Area of HBR and TP Fuels 4-8
4-6. Estimated Surface Area Per Unit Length (mm^2/mm) of ATM-101 Fuel 4-9
4-7. Average Fractional Radionuclide Release Rates (d^{-1}) from Rod Segment Tests 4-10
4-8. Direct Input Data Summary 4-11

6-1. Included FEPs for This Model Report and Their Disposition in the TSPA-LA Model 6-16
6-2. Summary of the Gap and Grain-Boundary Inventory Data 6-21
6-3. Comparison of Input Gap and Grain-Boundary Inventory Data Distribution Characteristics to the Corresponding Distribution Characteristics of the Superceded Data 6-22
6-4. Linear Regression: Combined CSNF and UO_2 Data, Model 1 6-28
6-5. Linear Regression: Combined CSNF and UO_2 Data, Model 2 6-28
6-6. Nonlinear Regression Model: Combined CSNF and UO_2 Data 6-28
6-7. Linear Regression Model: CSNF Data 6-29
6-8. Linear Regression Model: UO_2 Data 6-29
6-9. Summary of Geometric-Specific Surface Area Estimates 6-33
6-10. Average Radionuclide Release Rates (d^{-1}) from Rod Segment Tests 6-35
6-11. Average Fractional Release Rates (d^{-1}) in the Fuel Fragment Tests 6-38
6-12. Summary of CSNF Waste Form Degradation Analysis Inputs 6-40
6-13. Alternative Conceptual Models Considered 6-46

7-1. Data and Alternative Model Sources Used for Validation 7-4
7-2. Instantaneous Fractional Release - Rod Segment Tests 7-5
7-3. Comparison of Instantaneous Release Fraction Data from Rod Segment Tests to Model Distribution Ranges for the Gap and Grain-Boundary Inventories 7-5
7-4. Literature Data - Combined Gap and Grain-Boundary Inventories 7-6
7-5. Calculations of Equivalent Intrinsic Dissolution Rates of H. B. Robinson Fuel at 25°C 7-10
7-6. Calculations of Equivalent Intrinsic Dissolution Rates of H. B. Robinson Fuel at 85°C 7-11
7-7. Calculations of Equivalent Intrinsic Dissolution Rates of Turkey Point Fuel at 85°C.. 7-12
7-8. Summary of the NNWSI Series 3 Fractional Release Rate (d^{-1}) Results for Last Sampling Period 7-13
7-9. Average Fractional Release Rates (d^{-1}) Measured in the Series 11 Tests on Fuel Rod Segments with Different Burnups and in the Series 3 Tests on Fuel Fragments 7-13
7-10. Fractional Release Rates (d^{-1}) Measured Under Acidic Conditions in the SKB Series 3 and 11 Tests 7-14

TABLES

Page

7-11. Comparison of Data from Tait and Luht (1997 [DIRS 114435]) with the Alkaline Model 7-15
7-12. Experimental UO_2 Dissolution Rates as a Function of Temperature and Bicarbonate Concentration 7-16
7-13. Measured UO_2 Flow-Through Dissolution Data with Variation of Oxygen and pH 7-17
7-14. Comparison of the Base-Case Model to Alternative Models 7-20
7-15. Paragenesis of Uranium Minerals at Nopal I 7-23

8-1. Characteristic Values of the Triangular Probability Distribution Functions for Instantaneous Fractional Releases of Cesium, Iodine, Technetium, and Strontium..... 8-1
8-2. Parameter Values and Associated Characteristic Values of the Uncertainty Distributions for the Alkaline Conditions Model 8-2
8-3. Parameter Values and Associated Characteristic Values of the Uncertainty Distribution for the Acidic Conditions Model 8-3
8-4. Summary of Output Developed in This Model Report..... 8-6

ACRONYMS

ANL	Argonne National Laboratory
ATM	Approved Testing Material
BET	Brunauer, Emmett, and Teller equation
CANDU	Canada Deuterium Uranium
CSNF	commercial spent nuclear fuel
DOE	U.S. Department of Energy
DR	Dissolution Rate
EM	error metric
FEPS	features, events, and processes
FGR	fission gas release
GBI	grain-boundary inventory
GI	gap inventory
HBR	H.B. Robinson
IT	Inverse of the Absolute Temperature
LgDR	log10(dissolution rate per unit area)
NNWSI	Nevada Nuclear Waste Storage Investigations
QA	quality assurance
RH	relative humidity
SPFT	single-pass flow-through
TP	Turkey Point
TPSA	total system performance assessment
TSPA-LA	Total System Performance Assessment for the License Application
YMP	Yucca Mountain Project

INTENTIONALLY LEFT BLANK

1. PURPOSE

The purpose of this model report is to describe the development and validation of models that can be used to calculate the release of radionuclides from commercial spent nuclear fuel (CSNF) following a hypothetical breach of the waste package and fuel cladding in the repository. The purpose also includes describing the uncertainties associated with modeling the radionuclide release for the range of CSNF types, exposure conditions, and durations for which the radionuclide release models are to be applied.

This document was developed in accordance with *Technical Work Plan for: Regulatory Integration Modeling and Analysis of the Waste Form and Waste Package* (BSC 2004 [DIRS 169944]).

This document considers radionuclides to be released from CSNF when they are available for mobilization by gas-phase mass transport, or by dissolution or colloid formation in water that may contact the fuel. Because other reports address limitations on the dissolved and colloidal radionuclide concentrations (BSC 2004 [DIRS 169944], Table 2-1), this report does not address processes that control the extent to which the radionuclides released from CSNF are mobilized and transported away from the fuel either in the gas phase or in the aqueous phase as dissolved and colloidal species. The scope is limited to consideration of degradation of the CSNF rods following an initial breach of the cladding. It considers features of CSNF that limit the availability of individual radionuclides for release into the gaseous or aqueous phases that may contact the fuel and the processes and events expected to degrade these CSNF features. In short, the purpose is to describe the characteristics of breached fuel rods and the degradation processes expected to influence radionuclide release.

The availability of individual radionuclides for release once the CSNF waste package and fuel cladding are breached is limited by the structure, microstructure, physicochemical properties of the irradiated fuel, distribution of the fission products within the fuel rods, and degradation of the fuel rods and fuel matrix. As discussed in more detail in Section 6.2.1.1, most radionuclides, and essentially all of the rare earth and actinide radionuclides, are retained within the fluorite structure of the fuel matrix. The transition metals (molybdenum, technetium, ruthenium, rhodium, and palladium) are partly partitioned into five-metal metallic alloy phases embedded in the fuel grains and at the fuel grain boundaries. The part of the radionuclide inventory that is present either as a solid solution in the fuel matrix, or embedded as discrete phases within the fuel grains, is not available for dissolution until the fuel matrix is dissolved or otherwise altered. This part of the inventory is referred to as the "matrix inventory" (I_i^M, where the subscript "i" is a radionuclide index). A fraction of the inventory of fission gases and of some of the more volatile radioelements (e.g., cesium, iodine, and technetium) migrates out of the matrix during in-reactor operations and accumulates as gaseous and minor condensed phases in locations collectively referred to as the "gap region" (e.g., the interface between the pellets and the cladding, the rod plenum regions, and pellet fracture surfaces). As discussed in Sections 6.2.1.1 and 6.3, experimental evidence indicates a small fraction of the total radionuclide inventory resides at the interfaces between the fuel grains. Because this "grain-boundary inventory" may be released rapidly, it is useful, for modeling purposes, to view the radionuclide inventory in CSNF rods as being divided into two fractions: the matrix inventory and the combined gap and

grain-boundary inventories. The latter fraction of the inventory is referred to as the "gap and grain-boundary inventory (I_i^G)."

Separate models are developed for release of the gap and grain-boundary inventory (I_i^G) and the matrix (I_i^M) inventory because the features, events, and processes (FEPs) that affect the release of each of these fractions of the inventory are different. The "matrix release" models address release of the fraction of the radionuclide inventory that is in the fuel matrix; while the "instantaneous release" model addresses release of the fraction of the radionuclide inventory that is not contained in the fuel matrix (i.e., the gap and grain-boundary inventory).

The gap inventory is available for immediate gas-phase mass transport or dissolution when the cladding is breached. Release of the gap inventory of fission gases is modeled as an "instantaneous release" upon failure of the cladding. The gap inventory of other radionuclides is also modeled as an "instantaneous release" upon contact of the breached fuel with water. Although the evidence for preferential degradation at the grain boundaries (compared to the fuel grain matrix) and the consequent preferential release of the grain-boundary inventory is limited, the grain-boundary inventory is combined with the gap inventory in estimating the instantaneous release fraction. This approach overestimates the rate of release of the grain-boundary inventory and therefore represents a conservative modeling approach.

The inventory available for instantaneous release (I_i^G) can be expressed as a fraction of the total inventory of radionuclide, *i,* in the fuel (I_i):

$$I_i^G = f_i \, I_i \qquad \text{(Eq. 1)}$$

where

f_i = instantaneous release fraction

As shown in *Technical Work Plan for: Regulatory Integration Modeling and Analysis of the Waste Form and Waste Package* (BSC 2004 [DIRS 169944], Table 2-1) the total inventory of radionuclide *i* in the fuel (I_i) is addressed elsewhere. Hence, one purpose of this document is to model the instantaneous release by providing a probability distribution function, based on available data, to estimate the instantaneous release fraction (f_i) and the associated uncertainties.

For the radionuclides in the CSNF matrix, the rate of radionuclide release (R_i) can be expressed as:

$$R_i = I_i^M F_i \qquad \text{(Eq. 2)}$$

where

I_i^M = matrix inventory

F_i = Fractional release rate (i.e., the fraction released per unit time) of any radionuclide

The matrix inventory (I_i^M) in Equation 2 can be calculated given the instantaneous release fraction (f_i) and the total inventory (I_i). The matrix inventory can be expressed as:

$$(I_i^M) = (1 - f_i) I_i \qquad \text{(Eq. 3)}$$

This document describes the development and validation of models that can be used to calculate the fractional radionuclide release rate from the fuel matrix (i.e., the dependent variable of interest is F_i).

As discussed in Section 6.2.2, the oxidative dissolution is the primary process expected to degrade the CSNF matrix in the repository environment. This process begins with the oxidation of uranium in the plus four oxidation state, U(IV), to uranium in the plus six oxidation state, U(VI), followed by dissolution of U(VI). Using the simplifying assumption (Assumption 5.1) that the fractional rate of release of radionuclides from the CSNF matrix is equal to the fractional rate of degradation of the matrix, the fractional radionuclide release rate can be expressed as the product of the specific surface area (A) of the fuel, and the rate of corrosion of the fuel per unit area (R_d):

$$F_i = A\, R_d \qquad \text{(Eq. 4)}$$

where

A = Specific surface area (i.e., the surface area per unit mass) of the fuel
R_d = Rate of oxidative dissolution of the fuel per unit surface area.

This document describes how available experimental data are used for developing and validating the models for the fractional release rate of the matrix radionuclide inventory (i.e., the model, discussed in Sections 6.4.1 and 7.2, for which the dependent variable is F_i).

This document also describes how the models' parameter values and the associated uncertainties are determined by regression analysis of available experimental data. The range of qualified experimental data spans CSNF with burnup in the range 15 to 65 (MWd/kgU) and percent fission gas release in the range 1percent to 18 percent. It also spans pH values from 2 to 10.3, temperatures from 25°C to 90°C, oxygen partial pressure from 0.002 to 0.2 atmospheres, and carbonate–bicarbonate concentrations from 0 (i.e., water sparged with CO_2-free air) to 2×10^{-2} molar. Restrictions on the domain of application of the models (i.e., restrictions on range of CSNF characteristics and environmental factors over which the models are valid) are described in Section 8.2. With the exception of temperature, for which the upper end of the temperature domain is extended to 100°C (Section 7.2 for justification), the models' application domain is restricted to the data domain. A conservative bounding model is used for any fuel exposed to air at temperatures greater than 100°C (Section 6.2.2.2).

This report receives no direct inputs from other reports or their technical product output data tracking numbers (DTNs). It provides direct inputs to the TSPA-LA model.

INTENTIONALLY LEFT BLANK

2. QUALITY ASSURANCE

This document was developed in accordance with AP-SIII.10Q, *Models*, and *Technical Work Plan for: Regulatory Integration Modeling and Analysis of the Waste Form and Waste Package* (BSC 2004 [DIRS 169944]). Section 8 of the technical work plan (TWP) states that modeling activities performed under the TWP are subject to *Quality Assurance Requirements Description* (DOE 2004 [DIRS 171386]).

Technical Work Plan for: Regulatory Integration Modeling and Analysis of the Waste Form and Waste Package (BSC 2004 [DIRS 169944], Appendix A), contains the process control evaluation used to evaluate the control of electronic management of data during the modeling and documentation activities. The evaluation determined that the methods in the implementing procedures are adequate. No deviations from these methods were used.

INTENTIONALLY LEFT BLANK

3. USE OF SOFTWARE

The software applications used to support the CSNF analysis and modeling activities described in this document are Microsoft Excel 2002, Service Pack 2, running under Microsoft Windows 2000 Professional, Service Pack 2, on a Dell OptiPlex GX240 computer at Argonne National Laboratory; SigmaPlot 2002 for Windows, Version 8.0, running on a Dell PW5650 Workstation in Las Vegas (tag number WSB501356); and Mathcad 2001i Professional, running on a Dell PW5650 Workstation in Las Vegas (CRWMS M&O tag WSB 501356).

Microsoft Excel 2002 was used to perform calculations using user-defined formulas and the application's standard functions. Inputs to, outputs from, and formulas and standard functions used in the Excel spreadsheets are described at the points where they were used for calculations described throughout this document. SigmaPlot was used for the linear and nonlinear regression analyses discussed throughout the document. Mathcad 2001i Professional was used for the regression analysis documented in Appendix II. The built-in regression functions in the SigmaPlot for Windows, Version 8.0, and in Mathcad 2001i Professional were used without modification.

The Microsoft Excel 2002, Mathcad 2001i Professional, and SigmaPlot software applications are commercial off-the-shelf software and are not required to be qualified, per Section 2.1.6 of LP-SI.11Q-BSC, *Software Management*. Only standard functions of these software applications were used; no software routines or macros were used.

Regression analysis is used to determine the values of the model's parameters that most closely describe the data. It does so by minimizing the sum of the squared residuals (i.e., differences between the predicted and observed values of the dependant variable) where the sum of the squared residuals is given by:

$$SR = \sum_{i=1}^{n} (DR_i^m - DR_i^c)^2 \qquad \text{(Eq. 5)}$$

where

- SR = sum of the squared residuals
- DR_i^m = log of measured dissolution rate for run i
- DR_i^c = log of the calculated dissolution rate for run i
- n = number of runs included in the analyses

The user interface for the SigmaPlot application is designed for point-and-click implementation of functions available in pull-down menus and tool bars, much like those used in Microsoft Excel. The inputs for multivariate linear regression analyses are the identification of spreadsheet columns containing the data for the dependent and independent variables in the model.

The inputs for the nonlinear regression analyses are:

- The mathematical form of the model to be regressed to the data set (Section 6.4.1.2, Table 6-6). This mathematical form identifies the dependent variable, independent variables, and model parameters.
- Initial (estimated) values for each of the model parameters.
- The name of the dependent variable in the model and identification of a spreadsheet column for the corresponding data set to which the dependent variable in the model is to be fitted.
- The spreadsheet columns for each of the independent variable data sets for which independent variable data are available.

The input data for SigmaPlot regression analyses are the data in Tables 4-2, 4-3, and 4-4. The outputs from the SigmaPlot for Windows software are the regressed values for each of the model parameters, the standard errors in the values of these model parameters, and statistics for the goodness of fit of the model to the data set (Tables 6-4, 6-5, 6-6, 6-7, and 6-8). The listing of the input data, the form of the model, and the output parameter values allow the results to be checked by hand calculation or by comparison with the output from a different software application capable of performing multivariate linear and nonlinear regression analyses.

The regression analysis documented in Appendix II utilizes the matrix and vector manipulation features of Mathcad 2001i Professional. The regression equations described in Equation 5 are posed in their normal form, which admits to a direct solution, involving only matrix inversion and matrix-vector multiplication. The details of the algorithm are given in the two Mathcad sheets in Appendix II.

The input data for the Mathcad analysis is the same as that for the SigmaPlot analysis, Tables 4-2, 4-3, and 4-4. The outputs from the Mathcad 2001i Professional software are the same regressed values for the model parameters, standard errors and goodness of fit statistics. The covariance matrix is an additional output from the Mathcad calculation. The covariance matrix is required to implement uncertainty in the regression coefficients, in a way that accounts for the correlation between parameters and is consistent with the range of the dissolution rates and other data used to obtain the regressed values. Mathcad was also used to calculate the Cholesky decomposition of the covariance matrix (Appendix II). The Cholesky decomposition facilitates implementation of regression coefficient uncertainty in the TSPA model file.

The detailed presentation of the Microsoft Excel and Mathcad analyses in Appendices I and II allows the results to be checked by hand calculation or by using any other software application that performs standard mathematical operations and matrix and vector manipulations.

4. INPUTS

This section addresses the data inputs directly used for model development. In general, these inputs include data and associated measurement uncertainties chosen because they are the most current and relevant data available to support the purposes of this report (Section 1). All other data and sources of information used in discussing the scientific basis for the models or used for corroborative and model validation purposes are included is Sections 6 and 7.

In the following sections, the appropriateness of the input data is addressed by discussing the use of the data and aspects of the testing methods and testing conditions pertinent to considering the suitability of the data for the intended use.

4.1 DIRECT INPUT

As stated in the Section 1, this document is intended to develop a probability distribution for the instantaneous release fraction (f_i) for each radionuclide, i, and to derive parameters for modeling the matrix fractional release rate (F_i) by analysis of suitable experimental data. Qualified data are used as input for these analyses and the model parameter values and associated uncertainty estimates are the principal outputs (Sections 8.1 and 8.2).

The inputs are organized according to the principal model parameters they support and further organized according to the test types involved. On this basis, the experiments can be divided into three broad categories. The first addresses the gap and grain-boundary inventories and the instantaneous release fractions (f_i). The second is designed to address the parametric dependence of the matrix dissolution rate per unit of exposed surface area (i.e., R_d). The third measures the geometric-specific surface area of CSNF pellets. As discussed in Section 6.4.1.5, these geometric-specific surface area data are used to scale the area-specific dissolution rates based on the effective corroding surface area of CSNF in realistic degraded states and configurations. Within these three broad categories, the available test data can be further categorized by the test types and test conditions involved.

4.1.1 Instantaneous Fractional Release Data

This section includes data from measurements of the gap and grain-boundary inventory fractions of fission gases and fission product elements.

Table 4-1 shows available data for the gap inventory and grain-boundary inventories of cesium, technetium, strontium and iodine in CSNF from DTN: MO0407SEPGGBID.000 [DIRS 170619].

DTN: MO0407SEPGGBID.000 [DIRS 170619] data were obtained by exposing commercial spent fuel to mild leachant solutions and then measuring the concentrations of uranium, ^{137}Cs, ^{99}Tc, ^{90}Sr, and ^{129}I in the solution. For the gap inventory, the fuel was pushed out of the clad and the fuel fragments and cladding were exposed to the leachant (either deionized water or a buffered potassium-iodine solution) for periods of 1 day or up to 1 week. The solutions were then analyzed to determine the concentrations of the desired radionuclides. The fuel was then crushed to obtain individual grain particles and then again exposed to the leachant (either a buffered potassium iodine or 0.1 M HCl solution) for periods between two and 24 hours. The

solutions were then analyzed for the desired radionuclides to determine the grain-boundary inventories. The grain-boundary inventory was typically released within the first hour.

In using the methods described above, a small fraction of the fuel matrix dissolves and contributes to the measured ^{137}Cs, ^{99}Tc, ^{90}Sr, and ^{129}I concentrations. The gap and grain-boundary fractions for these radionuclides are, therefore, determined by subtracting the fractional dissolution of uranium (which indicates the fraction of the fuel matrix that dissolved) from the fractional dissolution of ^{137}Cs, ^{99}Tc, ^{90}Sr, and ^{129}I. Since the fractions involved are often small (the release fractions are typically less than one percent for technetium and strontium), subtraction of two small experimentally measured fractions, each of which have some measurement error, can result in a negative value. Such negative results are expected due to the measurement error inherent in determination of the small dissolution fractions but they have no physical meaning for an individual sample, as a negative inventory is not realistic. Such negative results are to be expected, especially for technetium where a significant fraction is located in the five-metal particles, which are more difficult to dissolve.

An examination of the reproducibility of the data in Table 4-1 shows that the majority of tests showed reproducibility, which is a measure of all of the uncertainties combined, within a factor of about 1.5. In one case (the cesium and iodine grain boundary data in the "0.59 FGR %" rows), the data differ by factors of about four and seven, respectively. However, it is important to note that the absolute values for these fractions is very small and, thus, these differences have little effect on total inventory available for instantaneous release (combined gap and grain-boundary inventory).

4.1.2 Matrix Dissolution Rate Data: Flow-Through Tests

CSNF, in the form of grain-sized powders, was tested in single-pass flow-through (SPFT) dissolution studies. These studies provide the parametric dependence of the "forward" matrix dissolution rate over a range of conditions that bracket the anticipated groundwater and environmental conditions to which CSNF may be exposed in breached waste packages in the repository. The test configuration, conditions, and methods are described elsewhere (Gray and Wilson 1995 [DIRS 100758], Section 2.0). The flow-through tests were designed to maintain constant test conditions and to eliminate the influence of back-reactions or secondary phase formation that could inhibit the overall reaction rate (hence the use of the term "forward" to describe the dissolution rates measured in these tests). The effect of feedback from the dissolved uranium concentration on the rate of release of ^{137}Cs from fuel grains was examined but the results were ambiguous. An increase of the dissolved uranium (U) concentration to 6 to 8 mg/L (about half the saturation concentration) in single-pass flow-through leachate resulted in no observable effect on the measured dissolution rate, indicating no feedback from the dissolved uranium. However, when uranium-free water was again pumped through the system, an increase of approximately 50 percent was observed for uranium and ^{137}Cs release (Gray and Wilson 1995 [DIRS 100758], Section 3.3.5), indicating the dissolved uranium may have some effect on the dissolution rate.

Table 4-1. Light Water Reactor SNF Gap and Grain-Boundary Inventories

FGR (%)	^{137}Cs		^{99}Tc		^{90}Sr		^{129}I	
	GI (%)	GBI (%)	GI (%)	GBI (%)	GI (%)	GBI (%)	GI (%)	GBI (%)
1.1	1.18E+00	1.98E-01	-2.30E-02	5.04E-02	3.97E-02	2.14E-02		
7.85	7.21E-01	1.17E+00	3.44E-05	-7.75E-02	8.70E-03	2.38E-02		
7.85	8.02E-01	3.67E-01	-1.85E-02	4.76E-02	3.68E-02	5.75E-02		
7.85	2.23E+00						1.52E+00	
7.85	1.55E+00						3.28E+00	
7.85		6.24E-01						5.15E+00
0.59	2.07E-01	1.88E-01		6.63E-02	1.97E-02	8.00E-02	1.68E-02	
0.59	2.78E-01						1.15E-01	
0.59		7.37E-01						2.09E+00
7.4	1.80E+00						9.37E-02	
7.4		6.96E-01						7.98E+00
7.4		6.48E-01						7.53E+00
11.2	2.57E+00	1.00E+00	1.51E-02	1.54E-02	2.30E-02	1.34E-01		
11.2	2.32E+00		8.22E-03		1.22E-02			
11.2	3.21E+00						1.44E+00	
11.2	3.00E+00						1.08E+00	
11.2		7.64E-01						7.48E+00
11.2		8.14E-01						9.13E+00
18	4.25E+00	9.34E-01	5.42E-02	1.33E-01	9.70E-02	8.65E-02		
18	5.05E+00		2.55E-02		4.08E-02			
18	7.46E+00						1.82E+01	
18	1.05E+01						1.23E+01	
18		1.10E+00						8.32E+00
18		1.23E+00						8.54E+00

Source: DTN: MO0407SEPGGBID.000 [DIRS 170619]

NOTES: GI = gap inventory; GBI = grain-boundary inventory; FGR = fission gas release.
Blank table cells indicate no data.

An inter-laboratory comparison of UO_2-dissolution rates measured by the SPFT method was conducted using portions of the same batch of unirradiated UO_2 and similar test conditions at each of the three participating laboratories (Gray et al. 1994 [DIRS 170109]). The dissolution rates from each of the three laboratories (2.2 ±0.5, 1.5 ±0.9, and 5.5 ±2.7 mg/m^2/day ±2σ) indicated good reproducibility of the results obtained using this test method.

In the SPFT tests, the principal test response is the oxidative-dissolution rate of the matrix. Because the available data set spans a wide range of dissolution conditions, these data are suitable for analysis of the functional dependence of the oxidative-dissolution rate (R_d) on environmental factors. The range of qualified SPFT data spans the pH range from 2 to 10.3, the temperature range from 25°C to 78°C, oxygen partial pressure from 0.002 to 0.2 atmospheres, and carbonate–bicarbonate concentrations from 0 to 2×10^{-2} molar.

The CSNF flow-through test data for alkaline conditions are shown in Table 4-2. Unirradiated UO_2 flow-through test data used as input in developing the alkaline conditions model are shown in Table 4-3. CSNF flow-through test data for acidic conditions are shown in Table 4-4, which includes Run #66, a dissolution rate for ATM-103 of 109 mg/(m^2×d) at a pH of 3.25 from

DTN: MO0302PNLDUFTD.000 [DIRS 162385] and data from DTN: MO0304PNLLPHDD.000 [DIRS 163441]. It also includes data for one test (Y6-A7B) conducted at a pH of 7.29 as part of the acidic conditions test series (DTN: MO0304PNLLPHDD.000 [DIRS 163441]). All of the tests listed in Table 4-4 were conducted under carbonate-free conditions (i.e., the solutions used were continuously stirred and sparged with air containing less than 3 ppm CO_2).

As described in the ReadMe files associated with these input data, the tabulated results are based on the steady state test conditions. The initial data, which are associated with transient and irrelevant surface phenomena (e.g., dissolution of fuel fines or dissolution of oxidized or otherwise altered surface features, or both), are not used. Such initially high and transient dissolution rates are commonly observed in laboratory dissolution studies and have been attributed to disruption of grain surfaces during sample preparation and/or early dissolution of ultrafine particles that adhere to larger grains (e.g., Aagaard and Helgeson 1982 [DIRS 101530], p. 244). The effects of oxidized surface layers on the initial dissolution of UO_2 are described by Jegou et al. (2001 [DIRS 162397], pp. 476 to 478). For acidic conditions, the data obtained after a significant fraction (more than approximately 30 percent) of the sample has been dissolved are not used because of the uncertain state of the sample material (including its specific surface area and the effects of accumulated insoluble residues) after such extensive dissolution.

Table 4-2. CSNF Flow-Through Test Dissolution Data (Alkaline Conditions)

Run No.	Burnup (MWd/kg U)	Specific Surface Area (m^2/g)	Temp. (°C)	Total Carbonate (mol/L)	O_2 Partial Pressure (atm)	pH	Dissolution Rate Normalized to Surface Area ($mg/m^2/day$)	Standard Deviation for Dissolution Rate ($mg/m^2/day$)	Slope of the Cumulative Release Curve (fraction released/day)
1	30	0.0858	49	2.E-03	0.2	9.06	7.58	0.35	6.476E-04
2	30	0.0858	51	2.E-03	0.2	9.06	8.55	0.76	7.194E-04
3	30	0.0858	50	2.E-03	0.2	9.06	6.31	0.97	5.177E-04
4	30	0.0858	24	2.E-02	0.2	8.18	4.15	0.33	3.426E-04
5	30	0.0858	73	2.E-02	0.2	10.14	13.81	1.36	1.124E-03
5A	30	0.0858	77	2.E-02	0.2	10.03	21.38	2.39	1.878E-03
6	30	0.0858	75	2.E-04	0.2	8.13	10.52	1.60	9.265E-04
6A	30	0.0858	72	2.E-04	0.2	8.13	9.90	0.82	8.683E-04
7	30	0.0858	23	2.E-04	0.2	10.07	0.58	0.22	4.751E-05
7A	30	0.0858	20	2.E-04	0.2	10.02	1.08	0.29	8.653E-05
8	30	0.0858	24	2.E-02	0.2	9.12	3.25	0.31	2.755E-04
9	30	0.0858	24	2.E-03	0.2	10.11	2.47	0.25	2.128E-04
10	30	0.0858	27	2.E-04	0.02	8.00	2.12	0.16	1.819E-04
11	30	0.0858	78	2.E-04	0.02	9.86	1.77	0.15	1.552E-04
12	30	0.0858	26	2.E-02	0.02	10.04	2.46	0.21	2.082E-04
13	30	0.0858	77	2.E-02	0.02	8.10	3.57	0.34	3.027E-04
14	30	0.0858	23	2.E-02	0.002	8.25	2.94	0.09	2.494E-04
15	30	0.0858	75	2.E-02	0.002	10.12	0.95	0.32	8.624E-05
16	30	0.0858	76	2.E-04	0.002	8.00	1.41	0.15	1.225E-04
17	30	0.0858	20	2.E-04	0.002	10.00	0.76	0.19	6.042E-05
18	30	0.0858	50	2.E-02	0.002	10.05	1.20	0.16	1.076E-04
19	30	0.0858	22	2.E-03	0.002	8.97	1.95	0.33	1.808E-04
20	30	0.0858	74	2.E-02	0.02	10.11	5.65	1.05	4.569E-04
21	31	0.0984	50	2.E-03	0.2	9.05	6.61	0.54	6.578E-04
22	50	0.277	26	2.E-02	0.2	8.27	1.63	0.32	4.376E-04
23	31	0.0678	23	2.E-02	0.2	8.02	4.04	0.87	2.837E-04
24	31	0.0678	76	2.E-02	0.2	8.04	9.41	2.82	6.457E-04
25	31	0.0678	23	2.E-04	0.2	7.93	2.64	0.34	1.805E-04

Table 4-2. CSNF Flow-Through Test Dissolution Data (Alkaline Conditions) (Continued)

Run No.	Burnup (MWd/kg U)	Specific Surface Area (m^2/g)	Temp. (°C)	Total Carbonate (mol/L)	O_2 Partial Pressure (atm)	pH	Dissolution Rate Normalized to Surface Area ($mg/m^2/day$)	Standard Deviation for Dissolution Rate ($mg/m^2/day$)	Slope of the Cumulative Release Curve (fraction released/day)
26	31	0.0678	75	2.E-04	0.2	7.75	10.99	1.72	7.918E-04
27	44	0.136	23	2.E-02	0.2	8.27	3.62	0.64	4.453E-04
28	50	0.1023	25	2.E-02	0.2	8.30	3.83	0.22	3.873E-04
29	50	0.1023	76	2.E-02	0.2	8.30	6.90	1.04	6.939E-04
30	50	0.1023	25	2.E-04	0.2	7.56	2.85	0.56	2.737E-04
31	50	0.1023	74	2.E-04	0.2	7.56	9.45	1.37	9.902E-04
33	50	0.1023	75	2.E-02	0.002	8.06	1.35	0.36	1.552E-04
34	50	0.1023	27	2.E-04	0.002	7.76	2.03	0.20	2.071E-04
35	50	0.1023	74	2.E-04	0.002	7.74	3.50	0.46	3.612E-04
36	15	0.0837	27	2.E-02	0.2	8.02	3.24	0.54	2.739E-04
37	15	0.0837	76	2.E-02	0.2	7.96	11.94	3.97	9.558E-04
38	15	0.0837	27	2.E-04	0.2	7.62	3.74	0.47	3.050E-04
61	65	0.133	26	2.E-02	0.2	8.14	3.94	0.52	5.262E-04
62	65	0.133	76	2.E-02	0.2	8.12	5.61	1.56	7.769E-04
63	65	0.133	26	2.E-04	0.2	7.63	2.49	0.89	2.908E-04
64	65	0.133	76	2.E-04	0.2	7.16	6.77	1.49	9.008E-04
65	65	0.133	76	2.E-02	0.002	8.07	0.85	0.19	1.217E-04

Source: DTN: MO0302PNLDUFTD.000 [DIRS 162385]

Table 4-3. Unirradiated UO_2 Flow-Through Test Dissolution Data (Alkaline Conditions)

Sample	T (°C)	Total CO_3 (mmol/L)	O_2 (%)	pH	DR (mg/m^2d)
4	25	20	20	8.7	2.42
5	75	20	20	10.3	77.4
6	75	0.2	20	9.1	10.9
7	25	0.2	20	9	2.55
8	25	20	20	9.4	6.72
9	25	2	20	9.3	9.34
10	26	0.2	2	7.8	0.12
11	75	0.2	2	9.7	9.21
12	26	20	2	10.1	1.87
13	75	20	2	8.5	5.11
14	25	20	0.2	8	0.22
15	75	20	0.2	9.8	5.61
16	75	0.2	0.2	8.7	0.51
17	26	0.2	0.2	9.3	0.23
18	50	20	0.2	9.9	4.6
19	26	2	0.2	9	1.52
21	50	2	2	8.9	12.3
22	50	2	2	8.8	7.96
23	50	2	2	8.9	10.4
24	75	0.2	20	9.5	6.48
25	75	2	20	9.6	23.3
26	75	20	20	8.5	54

Source: DTN: MO0407SEPUDISR.000[DIRS 170618]; Appendix I, CSNF MR REV2.xls, Sheet A1

NOTES: T = temperature; Total CO_3 = $[HCO_3^-]$ + $[CO_3^{2-}]$ in millimolar units; O_2 = oxygen percent in atmospheres; DR = dissolution rate in $mg/(m^2 \cdot d)$;

Table 4-4. CSNF Flow-Through Test Dissolution Data - Acidic Conditions

Test Identification	Burnup (MWd/kgM)	Temp (°C)	O_2 Partial Pressure (atmospheres)	pH	Dissolution Rate Normalized to Surface Area ($mg/m^2/day$)	Standard deviation for Dissolution Rate	Slope of the Cumulative Release Curve (fraction released/day)
Y6-A2B	50	27	0.2	2.02	5.02E+01	6.21E+00	1.406E-02
Y6-A3B	50	27	0.2	3.01	3.45E+01	5.37E+00	1.045E-02
Run #66	31	24	0.2	3.25	1.09E+02	6.35E+00	9.043E-03
Y6-A4B	50	27	0.2	3.80	5.39E+01	1.66E+01	1.756E-02
Y6-A5B	50	26	0.2	5.07	7.18E+00	7.24E-01	2.019E-03
Y6-A6B	50	26	0.2	5.82	3.80E+00	1.17E+00	8.932E-04
Y6-A7B	50	26	0.2	7.29	3.45E+00	1.04E+00	8.381E-04

Source: DTN: MO0302PNLDUFTD.000 [DIRS 162385] (RUN # 66 Data); MO0304PNLLPHDD.000 [DIRS 163441]; Excel Spreadsheet file: CSNF MR REV2.XLS, Sheet A3 of Appendix I

4.1.3 CSNF Surface Area Data

Tables 4-5 and 4-6 show available data on the geometric surface area of irradiated CSNF. The data in Tables 4-5 and 4-6 were obtained using different methods described in the following paragraphs.

Table 4-5 shows estimated geometric-specific surface areas for irradiated fuel from the H. B. Robinson (designated "HBR") and from the Turkey Point (designated "TP") nuclear power plants (Wilson 1990 [DIRS 100793], Appendix E). These estimates were obtained by determining the distribution of particle weights in a fuel sample and approximating the particle's shape as a uniform "right-angle wedge." The average geometric-specific surface areas for each fuel were calculated by dividing the sum of the particle areas by the sum of the particle weights for each fuel type (107 particles for HBR and 89 for TP). The ratio of the height to the length of the sides of the square-shaped base (h) of the right-angle wedge shape used to calculate the particle areas, was treated as a parameter. Table 4-5 lists the specific surface areas that were calculated for three values of 'h' selected on the basis of photographic examination of the shape of the fuel fragments.

Table 4-5. Estimated Geometric-Specific Surface Area of HBR and TP Fuels

Fuel Type	h = 0.50	h = 0.67	h = 1.00
HBR (cm^2/g)	2.57	2.40	2.29
TP (cm^2/g)	2.37	2.21	2.11

Source: Wilson 1990 [DIRS 100793], Appendix E

Table 4-6 shows estimates of the surface area per unit length of the H. B. Robinson fuel (designated as ATM-101) and as-fabricated characteristics of this fuel necessary to convert these data to specific surface areas (Barner 1985 [DIRS 109194], Tables 4.1 and4.6). In this case, the surface area estimates are based on examination of the cracking patterns revealed in transverse and longitudinal ceramographic sections of the N-9 fuel rod (Barner 1985 [DIRS 109194], Appendix B). A three-step approach was used to estimate the surface area per millimeter length of fuel based on the observed cracking patterns. First, the sum of the lengths of the major radially oriented longitudinal cracks was estimated from the transverse micrographs. The contribution of these cracks to the surface area per unit length of fuel was estimated by multiplying the sum of the crack lengths by the pellet radius and by two to account for the two facing surfaces defining each crack. Second, the areas of transverse cracks were estimated by counting the primarily radial cracks (i.e., cracks oriented approximately normal to the cladding) in the longitudinal micrographs. For cracks that were found to intercept the cladding at an angle between approximately 45° and 80°, a value of half a transverse crack was assigned because of the possibility that it had been counted in the transverse micrograph. The area per unit length of the transverse cracks was estimated by using the sum of the crack lengths to estimate equivalent diameters, calculating the number of equivalent cross sections in the sample, multiplying by two to account for the two surfaces associated with each fracture, and dividing by the length of the sample. Third, the total surface area per unit length was obtained by adding the fracture surface area per unit length to the original pellet surface area per unit length.

Table 4-6. Estimated Surface Area Per Unit Length (mm^2/mm) of ATM-101 Fuel

Fuel Sections	Area of Longitudinal Cracks	Area of Transverse Cracks	Total Area of Cracks	Area of Original Surface	Total Surface Area of Fragments
N-9C-C&F	84	30	114	38	152
N-9C-I&K	74	35	109	38	147
N-9B-O&M	90	8	98	38	136

Source: Barner 1985 [DIRS 109194], Table 4.6

NOTE: For ATM-101 fuel pellets the as-fabricated pellet height =15.2 (mm); diameter = 9.30(mm); density = 10.08 (g/cm^3) (Barner 1985 [DIRS 109194], Table 4.1)

A number of factors (e.g., surface roughness, preferential corrosion at grain boundaries, and oxygen depletion in tight cracks) can influence the extent to which the CSNF geometrical specific surface area represents the appropriate value to use for the parameter A in modeling the fractional degradation rate of corroding CSNF (Equation 4). Parameter A can be considered to be a scaling parameter and will be referred to as the "effective specific surface area" of corroding CSNF to distinguish it from the geometric-specific surface area. The effects of initial surface roughness and preferential grain-boundary penetration on the estimated effective specific surface area of corroding CSNF have been assessed (Gray and Wilson 1995 [DIRS 100758], Sections 2.1.3, 4.1.1, and 4.1.6). Comparison of specific surface area measurements on grain-sized UO_2 powders using Brumauer, Emmett, and Teller (BET) and geometric particle-size distribution methods, showed that the BET results were three times larger than the geometric results (Gray and Wilson 1995 [DIRS 100758], Section 2.1.3). This factor of three difference was attributed to the effects of irregularities in the particle's shape and to surface roughness effects on the BET specific surface area results. Preferential grain-boundary penetration during the corrosion process was estimated to increase the effective specific surface area of corroding fuel fragments by a factor of six (Gray and Wilson 1995 [DIRS 100758], Sections 4.1.1 and 4.1.6). Based on these results, the specific surface area of CSNF corroded in single-pass flow-through tests was estimated to be 3.9×10^{-3} (m^2/g) (Gray and Wilson 1995 [DIRS 100758], Section 4.1.1, p. 4.2). This estimate, which includes the effects of surface roughness and grain boundary penetration, is used in Section 6.4.1.5 to determine the upper end of the uncertainty distribution range for the specific surface area parameter. Its suitability for this purpose is discussed in Section 6.4.1.5.

4.1.3.1 Qualification of CSNF Surface Area Input Data

The input surface area data (Wilson 1990 [DIRS 100793], Appendix E; Barner 1985 [DIRS 109194], Tables 4.1 and 4.6; Gray and Wilson 1995 [DIRS 100758], Section 4.1.1, p. 4.2) are qualified in Appendices IV and V in accordance with AP-SIII.2Q, *Qualification of Unqualified Data*. The qualification process used for these data involves a combination of the following methods (AP-SIII.2Q, Attachment 3):

- Technical Assessment
- Corroborating Data.

The qualification process attributes (AP-SIII.2Q, Attachment 4) used were attributes 1 through 6 and 10 with most emphasis on attribute 10 (i.e., Extent and quality of corroborating data or

confirmatory testing results). This qualification process is designed to provide the desired level of confidence and its intended use is only for this modeling report. The qualification plan is included as Appendix IV and the qualification report is included as Appendix V.

4.1.3.2 Radionuclide Fractional Release Rate Data - Rod Segment Tests

This section includes data on fractional radionuclide release rates from short fuel rod segments. Five tests were conducted on short segments of ATM-103 (1.5-, 2.6-, and 3.7-inch segments), ATM-106 (1.4-inch segment), and ATM-109 (3.2-inch segment) fuel rods in a configuration in which a simulated groundwater was allowed to percolate, under a low hydraulic head, through the fuel rod segment and the radionuclide release was determined by collecting and analyzing the effluent. These tests were conducted at 90°C. The test configuration, test matrix, and test methods are described in the data report (Goldberg 2003 [DIRS 162410]). The fractional release rate data from these tests are used as direct input to this report (Table 4-7). The slopes of regression lines fitted to the cumulative release data were used to estimate these fractional radionuclide release rates (Goldberg 2003 [DIRS 162410]). The zero intercepts of the linear regression lines through the cumulative release data for each nuclide gave the instantaneous fractional releases used for validating the instantaneous fractional release model in Section 7.1.1. Overall, uncertainties in the measured fractional radionuclide release rate data from these tests are estimated to be bounded by ±80 percent relative standard deviation (Goldberg 2003 [DIRS 162410]). Section 6.4.1.4 discusses other components of the uncertainty of these data pertinent to estimate the effective specific surface areas used in scaling CSNF matrix release rates.

The data in Table 4-7 are used as inputs to determine the lower end of uncertainty range for the specific surface area parameter (Sections 6.4.1.4 and 6.4.1.5). These data are appropriate for this purpose because, as discussed in Section 6.2.2.1, short fuel rod segments represent a plausible state of degraded fuel rods.

Table 4-7. Average Fractional Radionuclide Release Rates (d^{-1}) from Rod Segment Tests

Fuel	^{137}Cs	^{129}I	^{90}Sr	^{99}Tc
ATM-103, 1.5”	7.09E-7	8.94E-6	7.01E-7	4.01E-7
ATM-103, 2.6”	8.01E-7	1.52E-5	1.05E-6	5.17E-7
ATM-103, 3.7”	7.96E-7	1.37E-5	2.82E-7	6.31E-7
Average ATM-103	7.69E-7	1.26E-5	6.78E-7	5.16E-7
ATM-106, 1.4”	1.95E-6	1.03E-5	9.09E-7	1.93E-7
ATM-109, 3.2”	5.21E-7	5.07E-6	ND[a]	2.60E-8

Source: DTN: MO0301ANLSF001.450 [DIRS 162384]

NOTE: [a] Concentration not determined in test solution.

4.1.4 Input Data Summary

The input data described above in Sections 4.1.1, 4.1.2, and 4.1.3 are summarized in Table 4-8. The input data uncertainties and the effects of these uncertainties on the model output are discussed in Sections 6.3.1, 6.3.2, 6.4.1.1, and 6.4.1.4.

Table 4-8. Direct Input Data Summary

Data Name	Data Source	DTN	Data Use in this Model Report
Instantaneous Release Fraction			
Gap/Grain Boundary Inventory Fractions		MO0407SEPGGBID.000 [DIRS 170619]	Section 6.3.1
Matrix Dissolution Rate Per Unit Area			
CSNF Flow-Through Test Data - Alkaline Conditions		MO0302PNLDUFTD.000 [DIRS 162385]	Sections 6.4.1.2 and 6.4.1.3
UO_2 Flow-Through Test Data		MO0407SEPUDISR.000 [DIRS 170618]	Section 6.4.1.2
CSNF Flow-Through Test Data - Acidic Conditions		MO0304PNLLPHDD.000 [DIRS 163441]	Section 6.4.1.3
CSNF Geometric Surface Area Data			
Geometric-Specific Surface Area (cm^2/g) of HBR and TP Fuels	Wilson 1990 [DIRS 100793], Appendix E	N/A – Qualified per AP-SIII.2Q	Sections 6.4.1.4 and 6.4.1.5
Surface Area Per Unit Length (mm^2/mm) of ATM-101 Fuel	Barner 1985 [DIRS 109194], Tables 4.6 and 4.1	N/A – Qualified per AP-SIII.2Q	Sections 6.4.1.4 and 6.4.1.5
Rod Segment Tests - Fractional Release Rates	Goldberg 2003 [DIRS 162410], Tables 6, 7, 8, and 9	MO0301ANLSF001.450 [DIRS 162384]	Sections 6.4.1.4 and 6.4.1.5
Specific Surface Area of Corroded CSNF	Gray and Wilson 1995 [DIRS 100758], Section 4.1.1, p. 4.2	N/A – Qualified per AP-SIII.2Q	Section 6.4.1.5

4.2 CRITERIA

Project Requirements Document (Canori and Leitner 2003 [DIRS 166275]) contains requirements relevant to this document. The requirements are primarily contained in Section 3.4 of that document. The key requirements (referred to by their requirement identifier) are:

1. PRD-002/T-014, "Performance Objectives for the Geologic Repository After Permanent Closure" (Canori and Leitner 2003 [DIRS 166275], pp. 3 to 14)

   This section specifies the repository performance objectives that must be met following permanent closure. It includes a requirement for multiple barriers and limits on radiological exposure.

2. PRD-002/T-015, "Requirements for Performance Assessment" (Canori and Leitner 2003 [DIRS 166275], pp. 3 to 14)

   This section specifies the technical requirements to be used in performing a performance assessment. It includes requirements for calculations, including data related to site geology, hydrology, and variability in the models, and deterioration or degradation processes, including waste form degradation.

3. PRD-002/T-016, "Requirements for Multiple Barriers" (Canori and Leitner 2003 [DIRS 166275], pp. 3 to 15).

> This section specifies the requirements for the identification of the repository multiple barriers, describing the capabilities of the barriers to isolate waste, and provide the technical bases for the capability descriptions.

Work described in this document will support these requirements. More specific criteria exist in *Yucca Mountain Review Plan, Final Report* (NRC 2003 [DIRS 163274]). Applicable Yucca Mountain Review Plan acceptance criteria are presented below. Section 8.3 quotes the full text of the applicable acceptance criteria with pointers to the information within this report that pertains to the criteria.

System Description and Demonstration of Multiple Barriers Acceptance Criteria (NRC 2003 [DIRS 163274], Section 2.2.1.1.3)

- Acceptance Criterion 1–Identification of Barriers Is Adequate
- Acceptance Criterion 2–Description of Barrier Capability to Isolate Waste Is Acceptable
- Acceptance Criterion 3–Technical Basis for Barrier Capability Is Adequately Presented.

Degradation of Engineered Barriers (NRC 2003 [DIRS 163274], Section 2.2.1.3.1.3)

- Acceptance Criterion 1–System Description and Model Integration are Adequate
- Acceptance Criterion 2–Data Are Sufficient for Model Justification
- Acceptance Criterion 3–Data Uncertainty is Characterized and Propagated through the Model Abstraction
- Acceptance Criterion 4–Model Uncertainty is Characterized and Propagated Through the Model Abstraction
- Acceptance Criterion 5–Model Abstraction Output Is Supported By Objective Comparisons.

Radionuclide Release Rates and Solubility Limits Acceptance Criteria (NRC 2003 [DIRS 163274], Section 2.2.1.3.4.3)

- Acceptance Criterion 1–System Description and Model Integration Are Adequate
- Acceptance Criterion 2–Data Are Sufficient for Model Justification
- Acceptance Criterion 3–Data Uncertainty Is Characterized and Propagated Through the Model Abstraction
- Acceptance Criterion 4–Model Uncertainty Is Characterized and Propagated Through the Model Abstraction
- Acceptance Criterion 5–Model Abstraction Output Is Supported by Objective Comparisons.

4.3 CODES AND STANDARDS

Standard Practice for Prediction of the Long-Term Behavior of Waste Package Materials, Including Waste Forms, Used in Engineered Barrier Systems (EBS) for Geologic Disposal of High-Level Radioactive Waste (ASTM C 1174-97 [DIRS 105725]) applies to this report.

5. ASSUMPTIONS

Three assumptions were used in the development of the CSNF models.

5.1 FRACTIONAL DEGRADATION RATE BOUNDS RADIONUCLIDE RELEASE

Assumption: In developing the models for the rate of fractional radionuclide release from the CSNF matrix, it is assumed that the fractional degradation rate of the CSNF matrix conservatively bounds the rate of fractional release of radionuclides located in the fuel matrix.

Rationale: This assumption is based on the fact that there is no process, other than those involving prior degradation of the fuel matrix, which can enable fission products dissolved or embedded in the fuel matrix to be released. The processes that could cause some mobilization of fission products embedded in the matrix are discussed in Section 6.2.1.2. These processes will have a negligible effect on radionuclide release compared to the matrix oxidation and oxidative dissolution processes that are modeled (Table 6-1). This assumption is conservative because the CSNF matrix degradation models assume that the fission product and actinide elements embedded in the fuel matrix are made available for mobilization and behave (e.g., dissolve) as individual elements as the fuel matrix degrades. Fission product technetium is known to be partly in the form of noble five-metal alloy particles. The properties of the five-metal alloy particles are likely to control technetium release rate at a level much lower than the CSNF matrix degradation rate. Assuming that technetium release from the CSNF matrix is limited only by the matrix degradation rate is, therefore, conservative.

Confirmation Status: This assumption is conservative and does not require further confirmation.

Use in the Model: Section 6.2.1.2.

5.2 FUEL FRAGMENTS AND SHORT FUEL ROD SEGMENTS CONSERVATIVELY REPRESENT DEGRADED CSNF

Assumption: In assessing the effective specific surface area of corroding CSNF in fuel rods following breaching of the cladding, it is conservatively assumed that the configuration of the fuel is represented by fuel pellet fragments and short fuel rod segments.

Rationale: The basis for assessing the evolution of the state of fuel rods after the cladding is breached is provided in Section 6.2.2.1. As pointed out in Section 6.2.2.1, several scenarios are plausible for the progression of the degradation of fuel rods once the cladding is breached. However, because there is insufficient information to discriminate between the evolution scenarios, the conservative assumption is made that the degradation progresses rapidly leaving the fuel in the form of fuel pellet fragments or short rod segments.

Confirmation Status: This assumption is conservative and does not require further confirmation.

Use in the Model: Section 6.2.2.1.

5.3 SIMILARITY BETWEEN OXYGEN AND TEMPERATURE DEPENDENCE FOR ACIDIC AND ALKALINE CONDITIONS

Assumption: In developing the model for the specific dissolution rate of CSNF under acidic conditions, it is assumed that the model parameter values expressing dependence on temperature and oxygen fugacity and associated uncertainties developed for alkaline conditions also apply under acidic conditions.

Rationale: As discussed in Section 6.4.1.3, the rationale for using the same temperature and oxygen fugacity dependence under alkaline and acidic conditions is that the same redox reaction steps are likely to be involved under acidic and alkaline conditions in carbonate solutions. The effects of low pH are to promote dissolution of the partially oxidized $UO_{2.33}$ surface layer. This is also the effect of carbonate under alkaline conditions. The rate-controlling steps under acidic conditions are probably similar to those in alkaline carbonate solutions when the dissolution of the $UO_{2.33}$ surface layer does not control the overall reaction rate.

Confirmation Status: Evidence for this assumption is provided by the fact that the oxygen dependence reported for the rate of oxidative dissolution of UO_2 under acidic conditions (Torrero et al. 1997 [DIRS 114439]; Shoesmith 2000 [DIRS 162405], Section 3.1.2), which shows an oxygen concentration exponent value of 0.31, is similar to that in the base-case model for alkaline conditions (Section 6.4.1.2).

Use in the Model: Section 6.4.1.3.

6. MODEL DISCUSSION

6.1 MODELING OBJECTIVES

The modeling objectives are threefold. The first objective is to develop a probability distribution for the instantaneous release fractions (f_i). The second objective is to derive parameter values for modeling the matrix fractional release rate (F_i) by analysis of suitable experimental data and to assess and represent the uncertainty in these model parameter values. The third objective is to define the domain of application (i.e., range of CSNF characteristics and environmental factors for which the models and uncertainty analyses are expected to be valid); the output from this report (Section 8.2) includes a limitation that the models should not be applied outside this domain. A list of supporting and corroborative data and information is in the associated Document Input Reference System (DIRS) report.

6.2 BASIS FOR MODELING RADIONUCLIDE RELEASE

Modeling the release of radionuclides from failed CSNF requires a conceptual framework for understanding the state of the fuel rods and the processes likely to alter this state and cause radionuclide release. The important processes will depend on the environments to which the fuel is exposed. Until the waste package and the CSNF cladding are breached, the CSNF pellets and radionuclides in the fuel rods will be isolated from the external repository environment. If these barriers are eventually breached, the CSNF will be exposed to humid air or dripping groundwater, or both.

Section 6.2.1 discusses the basis for assessing the state of CSNF when the waste package and cladding are eventually breached. Section 6.2.2 discusses processes influencing the evolution of the state of CSNF and radionuclide release after the waste package and cladding are breached and, as appropriate, it also discusses the CSNF state and environmental factors that influence these processes. Section 6.2.3 summarizes the FEPs included in the CSNF models.

6.2.1 State of CSNF When Cladding is Breached

The state of CSNF rods, when the cladding is eventually breached, is assessed here by summarizing pertinent information on the state of freshly irradiated CSNF (i.e., up to a few decades out of light water reactors) and assessing how the known state of freshly irradiated fuel may change as a result of long-term evolution in the repository before the waste package and fuel cladding are breached.

Section 6.2.1.1 describes pertinent features of the initial state of freshly irradiated CSNF. Processes that may cause the initial CSNF state to change in the closed system environments to which the fuel will be exposed while either the waste package or the fuel cladding remain intact are discussed in Section 6.2.1.2.

6.2.1.1 Initial State of Irradiated CSNF

The term “initial state” is used here to refer to the characteristics of CSNF after it is discharged from the reactor and before it is emplaced in the repository. The state (microstructure, physicochemical condition, and distribution of fission products and actinide elements) in freshly

irradiated CSNF has been extensively investigated in postirradiation examinations conducted throughout the world. It is beyond the scope of this document to provide a comprehensive summary of the extensive literature in this area. However, such a comprehensive review has been performed recently (Dehaudt 2001 [DIRS 164019], Section 5.2). The following is intended to summarize the characteristics (features) relevant to modeling radionuclide release in the repository and is mainly abstracted from the review by Dehaudt (2001 [DIRS 164019], p. 49).

Features of irradiated CSNF that may influence the instantaneous release and the matrix release rate are the chemical composition of the fuel matrix, the macro- and micro-scale structure of the fuel (gap dimensions, fuel pellet fracturing, fuel connected porosity, and grain boundary structure), and the distribution of the fission product inventory within these fuel features.

After irradiation, the macroscale structure of CSNF rods is changed from the as-fabricated condition. The gap between the fuel pellets and the cladding decreases with increasing burnup (Dehaudt 2001 [DIRS 164019], p. 196) and the fuel pellets are extensively cracked with the cracks running radially and axially through the irradiated fuel pellets. This cracking results from the differential expansion and the associated tensile stresses caused by the radial temperature gradients in the fuel rod, mostly when it is subjected to initial power increase in the reactor. Although the fuel pellet fragments formed initially may subsequently undergo further fragmentation, much of the cracking occurs early in the irradiation history (Dehaudt 2001 [DIRS 164019], p. 87). The radial and transverse cracking of the fuel pellets result in the creation of 15 to 20 fragments per pellet with the number of cracks somewhat dependent on the fuel burnup (Dehaudt 2001 [DIRS 164019], pp. 106 and 176). Section 6.4.1.5 discusses specific surface area estimates for CSNF in its cracked condition following irradiation.

Although the as-fabricated fuel pellets have a few percent porosity, this porosity is mostly due to pore formers added during the pellet fabrication and is in the form of isolated pores usually referred to as “closed porosity” (Pelletier 2001 [DIRS 164034], Section 5.4.3.1.1). However, the release of fission gasses in CSNF irradiated at high power, or to high burnup, generates lens-shaped bubbles (often associated with metallic fission product inclusions) that can become interconnected on the grain boundary surfaces and form gas tunnels that conduct the fission gas to the gap region of the fuel rod. The fission gas release leaves some residual grain boundary decohesion and connected or “open” porosity at grain boundaries in the fuel pellets. At burnups higher than approximately 45 MWd/kgU, a “rim region” (150 to 250μm thick) is formed at the outer surface of the pellets characterized by a very fine-grained fuel microstructure, up to 10 to 15 percent porosity, and local burnup up to three times higher than the pellet average burnup. Further details of the microstructural features and effects of fission gas release on irradiated CSNF are summarized elsewhere (Dehaudt 2001 [DIRS 164019], Sections 5.2.5.2 and 5.2.5.3; Barner 1985 [DIRS 109194], pp. 4.14 and 4.15). The effects of these microstructural features of CSNF (particularly the effects of the connected porosity) on the specific surface area of CSNF are discussed in Section 6.4.1.5.

The chemical state and distribution of fission product elements in irradiated CSNF have been studied using thermodynamic equilibrium calculations and experimental measurements (Dehaudt 2001 [DIRS 164019], Section 5.2.6.3). Most fission product elements are retained within the fluorite lattice structure of the fuel matrix. However, because some of the fission product elements are not soluble in the CSNF matrix, a fraction of the inventory of these

elements migrates out of the fuel grains under normal reactor operating conditions (Pelletier 2001 [DIRS 164034], Section 5.4). The extent of migration of these fission products out of the fuel grains and the subsequent migration and accumulation at the grain boundaries and in gap regions of the fuel depend on the diffusion coefficients of the individual fission product elements in the CSNF matrix and the available mechanisms for migration and accumulation at the grain boundaries and in the gap region of the fuel rods. The factors controlling the diffusion and release of fission gasses from CSNF grains are described by Pelletier (2001 [DIRS 164034], Sections 5.4.5 and 5.4.6). The factors and processes that are involved in migration from the grain boundaries to the gap regions are also discussed (Dehaudt 2001 [DIRS 164019], Section 5.2.9). Correlation of relative release rates of fission product elements with their electronegativity (Pelletier 2001 [DIRS 164034], Section 5.4.6.2 and Table 41) provides a basis for assessing their release relative to the release of the fission gasses. The percentage of the fission gas (krypton and xenon) released from the fuel during irradiation has been measured in CSNF postirradiation studies (Barner 1985 [DIRS 109194], p. 4.6; Guenther et al. 1988 [DIRS 109206], Section 4.4; Guenther et al. 1988 [DIRS 109205], Section 4.4.2). Dehaudt (2001 [DIRS 164019], Section 5.2.9.4) states that for high-burnup CSNF (approximately 60MWd/kgU), the overall range of fission gas release to the free volume of the fuel rod (i.e., to the gap region) is about 1 to 4 percent. The percent fission gas release to the grain boundaries is about 10 percent (Dehaudt 2001 [DIRS 164019], Table 29). As discussed in Section 6.3.1, these data are useful in assessing the plausible upper bound for the gap and grain-boundary inventories of other radioelements.

Like the fission gasses, some of the fission product cesium and iodine diffuses out of the fuel grains and is found at the grain boundaries and in the gap region between the fuel pellets and the cladding (Dehaudt 2001 [DIRS 164019], Section 5.2.9.6). After irradiation, part of the fission product molybdenum, ruthenium, technetium, rhodium, and palladium inventory is found in the form of metallic alloy particles located within the fuel grains and at grain boundaries. This accumulation of noble metals in alloy particles is more evident in the higher-powered regions of the fuel (Barner 1985 [DIRS 109194], p. 4.17; Guenther et al. 1988 [DIRS 109206], Section 4.6). The extent to which the metallic fission products, cesium and iodine migrate depends on the fuel burnup, operating temperatures, and temperature gradients, as determined by the fuel's linear power history in the reactor (Guenther et al. 1988 [DIRS 109205], Sections 4.3 and 4.5.2).

6.2.1.2 Evolution of CSNF State Before Cladding is Breached

This section addresses the effects of processes that may influence the state of CSNF while the cladding is intact and while the internals of the fuel rods remain in a closed system that isolates them from the external repository environment. Consideration of these effects is important because test data from freshly irradiated CSNF testing materials is used to predict the behavior of CSNF after potential cladding failure in the distant future. The possible effects of radioactive decay of short-lived fission products (e.g., ^{137}Cs and ^{90}Sr) and alpha decay of the actinide elements in the fuel must be considered. Also, although the interior gas-phase environment in the fuel rods is an inert noble gas environment, the closed system (consisting of the irradiated fuel matrix, embedded fission products, and cladding envelope) is not in thermodynamic equilibrium. Hence, possible changes in the physicochemical state must be assessed.

The long-term closed system evolution of fuel rods has been assessed (Piron 2001 [DIRS 162396], Section 5.1). This reference examined the chemistry evolution (specifically oxygen potential) of the fuel due to decay of radionuclides (principally $^{137}Cs \rightarrow {}^{137}Ba$ and $^{90}Sr \rightarrow {}^{90}Y \rightarrow {}^{90}Zr$). It also examined the evolution of the physical state of the pellets and the potential migration of radionuclides and changes in the radionuclide distribution.

On the basis of thermal-chemical and oxygen balance calculations (Piron 2001 [DIRS 162396], Section 5.1), it was concluded that the chemical composition of CSNF is not sufficiently altered by radioactive decay to change the oxidation state of the fuel matrix. Although thermally activated diffusion of radionuclides within the grains is negligible, the effects of accumulation of alpha radiation damage in the matrix could play a role in activating diffusion and, also, long-term thermal annealing of radiation damage could cause some mobilization of fission products and thereby influence the gap and grain-boundary inventories. Also, the accumulation of helium from alpha decay (particularly for high-burnup fuel) may cause microcracking and decohesion at grain boundaries (Piron 2001 [DIRS 162396], Section 5.1.4).

To accommodate these uncertainties, the grain-boundary inventories are combined with the gap inventory estimates in estimating the instantaneous release fractions and the range of specific surface area estimates used allows for uncertainty in the extent of grain boundary decohesion (Sections 6.3.2 and 6.4.1.5).

6.2.2 Processes Influencing CSNF State and Radionuclide Release after Cladding Breach

After the cladding is breached within a failed waste package, the interior of the fuel rod will be exposed to the repository environment. Section 6.2.2.1 addresses the evolution of the fuel rod degradation when a breached fuel rod is exposed to humid air. Section 6.2.2.2 addresses the corrosion of the fuel matrix exposed to humid air, and Section 6.2.2.3 addresses the oxidative dissolution of the fuel exposed to humid air and groundwater. The experimental basis for assessing the degradation processes involved and the rates at which they proceed, is based in large part on experiments involving freshly irradiated CSNF test materials. However, the conclusions from these data are conservatively biased because the radiolytic effects due to the short-lived fission product (^{137}Cs and ^{90}Sr) will not be significant after about 300 years. The effects of beta and gamma radiolysis (associated with ^{137}Cs and ^{90}Sr decay) on the oxidative dissolution rate of CSNF are, therefore, discussed in Section 6.2.2.3.

6.2.2.1 Degradation of Fuel Rods after the Cladding is Breached

The rate of radionuclide release from CSNF rods with breached cladding depends on the evolution of the CSNF rod degradation following the initial cladding breach. The objective of this section is to discuss plausible evolution scenarios for the state of CSNF rods following initial breaching of the cladding. The effects of corrosion of the CSNF pellets and fuel-side corrosion of the cladding are considered; effects of external forces (e.g., forces associated with seismic events and external mechanical loads) are addressed in other model reports and are not considered here.

If the cladding is eventually breached, the fuel rod will be exposed to ingress of water or humid air, or both. Under these conditions, several distinct scenarios are considered plausible for the

evolution of the degradation of the fuel rods (fuel pellets and cladding). Results from accelerated tests that were designed to identify potential evolution scenarios for fuel rods with breached cladding are discussed below.

Accelerated tests were conducted to examine the corrosion behavior of fuel and cladding. The test conditions were selected to determine how the state of CSNF, with breached cladding, may evolve under unsaturated repository conditions (Cunnane et al. 2003 [DIRS 162406]). The results discussed here were obtained from two test samples, each consisting of approximately 3.5-in. segments of ATM-103, a moderate-burnup (approximately 30 GWd/MTU) pressurized water reactor fuel. These tests were conducted in closed test vessels with humid air at 175°C to accelerate the degradation processes so that their effects could be observed in reasonable experimental time frames. The test conditions (i.e., 175°C in combination with 100 percent relative humidity) cannot occur in the repository because the water vapor pressure in the repository cannot exceed one atmosphere; the maximum relative humidity at 175°C is approximately 11%. However, the results are relevant for assessing fuel and fuel-side cladding degradation processes that may occur at lower temperatures (<100°C) when the relative humidity approaches 100 percent. Visual examination of the samples after 1.5 years revealed that each had developed an axial crack that passed through a drilled hole in the cladding and ran the full length of the sample. These tests are described more fully in Section 2a of *Yucca Mountain Project Report, Waste Form Testing Work* (Cunnane et al. 2003 [DIRS 162406]). As illustrated in Figure 6-1, destructive examination of the fuel and cladding showed that the cladding had experienced regions of extensive fuel-side corrosion. Transmission electron microscopy and electron diffraction analyses showed that the corrosion products were monoclinic ZrO_2. The results indicate that the fuel-side corrosion of the cladding and the specific volume increase associated with the formation of the corrosion products caused the hoop stresses that resulted in the observed axial splitting. Also, the extent of through-wall penetration of the cladding, at the locations of the observed fuel-side corrosion, was estimated to be about 18 percent. This result indicated that regions on the fuel side of the cladding had corroded actively under the humid (100 percent relative humidity) 175°C test conditions. It is likely that this corrosion was caused by the occurrence of some water vapor condensation in local regions of the fuel–cladding interface that served as an electrolyte within which corrosion potentials exceeded the Zircaloy repassivation potential or the passive layer breakdown potential. This condition may have been promoted by deliquescent fission product salts at those regions. Conditions under which breakdown of the Zircaloy passive layer may occur are described by Pan et al. (2001 [DIRS 162412], Section 3, p. 33).

Several hypothetical scenarios for the evolution of the state of a fuel rod following breach of its cladding are considered plausible. While the corrosion of the fuel and precipitation of alteration products in a breached fuel rod could quickly lead to axial splitting, or "unzipping," of the cladding, it is also possible that the precipitating alteration phases will seal the gap and fracture openings and, as a result, limit the rate of radionuclide release. Another possibility is that the fuel-side cladding corrosion will cause extensive cladding degradation and exposure of the fuel pellet fragments. Because of the widely different implications of these evolution scenarios for radionuclide release, conservative assumptions are adopted for the state of the breached fuel rods. Specifically, it is assumed that the state of a breached fuel rod will degrade rapidly

following initial breaching of the cladding to a condition in which the fuel pellet fragments or short fuel rod segments are exposed directly to the external repository environment.

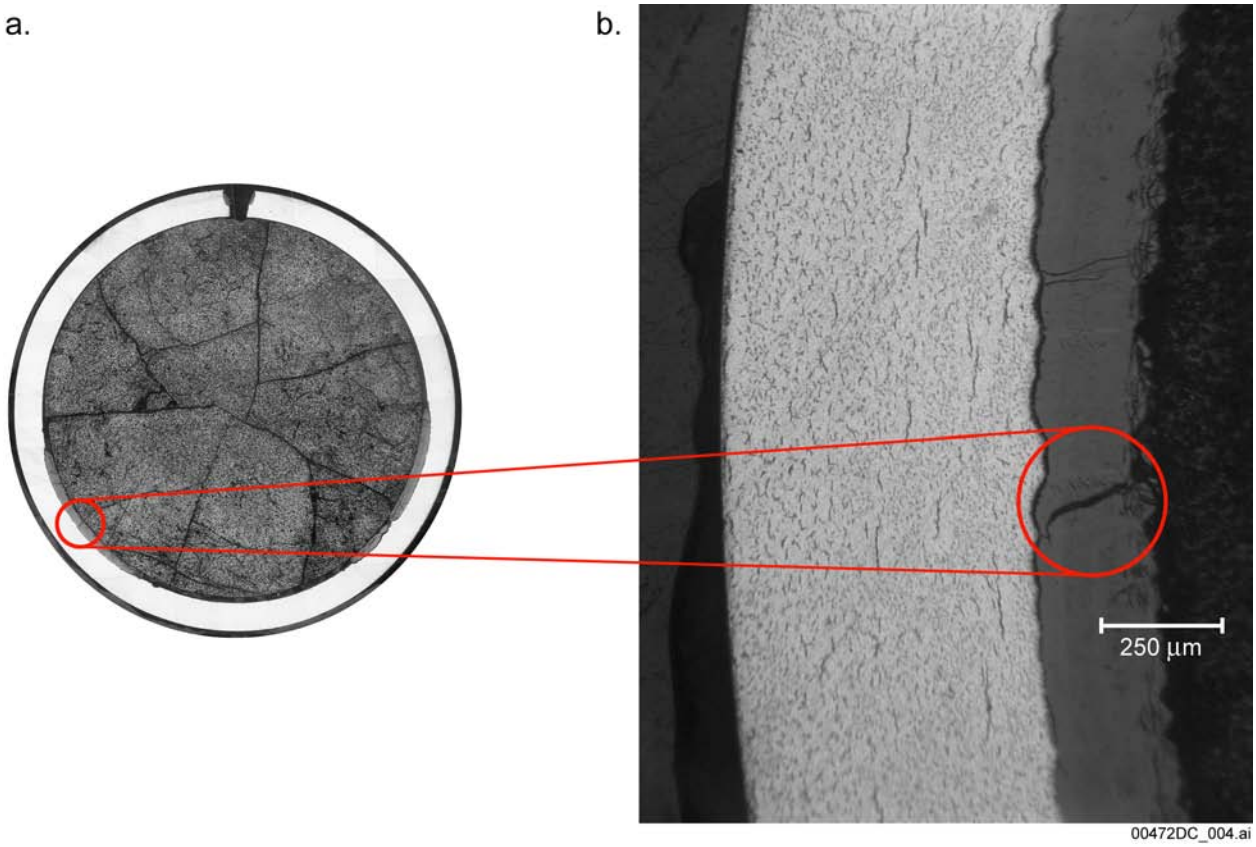

NOTES: Figure 6-1a shows a polished cross section illustrating two regions of fuel-side corrosion. Figure 6-1b illustrates the corrosion layer and the precipitated hydrides in the cladding adjacent to the corrosion layer.

Figure 6-1. Cladding Fuel-Side Corrosion Observed in Tests Conducted in Humid Air at 175°C

6.2.2.2 Corrosion of the CSNF Matrix in Humid Air

If the waste package and the cladding are breached, the CSNF will be exposed to the humid-air oxidizing environment expected in the repository. This section addresses the reactions of UO_2 and CSNF with the oxygen, water vapor and water films that may interact with the exposed CSNF under these conditions.

At temperatures well above the normal water boiling point, the air to which the fuel can be exposed has a maximum water pressure of 1 atm and can be characterized as "dry air" (dew point ≤ 100°C). UO_2 is known to be oxidized by pure steam under high temperature and pressure conditions (Olander 1986 [DIRS 170078]). For example, fuel in rods that fail during reactor service is known to be oxidized to U_3O_8 by pure steam between 500°C to 600°C (Olander et al. 1999 [DIRS 125562]). However, for the 1-atm pressure boundary conditions in the repository, the oxidation cannot exceed the UO_{2+x} single-phase region in the U–O phase diagram (Olander 1986 [DIRS 170078]). Such oxidation, by reaction with high temperature water vapor, would only be significant for fuel exposed to hot air as it cools down from approximately 1,000°C to which it could be exposed in an igneous intrusion scenario. As

discussed in the following paragraphs, reaction of fuel with water vapor is negligible for the nominal scenario temperature conditions and the oxidation of the CSNF matrix will proceed via solid-state reactions associated with the "dry air oxidation" process (CRWMS M&O 2000 [DIRS 149230]). As temperature decreases, the relative humidity to which the CSNF matrix will be exposed will increase and is expected to approach 100 percent when temperature decreases to 100°C and below. Under these conditions, water vapor complicates the oxidation process by facilitating formation of water films on the CSNF and formation of hydrated oxidation products. Not only are the reaction products different in the presence of water vapor, but the rates and mechanisms for reaction differ as well (Aronson 1958 [DIRS 117653], p. 94; Taylor et al. 1989 [DIRS 125792]). The following discussion summarizes information on the CSNF corrosion process in humid air. It specifically addresses the effects of water vapor in low relative humidity air on the rate of dry air oxidation. It also addresses whether the CSNF corrosion process, under exposure to air with relative humidities approaching 100 percent and temperatures at or below the water boiling point, is best characterized as an interaction between the water vapor and oxygen in the air that accelerates the solid-state oxidation process, or as an oxidative dissolution process in a film of water at the fuel surface.

Aronson (1958 [DIRS 117653]) studied the oxidation of UO_2 in water containing oxygen as a function of temperature. UO_2 powders were used with a specific surface area of 0.60 m^2/g (Aronson 1958 [DIRS 117653], p. 94), which is a factor of about three to eight times larger than the CSNF powders (approaching the size of typical individual grains) used in the flow through dissolution tests (Table 4-3). At 87°C, Aronson reports an oxygen-to-metal ratio of about 2.30 was achieved within 15 days. X-ray analyses of the partially oxidized samples identified dehydrated schoepite and additional water content tests confirmed the molecular ratio of water to oxide as about 0.8 (Aronson 1958 [DIRS 117653], p. 94). When the powder was exposed to degassed water, the sample did not oxidize or hydrate (Aronson 1958 [DIRS 117653], Figure 2, p. 94) even at 177°C. By comparing the activation energies (approximately 21 kJ/mol to 42 kJ/mol) of Aronson's tests (Aronson 1958 [DIRS 117653], p. 94) with those for dry-air oxidation (approximately 102 kJ/mol) (McEachern and Taylor 1998 [DIRS 113270], Table 3]) McEachern and Taylor (1998 [DIRS 113270]) were able to show that the oxidation of UO_2 in water requires the presence of dissolved oxygen and its mechanism is different from oxidation in air or gaseous oxygen.

The work of Danroc (as reported by Dehaudt 2001 [DIRS 164037], pp. 363 to 365) also shows that the hydration of very high surface area (2.5 m^2/g to 6 m^2/g) unirradiated UO_2 powders proceeds quickly in the presence of humid air (Dehaudt 2001 [DIRS 164037], Table 3). Within two years at 25°C and 100 percent relative humidity, a bulk oxygen-to-metal ratio of 2.22 is achieved with 18 percent per mole reacted being the hydrated phase schoepite (Dehaudt 2001 [DIRS 164037], Table 5). The reaction rate increases with temperature; a bulk oxygen-to-metal ratio of 2.48 was achieved within 70 days at 100°C and 60 percent humidity. When compared to dry air oxidation, which is almost negligible for these time frames (days) at the temperatures reported here, it is clear that the humid-air corrosion process is much more rapid than the rate of the solid-state oxidation process at this low temperature.

Sunder and Miller (1996 [DIRS 126463]) also studied oxidation of unirradiated UO_2 (disks cut from unirradiated, sintered Canada deuterium uranium [CANDU] pellets) at 150°C with an applied gamma radiation field. They confirmed formation of U_3O_8 within about two years on all

samples exposed to air or O_2 in the applied gamma field. The samples exposed to O_2 and 60 percent relative humidity underwent the most extensive oxidation, up to a factor of 20 higher U(VI)/U(IV) ratio, as measured by x-ray photo-electron spectroscopy, than samples in similar closed vessels containing only air. Hydrated phases and U_3O_8 were formed during the oxidation. However, virtually no oxidation occurred for samples exposed to 60 percent relative humidity in argon. Such a finding is consistent with the fact that UO_2 reaction with steam is relatively benign in this temperature range when oxygen is absent (Aronson 1958 [DIRS 117653], Figure 2, p. 94).

Woodley et al. (1989 [DIRS 122032], pp. 74 and 87) used thermogravimetric analysis tests to measure the oxidation of CSNF samples between 140°C to 225°C with the nominal dewpoint ranging from -70°C to +14.5°C. This range represents very low relative humidity. This variation in moisture content had little measurable effect on the oxidation rate, and, if anything, oxidation was somewhat faster in dry air. Einziger et al. (1991 [DIRS 126446], pp. 389 to 391) also examined oven dry-bath CSNF oxidation over the temperature range 110°C to 175°C and at nominal dewpoints of -55°C or +80°C. Again, the effect of water vapor on the oxidation from UO_2 to U_4O_9 was found to be minimal; however, oxidation was found to be somewhat faster in air with water vapor. These results indicate, at low dew points, the effects of water vapor on dry air oxidation of CSNF are small between 140°C and 225°C.

Taylor et al. (1989 [DIRS 125792]) studied the oxidation of UO_2 in air-steam mixtures at 200°C and 225°C. They report measurable UO_3 hydrate formation within 20 days at 200°C and 5 days at 225°C. More importantly, they found that below approximately 50 percent relative humidity, the rates and products of UO_2 oxidation are the same as for dry-air oxidation. Above approximately 50 percent relative humidity, UO_3-hydrated phases, primarily dehydrated schoepite ($UO_3 \cdot 0.8H_2O$) and schoepite ($UO_3 \cdot 2\ H_2O$), were observed. With water in excess of the amount necessary to saturate the test vessel's void volume, the specimens were fully wetted and much larger crystals of dehydrated schoepite were obtained. The relative humidities in the work of Woodley et al. (1989 [DIRS 122032]) and Einziger et al. (1991 [DIRS 126446]) were well below the approximately 50 percent relative humidity level (a maximum of 33 percent relative humidity according to Taylor et al. 1989 [DIRS 125792], p. 71). This could explain why no significant effect was observed. Below this 33 percent relative humidity threshold, there does not appear to be sufficient moisture to form a stable water film on the fuel surface necessary to provide a medium for uranium to dissolve and reprecipitate as a hydrated uranyl phase. However, as reported by Kohli et al. (1985 [DIRS 126191]), the presence of limited moisture during fuel oxidation may allow fuel to oxidize to an oxygen-to-metal ratio of about 2.9, as opposed to the 2.75 typical for dry-air oxidation (CRWMS M&O 2000 [DIRS 149230]).

Taylor et al. (1995 [DIRS 125815]) investigated the composition and microstructure of corrosion products formed on unirradiated UO_2 fuel exposed at 225 °C to humid air with a range of relative humidities. In dry air (RH < approximately 30 percent), they observed oxidation to U_3O_7 and U_3O_8 via a solid-state mechanism. At moderate relative humidities (30 to 70 percent), they observed surface and grain-boundary corrosion and fine-grained U_3O_8 and dehydrated schoepite crystals sparsely scattered over the surface. These observations were attributed to dissolution and precipitation of uranium within a thin (few molecules thick) and perhaps patchy layer of water on the fuel surface. At higher relative humidities (extending up to marginally unsaturated

conditions), a continuous and coarse-grained layer of U_3O_8 and dehydrated schoepite were found overlying a U_3O_7 layer. These results were attributed to dissolution and precipitation in a thicker film of water, which closely resembles a bulk liquid-phase film. When the test atmosphere was moisture-saturated (i.e., 100 percent relative humidity), large (tens to hundreds of micrometers in length) dehydrated schoepite crystals were observed consistent with growth from bulk solution.

Defective CANDU SNF (still in cladding) has also been studied to determine the effect of moisture on oxidation (Wasywich et al. 1993 [DIRS 125710]; Johnson and Taylor 1998 [DIRS 127125]). In these tests, SNF elements with small cladding defects were exposed to humid air at 150°C in five different experimental phases totaling almost 9.5 years. The initial approximately 7.75 years were at limited oxygen concentrations. For example, the oxygen concentration during the 720-day interval of Phase 4 showed a decrease in oxygen from the original 20 percent to less than 0.28 percent (Johnson and Taylor 1998 [DIRS 127125], Section 3.1). During Phase 5, it was found that the oxygen concentration dropped by a factor of approximately two within 25 days. Thus, the oxygen availability during most of the testing was very low and most likely greatly limited the extent of oxidation. Even during Phase 5 when the oxygen was replenished, the rate of alteration in regions near the defect was higher than the bulk average value.

In the dry-air experiments, Wasywich et al. (1993 [DIRS 125710]) found behavior comparable to other oxidation studies on CANDU SNF. That is, oxidation begins wherever the oxygen had direct access to the UO_2 surfaces, followed by preferential grain boundary oxidation. The U_3O_7-like phase then grew into the individual grains until conversion was complete. The behavior of the samples exposed to a moist-air environment was quite different, with alteration occurring throughout the length of the fuel element rather than being localized to the defect region. Because of the limited oxygen supply, bulk oxidation of grains was absent in the moist-air tests. At the end of the additional 660-day oxidation of Phase 5, where the oxygen supply was replenished to maintain full aeration, extensive bulk oxidation of individual grains to U_4O_9/U_3O_7 and formation of significant amounts of UO_3 hydrate occurred (Johnson and Taylor 1998 [DIRS 127125], Section 4.4.3.2).

The effects of humidity on the corrosion of irradiated and unirradiated UO_2 fuels are summarized in a review of the oxidation of UO_2 at temperatures below 400°C (McEachern and Taylor 1998 [DIRS 113270], Section 2.2). Humidity can influence air oxidation in this temperature range by forming hydrated-uranyl phases (e.g., by hydrous disproportionation of U_3O_8), by supporting oxidative dissolution in water films that form on the surface at higher relative humidities, by enhancing grain-boundary oxidation in SNF, and by supporting radiolytic processes at grain boundaries. These authors point out that because gas-phase diffusion is rapid along grain boundaries in SNF (Section 6.2.1.1 for discussion of the connected porosity at grain boundaries in CSNF), the oxidation of SNF can be considered to proceed simultaneously at grain boundaries throughout the fuel when it is exposed to humid air. At higher temperatures (e.g., between 500°C to 600°C), fuel in rods that fail during reactor service is known to be oxidized to U_3O_8 by pure steam (Olander et al. 1999 [DIRS 125562]).

The rate of dry air oxidation from $UO_{2.4}$ to $UO_{2.75}$ is about 3 times faster for samples that had schoepite present (CRWMS M&O 2000 [DIRS 149230], p. 44). Kansa et al. (1998 [DIRS 125636]) propose that the hydrated phases on the surface of the fuel essentially act as

"fins" to increase the surface area for oxygen absorption that is readily transferred to the unreacted fuel surface below the hydrated phase. The effect from these "fins" decreases as more of the fuel oxidizes to U_3O_8 and cracks or spalls from the surface. This is observed with the thermogravimetric analysis tests; after some initial transient following the plateau, the oxidation proceeds in a manner similar to that of the other samples that did not have hydrated phase present.

Results from the corrosion of spent UO_2 fuel stored at ambient temperatures in dry air for ten years, and subsequently stored in a humid air environment for fifteen years, have shown oxidation processes along the grain boundaries that weaken the intergranular bonding and cause grain-boundary decohesion (Leenaers et al. 2003 [DIRS 168991]). Examination of the fuel showed progression of a grain-boundary corrosion front that extended from the periphery to about the midradius of the pellets. Analysis of the gas phase in the storage vessel at the end of the storage period showed that it was enriched in hydrogen (approximately 40 vol %) and depleted in oxygen (approximately 1.7 vol %). These results were interpreted to be due to the combined effects of two reactions. One reaction consumes oxygen by direct oxidation of the UO_2 fuel to produce U_4O_9. The other produces hydrogen by oxidation of the fuel to U_4O_9 through reaction with H_2O_2 produced by radiolysis; the net reaction involves oxidation of the fuel by water and can be written as one mole of water reacting with four moles of UO_2 to produce one mole of U_4O_9 and one mole of hydrogen. The larger oxygen depletion observed in the humid-air exposure compared to dry-air exposure indicated that the oxidation of the fuel had progressed more rapidly in humid air than in dry air.

Long-term tests have been performed on UO_2 and CSNF fragments exposed to humid air and periodic "dripping" of a simulated groundwater composition (Wronkiewicz et al. 1996 [DIRS 102047]; Thomas 2003 [DIRS 163048]). The CSNF tests were designated "high drip rate," "low drip rate," and "vapor" tests. Each test used approximately 8 g of fuel in the form of fuel pellet fragments removed from the cladding, sieved to remove fuel fines, and contained in a Zircaloy-4 fuel "holder" supported on a ledge in a closed stainless steel test vessel. For the drip tests, water from well J-13 was equilibrated with tuff at 90°C and periodically injected into the test vessels. This water is referred to as "EJ-13 water." For the high drip-rate tests, 0.75 mL of EJ-13 water was injected twice weekly into the test vessel in a configuration that was designed to allow the injected water to drip onto the fuel in the fuel holder, percolate through the fuel fragments, drain through the bottom of the fuel holder, and accumulate in the bottom of the test vessel. The low drip-rate test design was similar to the high drip-rate test design, but the EJ-13 water injection rate (a twice-weekly injection of 0.075 mL) was a tenth of the high drip rate. The humid-air tests were conducted in the same test configuration as the high drip rate and low drip-rate tests but without any water injection. To expose the fuel to 100 percent relative humidity, approximately 5 mL of EJ-13 water was added to the base of the test vessels at the beginning of every test interval before the vessel was sealed and brought to the test temperature of 90°C ±2°C. Failure scenarios considered in the design of these tests include a scenario in which groundwater drips intermittently onto bare fuel fragments in a humid-air environment, reacts with the fuel, dissolves soluble components, and forms solid corrosion products. As illustrated in Figure 6-2, and discussed further in Section 6.2.2.3, the fuel matrix was found to react in a similar fashion in all three of these test types (Finch et al. 1999 [DIRS 127332]). The results in the vapor tests are consistent with corrosion of the fuel matrix occurring in a layer of water that condensed onto the corroding fuel surface.

The results summarized above indicate that grain-boundary corrosion and decohesion is likely to occur rapidly if CSNF pellets are exposed to humid air at temperatures greater than 100°C. Because some bulk oxidation of the CSNF grains exposed to these conditions may also occur, the effects of such oxidation on the oxidative dissolution rate of the matrix are addressed in Section 7.1.3. Although the results in Section 7.1.3 show that the dissolution rate per unit area of the higher oxides (up to U_3O_8) are somewhat greater than the UO_2 rates, the most important effect of oxidation is the very large increase in the specific surface area which causes the fractional dissolution rate to increase accordingly. Because of these results, an instantaneous radionuclide release rate model is used for any fuel that is exposed to humid air at temperatures greater than 100°C when it is subsequently contacted by water after the temperature drops below 100°C (Section 8.1).

In humid air, when the relative humidity approaches 100 percent, the fuel is probably covered by a film of condensate (perhaps promoted by dissolution of deliquescent fission product salts) and, as a result, CSNF is altered by the oxidative dissolution process under these conditions. The information summarized above is consistent with the hypothesis that the corrosion of CSNF exposed to humid air (approaching 100 percent relative humidity) at temperatures less than 100°C is due to oxidative dissolution of the fuel matrix in a film of water on the fuel surfaces.

6.2.2.3 Oxidative Dissolution of CSNF

This section provides a summary of the pertinent phenomena and chemical reactions associated with the oxidative dissolution process when CSNF is exposed to air-saturated groundwater and humid air. It specifically addresses pertinent observations as to how CSNF corrodes as a result of oxidative dissolution under conditions (limited amounts of groundwater and humid air) relevant to the repository and the factors that influence the rate of the process.

CSNF is a crystalline ceramic material with grains composed of mostly uranium dioxide. Much of the following is abstracted from recent reviews of SNF corrosion processes (Shoesmith 2000 [DIRS 162405]; Dehaudt 2001 [DIRS 164019]; Dehaudt 2001 [DIRS 164037]; Jegou et al. 2001 [DIRS 162397]; Pelletier 2001 [DIRS 164034]; Piron 2001 [DIRS 162396]).

Uranium(IV) minerals, primarily uraninite (UO_2) in the mined uranium-bearing ores, are relatively insoluble in nonoxidizing aqueous solutions; to dissolve, their uranium(IV) must first be oxidized to the much more soluble uranium(VI) oxidation state (hence the term "oxidative dissolution"). Oxidative dissolution is promoted by factors that cause oxidation to uranium(VI) and enhance dissolution of the oxidized U(VI) species. For example, uranium is extracted from natural uranium(IV) ores by oxidative dissolution with acidic iron(III) sulphate solutions or in alkaline carbonate solutions with oxygen under pressure. The overall oxidative dissolution process involves a coupled series of redox, surface complexation and dissolution, and precipitation reactions with the overall reactions depending on the fluid environment. For example upon contact with air-saturated condensate (i.e., pure water), UO_2 (and CSNF) is expected to undergo reactions of the following type to form dehydrated schoepite and metaschoepite:

$$UO_2\,(s) + \tfrac{1}{2}\,O_2\,(aq) + 0.8\,H_2O\,(l) = UO_3.\,0.8H_2O\,(s)$$

$$UO_2\,(s) + \tfrac{1}{2}\,O_2\,(aq) + 2\,H_2O\,(l) = UO_3.\,2H_2O\,(s)$$

Upon contact with groundwater containing silicate and alkali or alkaline-earth cations, the overall reactions form uranyl silicates:

$$UO_2\,(s) + \tfrac{1}{2}\,O_2\,(aq) + Na^+(aq) + Si(OH)_4\,(aq) + \tfrac{1}{2}\,H_2O = Na(UO_2)(SiO_3OH)(H_2O)_{1.5}\,(s) + H^+$$

The redox reactions involved in these overall reactions can be considered a sum of the electrochemical half-reactions:

$$UO_2 \Rightarrow UO_2^{2+} + 2e^- \qquad \text{(Eq. 6)}$$

$$\text{oxidant} + 2e^- \Rightarrow \text{reduced species} \qquad \text{(Eq. 7)}$$

These two half-reactions are affected by the solid, and particularly surface, properties of the fuel and by environmental factors that influence the rates of the oxidation and dissolution reactions involved.

For the slowly dissolving semiconductor oxides, which include UO_2, the rate of the oxidative dissolution process can be controlled either by: (1) redox reaction charge transfer at the dissolving surface, or (2) surface reactions (e.g., surface complexation and dissolution reactions). The factors that influence the rates of these reactions are discussed later in this section and in Sections 6.4.2.1 and 6.4.2.2. Also, the production or mass transport rates of oxidants to the corroding UO_2 surface can, under some circumstances, control and limit the rate of the oxidative dissolution process. In the following paragraph, the circumstances under which oxidant production rates and oxidant mass transport rates can limit the overall rate of oxidative dissolution are briefly summarized before discussing the factors that control the rate of the chemical reactions involved in the oxidative dissolution process.

In reducing repository environments, the radiolytic production rate of oxidants and the mass transport rate of dissolved species to and away from the corroding CSNF can control the overall rate of reaction and can provide the basis for modeling the dissolution rate (Jegou et al. 2001 [DIRS 162397], Section 8.2.4). For example, if the radiolytically produced oxidants from alpha decay were the only source of oxidants, then it would take more than 7,000 years after the CSNF is exposed to water to oxidize all of the fuel (Jegou et al. 2001 [DIRS 162397], Figure 88). In contrast to the reducing repository environment, air in the hydraulically unsaturated void spaces of the repository is likely to maintain an oxygen fugacity expected for humid air under the local relative humidity and temperature conditions (i.e., approximately 0.2 atmospheres at ambient temperatures and approximately 0.06 atmospheres at 90°C and 100 percent relative humidity) and provide an unlimited supply of dissolved oxygen to air–water interfaces. Therefore, in the repository, the dissolved oxygen concentration boundary condition at the air–water interface is controlled and buffered by the oxygen fugacity in the air space. In some configurations (e.g., within clad segments of CSNF rods), the rate of diffusion of dissolved oxygen from the air–water interface to parts of the corroding fuel surface may be sufficiently slow to limit the rate of the oxidative dissolution process (Section 6.4.1.4). The remainder of this section discusses pertinent experimental observations on how CSNF corrodes because of oxidative dissolution at temperatures less than 100°C and the factors that influence the kinetics of the chemical reactions involved.

Experimental evidence indicates that the long-term oxidative dissolution of UO_2 (and CSNF) under neutral to basic conditions involves oxidation of a thin layer of the UO_2 at the surface–

water interface to a higher oxide UO_{2+x} (e.g., U_3O_7) followed by further oxidation and dissolution of this layer (Casas et al. 1994 [DIRS 162386]; Shoesmith et al. 1989 [DIRS 162402]). Based on the results of x-ray photoelectron spectroscopy analyses, it has been shown that the corrosion of unirradiated UO_2 fuel in near neutral to alkaline solutions proceeds in two stages (Shoesmith et al. 1998 [DIRS 162404]; Christensen and Sunder 2000 [DIRS 162387]). The first stage is the rapid formation of a surface UO_{2+x} film that achieves a limiting composition of $UO_{2.33}$. The second stage involves the further oxidation of the $UO_{2.33}$ film at the film–water interface to form soluble secondary U(VI) phases (e.g., $UO_3.xH_2O$, hydrated schoepite). Under acidic and complexing (carbonate–bicarbonate) conditions that promote rapid dissolution of this layer, the solid surface is less oxidized (Casas et al. 1994 [DIRS 162386]; Torrero et al. 1997 [DIRS 114439]; Shoesmith 2000 [DIRS 162405]).

As discussed in Section 6.2.2.2, the more macroscopic scale corrosion phenomena that occur upon exposure of CSNF and UO_2 to dripping water and humid air have been studied in long-term experiments (Thomas 2003 [DIRS 163048]). After approximately five years, the surfaces of all fuel fragments in drip and vapor experiments developed yellowish to white crusts, obscuring the underlying (black) fuel. Analyses using a scanning electron microscope revealed these crusts to be predominantly uranium-bearing phases, including uranyl oxy-hydroxides and uranyl silicates (Section 7.3.2 provides further discussion of alteration phase identification and associated uncertainties). Similar phases were identified during corrosion studies of unirradiated UO_2 (Wronkiewicz et al. 1996 [DIRS 102047]) and occur at many oxidized uraninite deposits (Section 7.3.1). These results indicate that under the range of hydrologic conditions anticipated in the repository, the oxidative dissolution process involves oxidation of the fuel matrix to U(VI), dissolution of the oxidized U(VI), and precipitation of uranyl alteration phases back onto the corroding fuel surface. As illustrated in Figure 6-2, oxidative dissolution in humid air and dripping groundwater at 90°C occurs via general corrosion at fuel-fragment surfaces. Dissolution along fuel-grain boundaries is also evident. Apparent dissolution of fuel along defects that intersect grain boundaries has created dissolution pits that are 50 to 200 nm in diameter. These dissolution pits penetrate 1 to 2 μm into each grain, producing a "worm-like" texture along fuel-grain boundaries (Figure 6-2). Fuel shards smaller than a micrometer are common between fuel grains and may contribute to the reactive surface area of fuel exposed to groundwater. Similar grain-boundary dissolution and a "wormy" texture were observed in fuel specimens exposed to Na-bicarbonate water in flow-through dissolution experiments (Gray and Wilson 1995 [DIRS 100758], Sections 3.3.4, 4.1.4, and 4.1.6, Figures A.46 to A.60). The effects of this "wormy" fuel grain texture on the effective specific surface area of the corroding fuel is addressed in Section 6.4.1.5. Outer surfaces of reacted fuel fragments develop a fine-grained layer of corrosion products adjacent to the fuel. A more coarsely crystalline layer of corrosion products covers the fine-grained layer, the thickness of which varies considerably among samples. Corrosion-layer compositions depend strongly on water composition, with uranyl oxy-hydroxides predominating in humid-air experiments, and alkali and alkaline earth uranyl silicates predominating in high drip-rate experiments (Section 7.3.2).

Figure 6-2 indicates that the SNF matrix dissolves by three modes: (1) dissolution through the outer surface of fuel fragments (general corrosion); (2) dissolution along grain boundaries and defects associated with grain boundaries (Figure 6-2a); and (3) dissolution of micrometer-sized intergranular fuel particles (Figure 6-2b). Dissolution of fuel fragments in samples from all three types of unsaturated tests (humid air, low drip rate, and high drip rate) has proceeded through the

outermost grains, with little or no preferential bulk dissolution of the matrix along adjacent grain boundaries (general corrosion). Similar results were reported by Gray and Wilson (1995 [DIRS 100758], Figure A.57). These results indicate, although the CSNF oxidative dissolution process is a general corrosion process with the dissolution occurring mostly at the outermost exposed surfaces, the effective specific surface area of the corroding fuel could differ from surface area estimates of the starting material (Section 6.4.1.5).

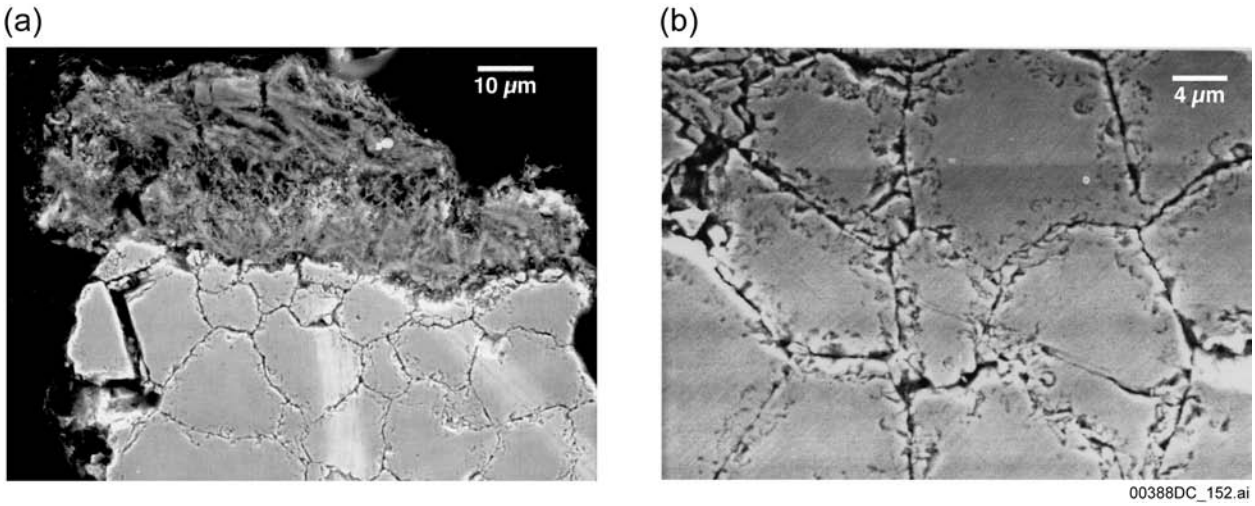

Source: Finch et al. 1999 [DIRS 127332]

NOTES: Figure 6-2a. Backscattered-electron image of a polished section through a fuel particle (bright contrast) from a high drip rate experiment with a corrosion layer (intermediate contrast) predominantly composed of Na-boltwoodite (ATM-103 high drip rate 3.7 years).
Figure 6-2b. Backscattered-electron image of a polished section showing curvilinear features at fuel-grain boundaries, which may result from dissolution along defects. The darkest contrast (black) is epoxy.

Figure 6-2. Scanning Electron Microscopy Images of Corroded CSNF

Environmental factors (e.g., temperature, dissolved oxygen concentration, pH, and carbonate concentration) that influence the oxidative dissolution of CSNF are discussed extensively in recent reviews (Shoesmith 2000 [DIRS 162405]; Jegou et al. 2001 [DIRS 162397], Section 8.2.3). The following paragraphs provide an overview of the effects of these environmental parameters; additional discussion of the mechanistic effects of these factors is provided in Sections 6.4.2.1 and 6.4.2.2.

The species available for oxidizing CSNF in the repository include dissolved oxygen and water or humid-air radiolysis products. Oxidants such as H_2O_2 and HNO_3 will be supplied by radiolysis of water or humid air. A wide range of reaction orders with respect to dissolved oxygen concentration has been reported and there is evidence that the reaction order depends on the dissolved oxygen concentration and temperature (Jegou et al. 2001 [DIRS 162397], Section 8.2.3.3.1; Shoesmith 2000 [DIRS 162405], Section 5.4; Oversby 1999 [DIRS 163420]). For example, reaction orders ranging between 1 and 0.1 have been reported for the rate of UO_2 corrosion depending on the dissolved oxygen concentration (Jegou et al. 2001 [DIRS 162397], p. 476). The fact that the reaction is first order at low dissolved oxygen concentrations, whereas the reaction order is lower at high oxygen concentrations, is attributed to adsorption of dissolved oxygen being the rate-limiting step in the oxidative dissolution process; a fractional reaction order is obtained when the surface absorption sites approach saturation. The influence of β/γ

radiolysis on the oxidative dissolution rate of UO_2 in aerated and oxygenated solutions shows a power law dependence of the dissolution rate on the dose rate (Shoesmith 2000 [DIRS 162405], Section 5.7.1; Jegou et al. 2001 [DIRS 162397], Section 8.2.3.4). Since the β/γ fields associated with CSNF decay within hundreds of years, corrosion tests on fresh CSNF (less than 30 years out of reactor) may overestimate the corrosion of CSNF in the long term. However, authors who have compared the corrosion rates of unirradiated UO_2 and CSNF have found that there is no significant difference under air-saturated groundwater conditions (Serrano et al. 1998 [DIRS 162399]; Jegou et al. 2001 [DIRS 162397], p. 542; Shoesmith 2000 [DIRS 162405], Figure 29). The reaction order for dissolved oxygen is different for SNF and UO_2 in the Canadian (Tait and Luht 1997 [DIRS 114435]) and U.S. studies (Stout and Leider 1998 [DIRS 111047], p. 2-225). It is also probably because the effects of radiolytic oxidizing species produced when CSNF corrodes mask the effects of the dissolved oxygen (Oversby 1999 [DIRS 163420], p. 10).

Carbonate present in groundwaters, including those at Yucca Mountain, is a strong complexing agent for the, U(VI) species (Grenthe et al. 1992 [DIRS 101671]; Shoesmith 2000 [DIRS 162405]) and promotes dissolution of the oxidized uranium. The influence of carbonate on the corrosion of UO_2 and CSNF is described as a function of concentration (Shoesmith 2000 [DIRS 162405], Sections 3 and 5; Jegou et al. 2001 [DIRS 162397], pp. 479 to 480) and is explicitly modeled in Section 6.4.2.2. Shoesmith (2000 [DIRS 162405], Section 3.1.3) describes the influence of different carbonate concentration ranges on the rate of UO_2 oxidative dissolution as follows. With no carbonate, an oxidized corrosion product layer (e.g., $UO_{2.33}$) accumulates and suppresses the rate of the oxidative dissolution process. With less than 10^{-3} molar total carbonate, the predominant influence of carbonate is to complex UO_2^{2+}, thus reducing alteration product buildup. With between 0.001- and 0.1-molar total carbonate, carbonate is kinetically involved in the dissolution process via carbonate surface complexes (Section 6.4.2.2). With higher carbonate concentrations, formation of UO_2CO_3 on the surface may inhibit dissolution, and carbonate dependency may lessen. It is not surprising, given these various effects of CO_3^{2-}, that the reported reaction orders for carbonate in the concentration range of approximately 2×10^{-3} M are complex and depend on the redox conditions and temperature under which the corrosion occurs (Shoesmith 2000 [DIRS 162405], Section 5.5). The combined effect with redox conditions is explained by the fact that carbonate is a strong complexant for UO_2^{2+} but not for U^{4+} and, as a consequence has a larger effect on the dissolution rate under more oxidizing conditions. The combined effect with temperature (a larger effect of carbonate concentration at higher temperature) has been attributed to a switch in the rate determining step from the rate of surface oxidation to the rate of U(VI) dissolution, which is promoted by carbonate complexation.

Information on the influence of pH on the oxidative dissolution rates of UO_2 and CSNF has been summarized in recent reviews (Shoesmith 2000 [DIRS 162405], Sections 3.1.2 and 5.3; Jegou et al. 2001 [DIRS 162397], pp. 478 to 479). For basic pH values, there is little, if any, effect. For acidic pH values, the dissolution rate increases with decreasing pH and has a power law dependence (exponent approximately equal to 0.4) on the hydrogen ion concentration. Radiolysis of a moist-air environment has been shown to increase acidity via production of HNO_3 (Reed and Bowers 1990 [DIRS 113577]). When pure water is irradiated, either by alpha particles or by beta particles or gamma rays, there is no pH change. Irradiation of water or air systems results in the fixation of nitrogen from the gas phase, the formation of nitric acid

(probably also in the gas phase), and its condensation into the liquid water phase (Reed and Bowers 1990 [DIRS 113577]).

Information on the effects of temperature on the oxidative dissolution rates of UO_2 and CSNF has been summarized in recent reviews (Shoesmith 2000 [DIRS 162405], Section 5.6; Jegou et al. 2001 [DIRS 162397], pp. 480 to 481). A range of apparent activation energies between 20 and approximately 70 kJ/mol have been reported for different conditions with acidic and complexing solutions giving values toward the upper end of this range and noncomplexing neutral solutions giving values toward the lower end of the range. These different apparent activation energies are consistent with the evidence that the formation and accumulation of secondary deposits on the corroding surface in noncomplexing solutions can counterbalance the effects of temperature and give an apparent activation energy at the lower end of the range cited above. In acidic and carbonate solutions that minimize the buildup of secondary deposits and the formation of an intermediate $UO_{2.33}$ layer, higher apparent activation energies are observed because these counterbalancing effects are minimized. The activation energies discussed here are referred to as "apparent" activation energies because a number of mechanistic features of the oxidative dissolution process change with increasing carbonate concentration over the temperature range 20°C to 75°C (Shoesmith 2000 [DIRS 162405], Section 5.6).

Other important groundwater species are calcium and silicon ions, which can greatly reduce the rate of oxidative dissolution rate by forming a protective layer of stable corrosion products with low solubilities (Gray and Wilson 1995 [DIRS 100758], p. 4.13; Shoesmith 2000 [DIRS 162405], Section 5.9). Electrochemical studies have shown, although these groundwater species can form very thin and protective corrosion product films that significantly reduce the rate of the oxidative dissolution process, this effect can be counteracted by the effects of carbonate (Shoesmith 2000 [DIRS 162405], Sections 3.1.4 and 5.9).

6.2.3 FEPs Included in the Model

Based on the discussion in Section 6.2.2, this model report includes consideration of features of the CSNF, its disposal environment, and the events and processes that are expected to influence the rate of radionuclide release (DTN: MO0407SEPFEPLA.000 [DIRS 170760]). These FEPS, along with their disposition into the Total System Performance Assessment for the License Application (TSPA-LA) model, are summarized in Table 6-1. Other screened out CSNF FEPs and the basis for their screening decisions are described in *Miscellaneous Waste-Form FEPs* (BSC 2004 [DIRS 163116]).

Table 6-1. Included FEPs for This Model Report and Their Disposition in the TSPA-LA Model

FEP Number	FEP Name	Section Where Disposition is Described
2.1.02.02.0A	CSNF degradation (alteration, dissolution, and radionuclide release)	Sections 6.2.2 and 6.4.1.
2.1.02.07.0A	Radionuclide release from gap and grain boundaries	Sections 6.2.1 and 6.3.

6.3 MODELING THE INSTANTANEOUS RELEASE FRACTIONS

6.3.1 The Gap and Grain-Boundary Inventory Data Input and Uncertainties

The input data for modeling the instantaneous radionuclide release fractions (f_i) are the gap and grain-boundary inventory fraction data described in Section 4.1.1. Section 6.2.1.1 provides a general discussion of the factors that influence the distribution of fission products in irradiated CSNF. The following paragraphs provide a discussion of the available data that are pertinent for assessing instantaneous release in irradiated UO_2 fuels and that provide a basis for assessing the extent to which the available data represent the CSNF population.

As discussed in Section 6.2.1.1, some fission-produced radionuclides migrate from the UO_2 matrix of light water reactor CSNF at the high fuel temperatures of reactor operation and deposit onto the cooler grain boundaries and fuel–cladding gap surfaces. Cesium and iodine, in addition to the fission gases, are the most conspicuous elements in this category. If water enters fuel rods with breached cladding in the repository, these soluble radionuclides can dissolve quickly. The fraction of the inventory that is available for such rapid dissolution is therefore modeled as an "instantaneous" release fraction.

Laboratory measurements of light water reactor CSNF show that the gap and the grain-boundary inventories of ^{99}Tc and ^{90}Sr are near the detection limits of the methods used (i.e., less than 0.2 percent of the total inventories of these elements) (Gray et al. 1992 [DIRS 162393]). However, some of the ^{99}Tc resides at the grain boundaries in the form of relatively insoluble metallic particles and may not be detected by these tests (Gray et al. 1992 [DIRS 162393]).

Fission gas release fractions have been used as a basis for comparison to release of other fission product elements from the fuel matrix because the gasses are chemically inert and are quickly released from the gap and grain boundary upon breach of the cladding. For ^{137}Cs, the combined gap and grain-boundary inventories are approximately one third of the fission gas release fractions (Gray 1999 [DIRS 121407]). For the same fuels, the available data (Gray 1999 [DIRS 121407], Figure 1) indicate that the grain-boundary inventories of cesium-135 and ^{137}Cs are generally less than about 1 percent of the total inventories of these nuclides and that the gap inventories are equal to roughly one fourth of the percentage of fission gas release for a given fuel type.

The first column of Table 4-1 shows that the gap inventory (GI) and grain-boundary inventory (GBI) input data were obtained from CSNF with a broad range of fission gas release fractions. As pointed out in Section 6.2.1.1, the fraction of the fission product inventory that is located in the gap and at the grain boundaries in CSNF is related to the percent fission gas release. The mechanism by which fission gasses and other fission product elements migrate out of the fuel grains and accumulate at grain boundaries and in the gap regions of fuel rods (Dehaudt 2001 [DIRS 164019], Section 5.2.9; Pelletier 2001 [DIRS 164034], Section 5.4) provide a basis for assessing the extent to which the data in Table 4-1 is likely to represent the CSNF population in general. This mechanism involves thermal and athermal diffusion from the fuel grains to the grain boundaries, fission gas bubble accumulation at the grain boundaries, coalescence of the fission gas bubbles to form an interconnected porosity network at the grain boundaries, and migration of mobile fission products along the grain-boundaries by grain-boundary diffusion and

percolation through the interconnected porosity network. The relative rates of diffusion of the fission product elements are controlled by their diffusion coefficients. The relative rates of percolation through the connected porosity created by the fission gas bubbles is controlled by the difference between the gas pressure in the pores and the gap region as well as the permeability of the fuel. In the CSNF fluorite structure, fission product atom diffusion occurs by a substitution mechanism involving vacancies in the cation and anion lattices with the mobility through the oxygen anion lattice being greater than through the cation lattice. On this basis, the relative release rates of the fission product elements has been correlated with their electronegativities giving the following order for the relative release rates in high-temperature annealing experiments: iodine>xenon>cesium>technetium (Pelletier 2001 [DIRS 164034], Section 5.4.6.2). When the fission gas accumulation provides an interconnected porosity network allowing percolation of the fission products to the gap region of the fuel rods, the migration rate is controlled by the fission products' vapor pressure and hence by the axial temperature profile in the rods. Even though the diffusion rate of iodine probably exceeds that of the fission gasses in the CSNF matrix, its overall release is generally close to or bounded by the fission gas release. This is because the fission yield of cesium is much greater than that of iodine and iodine combines with cesium to form CsI, which then controls iodine migration as CsI vapor after it reaches the grain boundaries (Dehaudt 2001 [DIRS 164019], Section 5.2.9.6).

As pointed out in Section 6.2.1.1, the fraction of the fission product inventory that is located in the gap and at the grain boundaries in CSNF is related to the percent fission gas release. Because the fission gas release depends on fuel type, burnup and linear power density (Jegou et al. 2001 [DIRS 162397], Section 8.2.2) it is useful to compare CANDU and light water reactor fuels in considering the effects of these parameters. The Canadian studies allow a comparison of the gap and grain-boundary inventory results for CANDU and light water reactor fuels to see whether their characteristics can be explained by differences in power levels and burnups.

Light water reactor CSNF generally operates at lower power but is irradiated to higher burnups than CANDU fuel (Jegou et al. 2001 [DIRS 162397], p. 453). The linear power of U.S. light water reactor SNF is typically 20 to 30 kW/m (Gray 1999 [DIRS 121407]), which is a little lower than even the low power CANDU fuels. Lower power levels generally mean lower fuel temperatures; pellet centerline temperatures in operating CANDU reactors are in the range 1,000°C to 1,700°C while the centerline fuel pellet temperatures in pressurized water reactors are typically in the range 800°C to 1,000°C. The resulting smaller radial temperature gradient in the fuel rods during light water reactor operation reduces the flux of ^{129}I, ^{137}Cs, and fission gases diffusing out of the matrix into the grain boundaries and gap. However, CANDU SNFs have burnups of about 10 MWd/kgU, which is considerably lower than the light water reactor fuel burnups. Lower burnup means that less ^{129}I, ^{137}Cs, and fission gases were generated in the first place (Gray 1999 [DIRS 121407]). For CANDU fuels, the radionuclide migration to the gap and grain boundaries is lessened by a smaller concentration gradient rather than the smaller temperature gradient of the light water reactor CSNF and also by the fact that the lower fission gas inventory reduces accumulation, growth and coalescence of fission gas bubbles to form connected porosity at the grain boundaries. The combined effects of local fuel temperature and burnup on the behavior of fission gas bubbles in pressurized water reactor fuels is described in some detail by Dehaudt (2001 [DIRS 164019], Section 5.2.9.2).

Stroes-Gascoyne (1996 [DIRS 113639]) measured gap and grain-boundary inventories of ^{137}Cs, ^{129}I, ^{90}Sr, ^{99}Tc, and ^{14}C in 15 used (spent) CANDU fuel elements. There was a good correlation between the combined gap and grain-boundary inventories of ^{137}Cs and ^{129}I, indicating that these fission products exhibit similar behavior in CANDU fuel and light water reactor fuel. Results were divided into groups consisting of ten low-power (less than 42 kW/m) and five high-power (greater than 42 kW/m) CANDU fuels. This partition was necessary because of wide differences in the ^{129}I and ^{137}Cs gap and grain-boundary inventories of these two fuel groups. Correlation between combined gap and grain-boundary inventories of ^{137}Cs and ^{129}I with calculated fission gas release of CANDU fuels could be confirmed only for lower-power fuels (less than 42 kW/m). Combined gap and grain-boundary inventories of ^{90}Sr were higher than expected and showed no correlation with calculated fission-gas release. No values for the combined gap and grain-boundary inventories of ^{99}Tc were obtained because ^{99}Tc in SNF samples is very insoluble and requires oxidation prior to dissolution. Combined gap and grain-boundary inventories of ^{14}C were independent of fuel power or burnup. For eight out of the nine low-power CANDU fuels, almost all of the combined gap and grain-boundary inventories of ^{129}I and ^{137}Cs remained in the grain boundaries (Stroes-Gascoyne 1996 [DIRS 113639]). In contrast, a much greater proportion of the ^{129}I and ^{137}Cs migrated out of the grain boundaries into the gap in light water reactor fuels (Gray 1999 [DIRS 121407]). This difference between the CANDU and light water reactor fuels suggests that the grain boundaries in the CANDU fuels are tighter and have less connected porosity than CSNF.

As discussed in Section 6.2.1.1, the CSNF fission gas release fraction bounds the release fraction of other radionuclides. However, Jegou et al. (2001 [DIRS 162397], Section 8.2.2.4) conclude, based on their review of the available data, that there is no obvious function that describes the correlation between the radionuclide inventory available for instantaneous release and the percent fission gas release. An alternative to correlating the gap and grain-boundary inventory to the fission gas release is to use an empirical distribution function based on the available data tabulated in Table 4-1 for each radioelement. This approach is adopted here because it is based on data from fuels spanning a wide range of percent fission gas release and because it provides results that generally overestimate instantaneous release fractions compiled based on an extensive review of CSNF data (Jegou et al. 2001 [DIRS 162397], Section 8.2.2.4). Using this approach, any correlation between the instantaneous fractional release data for cesium, technetium, strontium, and iodine is lost when the distribution functions are sampled separately. However, as pointed out above, there is no obvious correlation between the fractional release data for these elements. Even if there is some unknown correlation, it is not significant because the instantaneous fractional releases are very small except for iodine and cesium. Table 6-2 shows the input data from Table 4-1 with the average and range of the data for each element rounded to the second decimal point. The "Combined GI and GBI Average" is obtained by adding the average values for the GI and GBI columns and rounding to the second decimal point. This approach gives equal weight to the results obtained from each sample and, since most of the results are from fuel samples that have high FGR values, is expected to give averages that are conservatively biased. The lower and upper ends of the range for the combined GI and GBI are obtained by adding the minimum and maximum values, respectively, in the GI and GBI data sets. This approach maximizes the range. Negative entries are not included in establishing the range minima because the gap and grain-boundary inventory fractions are bounded by 0 percent (Note: the negative entries in Table 4-1 are a consequence of measurement uncertainties and indicates that these inventory fractions are near zero).

Although the measurement uncertainties are not tabulated for the data in Table 6-2, the overall uncertainty in estimating the instantaneous fractional releases includes the experimental measurement uncertainties discussed in Section 4.1.1 and potential systematic bias introduced by the experimental approach and aleatory uncertainty due to variability in such factors as the linear power history, burnup, and fuel grain size of the CSNF inventory (Jegou et al. 2001 [DIRS 162397], Section 8.2.2). Systematic bias in the experimental approach could be caused by the fact that, because some of the technetium inventory is associated with insoluble metal particles, its full gap and grain-boundary inventory may not be detected (Gray 1999 [DIRS 121407]). Comparison of the gap and grain-boundary inventories to the instantaneous release fractions from rod segments (Table 7-2) indicates that the potential systematic bias in the gap and grain-boundary inventory data does not have a significant effect on the instantaneous release of technetium.

Uncertainties in the extent to which the data in Table 6-2 are likely to represent the gap and grain-boundary inventories for the CSNF to be disposed of in the repository can be assessed by comparing the average fission gas release for the data in Table 6-2 to data available on the fission gas release from CSNF in general. The fission gas release rates from pressurized water reactor fuel are generally in the range 1 to 4 percent (Dehaudt 2001 [DIRS 164019], Section 5.2.9.4). Also, data for fuel irradiated to a burnup of 60 MWd/kgU show 3 percent fission gas release and 10 percent of the fission gas inventory at the grain boundaries. By comparison, the average fission gas release for the data set shown Table 6-2 is 9.8 percent and the range is 0.59 to 18 percent. Because, as discussed above, the fission gas release bounds the release of other fission products, the comparison of the fission gas release data in Table 6-2 to the fission gas release data for CSNF in general indicates that the Table 6-2 data set are a somewhat conservative subpopulation to represent instantaneous radionuclide release from the overall CSNF population.

Table 6-2. Summary of the Gap and Grain-Boundary Inventory Data

FGR (%)	^{137}Cs		^{99}Tc		^{90}Sr		^{129}I	
	GI (%)	GBI (%)	GI (%)	GBI (%)	GI (%)	GBI (%)	GI (%)	GBI (%)
1.1	1.18E+00	1.98E-01	-2.30E-02	5.04E-02	3.97E-02	2.14E-02		
7.85	7.21E-01	1.17E+00	3.44E-05	-7.75E-02	8.70E-03	2.38E-02		
7.85	8.02E-01	3.67E-01	-1.85E-02	4.76E-02	3.68E-02	5.75E-02		
7.85	2.23E+00						1.52E+00	
7.85	1.55E+00						3.28E+00	
7.85		6.24E-01						5.15E+00
0.59	2.07E-01	1.88E-01		6.63E-02	1.97E-02	8.00E-02	1.68E-02	
0.59	2.78E-01						1.15E-01	
0.59		7.37E-01						2.09E+00
7.4	1.80E+00						9.37E-02	
7.4		6.96E-01						7.98E+00
7.4		6.48E-01						7.53E+00
11.2	2.57E+00	1.00E+00	1.51E-02	1.54E-02	2.30E-02	1.34E-01		
11.2	2.32E+00		8.22E-03		1.22E-02			
11.2	3.21E+00						1.44E+00	
11.2	3.00E+00						1.08E+00	
11.2		7.64E-01						7.48E+00
11.2		8.14E-01						9.13E+00
18	4.25E+00	9.34E-01	5.42E-02	1.33E-01	9.70E-02	8.65E-02		
18	5.05E+00		2.55E-02		4.08E-02			
18	7.46E+00						1.82E+01	
18	1.05E+01						1.23E+01	
18		1.10E+00						8.32E+00
18		1.23E+00						8.54E+00
Average:	2.95	0.75	0.01	0.04	0.03	0.07	4.23	7.03
Maximum:	10.50	1.23	0.05	0.13	0.10	0.13	18.20	9.13
Minimum:	0.21	0.19	-0.02	-0.08	0.01	0.02	0.02	2.09
Combined GI and GBI Average	3.69		0.05		0.10		11.26	
Range - Combined GI and GBI	0.40 to 11.73		0[a] to 0.19		0.03 to 0.23		2.11 to 27.33	

DTN: MO0407SEPGGBID.000 [DIRS 170619] is the source of the numbers except for the last five rows ; the numbers in the last five rows are calculated in the Appendix I, CSNF MR REV2.xls, sheet A13

NOTES: FGR = fission gas release; GBI = grain-boundary inventory; GI = gap inventory
[a] zero is used as the lower end of the range here because a negative value is nonphysical

6.3.2 The Instantaneous Release Fraction Model

The mode and range for the probability distributions used in modeling the instantaneous release fractions were based on data in the superceded DTN LL000107951021.107 [DIRS 135012]. Upon review of the data in the superseded DTN LL000107951021.107 [DIRS 135012], it was discovered that some of the fractional releases were reported as percentage release when in fact they were fractional releases. The data involved were therefore reanalyzed and the corrected data are in Table 4-1. In the course of correcting the data, changes were also made in the data analysis methods to improve the accuracy of the results (DTN: MO0407SEPGGBID.000 [DIRS 170619], ReadMe file). Thus, many numbers in this new table are different from the previous values, but typically by only a few percent. One row of data was removed because that testing had been performed as part of a different program and is not qualified for use as direct input in this report. Table 6-3 shows a comparison of the average and the range for gap and grain-boundary inventories in the DTN: MO0407SEPGGBID.000 [DIRS 170619] data set and the data from the superseded DTN: LL000107951021.107 [DIRS 135012].

Table 6-3. Comparison of Input Gap and Grain-Boundary Inventory Data Distribution Characteristics to the Corresponding Distribution Characteristics of the Superceded Data

Part A:

FGR (%)	^{137}Cs		^{99}Tc		^{90}Sr		^{129}I	
	GI (%)	GBI (%)	GI (%)	GBI (%)	GI (%)	GBI (%)	GI (%)	GBI (%)
Average:	2.95	0.75	0.01	0.04	0.03	0.07	4.23	7.03
Maximum:	10.50	1.23	0.05	0.13	0.10	0.13	18.20	9.13
Minimum:	0.21	0.19	-0.02	-0.08	0.01	0.02	0.02	2.09
Combined GI and GBI Average	3.70		0.05		0.10		11.26	
Range - Combined GI and GBI	0.40 to 11.73		0 to 0.18		0.03 to 0.23		2.11 to 27.33	

Part B:

FGR (%)	^{137}Cs		^{99}Tc		^{90}Sr		^{129}I	
	GI (%)	GBI (%)	GI (%)	GBI (%)	GI (%)	GBI (%)	GI (%)	GBI (%)
Average:	2.90	0.73	0.03	0.03	0.03	0.06	4.10	7.14
Maximum:	9.90	1.16	0.14	0.12	0.12	0.13	17.40	9.35
Minimum:	0.21	0.18	0.00	0.00	0.00	0.02	0.03	2.01
Combined GI and GBI Average	3.63		0.06		0.09		11.24	
Range - Combined GI and GBI	0.39 to 11.06		0.00 to 0.26		0.02 to 0.25		2.04 to 26.75	

Source: Appendix I, CSNF MR REV2.xls, sheet A13

NOTES: FGR = fission gas release; GBI = grain-boundary inventory; GI = gap inventory

Based on the discussion in Section 6.3.1, the instantaneous fractional releases for cesium, iodine, technetium, and strontium were modeled in Revision 01 of this report (BSC 2003

[DIRS 163824] as triangular distributions with the apex of the triangular probability distribution function located at the average release fractions shown in Table 6-3 and spanning the range shown for the DTN: LL000107951021.107 [DIRS 135012] data in this table for each element. Comparison of the average fractional release data and ranges for the DTN: LL000107951021.107 [DIRS 135012] data to the corresponding corrected data (the DTN: MO0407SEPGGBID.000 [DIRS 170619] data in Table 6-3) shows that the changes to the corrected values (DTN: MO0407SEPGGBID.000 [DIRS 170619]) are negligible considering the measurement uncertainties discussed in Section 4.1.1 and other uncertainties discussed at the end of Section 6.1.3. These differences are also small compared to the conservative bias discussed in Section 6.1.3. On this basis, the probability distributions described above are not changed in the current revision of this report. The triangular probability distribution is fully defined when the minimum, mode, and maximum values are defined because the area is equal to 1. The corresponding cumulative distribution function (CDF) is obtained by integrating the area under the triangular distribution.

6.4 MODELING THE CSNF MATRIX FRACTIONAL RELEASE RATES

This section describes models that have been developed for the oxidative matrix dissolution rate of CSNF and UO_2. Section 6.4.1 describes the models for CSNF matrix degradation under alkaline and acidic conditions, Section 6.4.2 describes the alternative models developed internationally, and Section 6.4.3 describes the CSNF barrier capability.

6.4.1 The CSNF Matrix Degradation Models

The general modeling approach for the specific dissolution rate of the CSNF matrix is to identify a suitable mathematical form for the matrix dissolution rate and to determine appropriate values for adjustable parameters in that expression by regression analyses using the input data in Section 4.1.2.

The following describes forms of the mathematical expressions developed to describe the kinetics of mineral dissolution in aqueous solutions and considers, including the "goodness of fit" to the input data set, to select the models to be used in TSPA-LA. The technical basis for the plausible mathematical forms that apply to the CSNF oxidative dissolution process is discussed in *Waste Form Characteristics Report* (Stout and Leider 1998 [DIRS 111047], Section 3.4.2). This discussion indicates that the chemical kinetic rate law, which has the general mathematical form of simple rate laws given in textbooks (e.g., Stumm and Morgan 1981 [DIRS 100829], p. 90, for dependence on the concentrations of reactants and products; and p. 95, for the temperature dependence) is useful as a first approximation in evaluating rate constants and reaction orders from given sets of experimental data:

$$\text{Rate} = k[A]^a[B]^b[C]^c...\exp(E_a/RT) \qquad \text{(Eq. 8)}$$

where

k, a, b, c, and E_a are model parameters; R is the gas constant; and

[A], [B], [C], and T are relevant independent variables; the bracket notation denotes solution molar concentrations of the relevant variables (e.g., hydrogen ion, total carbonate, and dissolved oxygen)

This expression has the same mathematical form as the general expression developed for the rates of heterogeneous reactions between minerals and aqueous solutions (Aagaard and Helgeson 1982 [DIRS 101530], p. 237; Lasaga et al. 1994 [DIRS 106466], Eq. 8, p. 2,367) when the solution feedback or "dissolution affinity" term is omitted. More recent emerging understanding of mineral dissolution in general, based on the role of energetically reactive surface sites (e.g., dislocation defects) shows how these surface features interact with the extent of solution undersaturation in initiating dissolution "step waves" (Lasaga et al. 1994 [DIRS 106466]; Lasaga and Luttge 2003 [DIRS 168087]). This understanding indicates that, while the dissolution rate decreases monotonically as the extent of solution undersaturation decreases, the rate may have a very nonlinear dependence on the extent of solution undersaturation. Because the data sets used here in the regression analyses are obtained from single-pass flow through tests in which the dissolved uranium concentration is kept low, the omission of terms that describe the solution feedback effects is appropriate for determining values for the parameters that express the dependence of the rate on temperature and solution chemistry factors (i.e., for determining a, b, c, and E_a in Equation 8).

The initial approach is to use the rate law (Equation 8), with parameter values (for the parameters a, b, c, and E_a), evaluated by numerical regression analysis over the input set of experimental data from single-pass flow-through tests. For implementation in the regression analyses, Equation 8 was converted to a linear mathematical form by taking logarithms of each side; negative logarithms of the water-chemistry variables are used to be consistent with the standard definition of pH: $-\log10[H^+]$. This gives the following model form:

$$\mathrm{Log}_{10}\, R_d = a_0 + a_1 \times IT + a_2 \times pCO_3 + a_3 \times pO_2 + a_4 \times pH \qquad \text{(Eq. 9)}$$

where

R_d is the rate of matrix degradation in $mg/m^2/day$

a_0, a_1, a_2, a_3, and a_4 are model parameters

and IT, pCO_3, pO_2, and pH are the independent model variables. IT is equal to the inverse of the absolute temperature, pCO_3 is the negative log of the total carbonate molar concentration, pO_2 is the negative log of the oxygen fugacity in atmospheres, and pH is the negative log of the hydrogen ion molar concentration

More recent work expresses the general rate laws for heterogeneous reactions in terms of the activities of adsorbed reactants on mineral surfaces (Lasaga et al. 1994 [DIRS 106466], Equations 11 and 12, p. 2,367). *Waste Form Characteristics Report* (Stout and Leider 1998 [DIRS 111047], Section 3.4.2.2) describes how chemisorption of reactants may lead to more complex mathematical model forms when the rates are expressed in terms of the solution concentrations as independent variables. These more complex models include some of these independent variables included in cross-product and quadratic terms. Such nonlinear models were examined (Section 6.4.1.1) to see if they could significantly improve the regression model's R_{sqr} values (i.e., to see if such regression models could account for a significantly greater fraction of the data variation).

The CSNF degradation rate model was developed in two steps. First, the input flow-through data (Tables 4-2, 4-3, and 4-4) were analyzed to determine the values for parameters that describe the dependence of the specific dissolution rate of the matrix on the independent

variables [H^+], [CO_3], fO_2, and T (oxygen fugacity (fO_2) rather than dissolved oxygen fugacity was used as the independent modeling variable because it is the experimental variable used in Tables 4-2, 4-3, and 4-4). Because the dissolved oxygen concentration varies with temperature at constant fugacity, the use of oxygen concentration as the independent modeling variable results in some convolution of the effects of oxygen fugacity and temperature. The model for the specific dissolution rate is developed as a piecewise continuous function for the basic and acidic pH regimes. Second, the specific dissolution rate is scaled to repository-relevant degraded fuel states (i.e., pellet fragments and rod segments) (Section 6.2.2.1).

6.4.1.1 Input Data and Uncertainties for Developing CSNF Matrix Degradation Models

The input data that were used to develop the base-case model for the specific dissolution rate of the CSNF matrix are the CSNF and UO_2 single-pass flow-through test data described in Section 4.1.2.

Flow-Through Test Results

Single-pass flow-through dissolution studies were performed to examine the effects of temperature and important water chemistry variables on the forward dissolution rates of the UO_2 matrix in unirradiated UO_2 and CSNF. The UO_2 data are pertinent because the dissolution behavior of unirradiated UO_2 is similar to the behavior of CSNF after the ^{137}Cs and ^{90}Sr have decayed and the associated radiolysis effects are no longer present (Shoesmith 2000 [DIRS 162405]). Details of the flow-through tests were reported by Stout and Leider (1998 [DIRS 111047]). Tests were selected to examine systematically the effects of temperature (25°C to 75°C), dissolved oxygen (0.002 to 0.2 atmospheres overpressure), pH (8 to 10), and carbonate concentrations (2×10^{-4} to 2×10^{-2} molar) on UO_2 and SNF dissolution (Stout and Leider 1998 [DIRS 111047], p. 2-221). The results for the CSNF tests are in Table 4-2 and the UO_2 results are given in Table 4-3. Results for a series of single-pass flow-through tests conducted over the pH range extending from 2.02 to 7.29 are shown in Table 4-4. As described in Section 4.1.2, these test results were obtained under carbonate-free conditions; test Y6-A7B provides data for the dissolution rate under carbonate-free alkaline conditions.

The forward reaction includes UO_2 oxidation and dissolution reaction steps. The forward dissolution rates of UO_2 and CSNF were determined by using a single-pass flow-through method (Stout and Leider 1998 [DIRS 111047], p. 2-220). The single-pass flow-through technique allows the flow rates and specimen size to be controlled so that the UO_2 dissolves under controlled conditions far from solution saturation (no precipitation of dissolved products). Under such conditions, the steady-state dissolution rates are directly proportional to the effective surface area of the test specimen. The input data shown in Tables 4-2, 4-3, and 4-4 are "normalized" based on the estimated effective surface area of the test material (i.e., the data are expressed in the form of dissolution rate per unit area).

Uncertainties associated with the use of the single-pass flow-through measurements on CSNF and UO_2 to assess the specific dissolution rate of aged CSNF (i.e., CSNF after the β/γ radiolysis effects associated with decay of ^{137}Cs and ^{90}Sr are gone) and its parametric dependence on the environmental factors identified above include:

- Measurement uncertainties (standard deviations for the measurement uncertainties are included in Table 4-2)
- Uncertainties due to uncontrolled experimental factors
- Uncertainties associated with use of test data obtained on fresh CSNF and UO_2 to assess the dissolution rate of the full range of aged fuel in the repository.

The following discussion addresses the extent to which the pertinent sources of uncertainty are likely to be properly quantified in the parameter uncertainty estimates based on regression analyses of the input data from the single-pass flow-through tests.

A fairly recent comparison and evaluation of worldwide specific dissolution rate data (including single-pass flow-through data) for UO_2, SIMFUEL, and CSNF noted that the data have a wide range (up to a factor of 100 for the SIMFUEL data) for nominally similar conditions (Oversby 1999 [DIRS 163420], p. 31). This range is a useful indicator of the combined uncertainty associated with uncontrolled experimental factors in the measurements and the variability in the test materials and procedures used by different investigators. The uncertainty and variability in the data was attributed to various sources including effects of sample surface state (specifically oxidation to UO_{2+x}) and differences in test procedures. The results of the interlaboratory comparison described in Section 4.1.2 provide an indication of the variability associated with implementation of the single-pass flow-through test procedure on the same test material at different laboratories. The insensitivity of the CSNF flow-through data to dissolved oxygen concentration at 25°C is noted (Gray and Wilson 1995 [DIRS 100758], p. 4.3). This indicates that the oxidative dissolution rate at lower temperatures is sufficiently slow such that the results may be controlled by the initial surface state of the sample rather than the steady state surface appropriate for the test conditions involved. This component of the uncertainty would cause the data to be biased toward higher dissolution rates. The potential effects of insoluble elemental components on the dissolution rate of a complex material such as urananite were discussed by Grandstaff (1976 [DIRS 113255]). Similarly, the very insoluble fission product and actinide elements in CSNF are probably not completely dissolved under the single-pass flow-through conditions and may influence the measured uranium dissolution rate as they accumulate at the dissolving CSNF surface. These uncertainty contributions, combined with the effects of other uncontrolled experimental factors, contribute to the variability noted by Oversby (1999 [DIRS 163420]) and to the conclusion that data variability causes parameter values that express the dependence of the specific dissolution rate on environmental factors to be poorly constrained (Oversby 1999 [DIRS 163420], Abstract).

Uncertainty associated with using data from fresh CSNF to assess the oxidative dissolution of aged CSNF (i.e., CSNF after decay of the ^{137}Cs and ^{90}Sr content) is due to the uncertain effects of radiolytic oxidants produced by the β/γ decay. As pointed out in Section 6.2.2.3, the magnitude of the effects of β/γ radiolysis on the oxidative dissolution rate of CSNF in aerated water is uncertain. However, it is important to note that the effects of β/γ radiolysis will cause the modeled dissolution rate for aged CSNF to be biased on the high side.

In considering the effects of the uncertainties discussed above on modeling, it is useful to categorize them as uncertainties that cause variability in the data and uncertainties that may cause the data to be systematically biased, either conservatively or nonconservatively. The former category is addressed by propagating the uncertainties indicated by the data variability

into estimated uncertainties in the modeling parameters; the latter is addressed by assessing indications of systematic modeling bias through the model validation (Section 7).

6.4.1.2 Model for the Specific Dissolution Rate under Alkaline Conditions

This section discusses the modeling of the specific oxidative dissolution rate of CSNF under alkaline conditions. It summarizes the rate model functional form, presents the regression analysis of several forms of the model, and presents the recommended alkaline model. The approach adopted here for the alkaline conditions model uses experimental input data from flow-through dissolution tests for a set of specific CSNF types (approved testing material) and for unirradiated UO_2 over a range of controlled water chemistries and temperatures (Tables 4-2 and 4-3). Regression analyses of these data are used to evaluate empirical parameters in the rate law that expresses the corrosion rate dependence on the important experimental factors.

Regression Analysis of Alkaline Data

As discussed in Section 6.2.2.3 the principal environmental factors that influence the rate of oxidative dissolution of CSNF and UO_2 are temperature, pH, and carbonate and dissolved oxygen concentrations. Based on the discussion of mathematical forms appropriate for expressing the reaction rate kinetics the intrinsic CSNF dissolution model can be expressed in the following form:

$$\mathrm{LgDR} = a_0 + a_1 \times \mathrm{IT} + a_2 \times pCO_3 + a_3 \times pO_2 + a_4 \times \mathrm{pH} \qquad \text{(Eq. 10)}$$

where

LgDR, the dependent variable, is equal to $\mathrm{Log}_{10}\, R_d$;
a_0, a_1, a_2, a_3 and a_4 are model parameters; and
IT, pCO_3, pO_2, and pH are the independent model variables.

IT is equal to one over the absolute temperature; pCO_3 is the negative log of the total carbonate molar concentration; pO_2 is the negative log of the oxygen fugacity; and pH is the negative log of the hydrogen ion concentration. The negative logarithms of the water chemistry variables are used to be consistent with the standard definition of pH (i.e., $-\log_{10}[H^+]$).

Values for the model parameters a_0, a_1, a_2, a_3, and a_4 and associated uncertainty estimates were obtained by regression analyses using the data sets in Tables 4-2 and 4-3 together and separately. The Microsoft Excel spreadsheets used to calculate the values of the dependent and independent variables from the input data in Tables 4-2 and 4-3 are attached (Appendix I, CSNF MR REV2.xls, sheets A1 and A2). Tables 6-4, 6-5, 6-7, and 6-8 show results from the regression analyses with some statistics for the model's goodness-of-fit to the experimental data. The model forms that were used in the regression analyses are shown in the notes at the bottom of each of these tables. For example, Table 6-4 shows the regression results obtained when temperature, carbonate, and oxygen fugacity were used as the independent variables and the corresponding form of Equation 10 was regressed to the combined data in Tables 4-2 and 4-3. Equation 10, with the parameter values determined from this regression, is referred to as Model 1. Likewise, Table 6-5 shows the regression results obtained when temperature, carbonate, oxygen fugacity, and pH values were used as the independent variables and the

corresponding form of Equation 10 was regressed to the combined data in Tables 4-2 and 4-3. Equation 10, with the parameter values determined from this regression, is referred to as Model 2. Because, as discussed in Section 6.4.1, adsorption of reactants can lead to nonlinear models involving the independent variables in cross-product and quadratic terms, nonlinear multivariate regression analyses were also performed to determine if such nonlinear models would give a better fit to the data. Table 6-6 shows the regression analysis results obtained for a nonlinear model that includes cross-product terms between total carbonate and temperature and between oxygen fugacity and temperature.

Table 6-4. Linear Regression: Combined CSNF and UO_2 Data, Model 1

Model Term	Parameter	Standard Error	Significance
Constant	4.705	0.601	<0.001
IT	-1,093.826	186.829	<0.001
pCO_3	-0.102	0.0471	0.034
pO_2	-0.338	0.0506	<0.001

Source: CSNF MR REV2.xls, Spreadsheets A1 and A2 contain the derived values for the model variables that were used for this regression analysis; SigmaPlot regression file CSNF-UO2.JNB is in Appendix I and the Mathcad regression results are in Appendix II.

NOTES: $LgDR = 4.705 - (1{,}093.826 \times IT) - (0.102 \times pCO_3) - (0.338 \times pO_2)$
N = 67; R = 0.749; Rsqr = 0.561; Adj R sqr = 0.540
Standard Error of Estimate = 0.347

Table 6-5. Linear Regression: Combined CSNF and UO_2 Data, Model 2

Model Term	Parameter	Standard Error	Significance
Constant	4.224	0.758	<0.001
IT	-1,091.611	186.712	<0.001
pCO_3	-0.0933	0.0479	0.056
pO_2	-0.345	0.0509	<0.001
pH	0.0523	0.0502	0.301

Source: CSNF MR REV2.xls, Spreadsheets A1 and A2 contain the derived values for the model variables that were used for this regression analysis; SigmaPlot regression file CSNF-UO2.JNB is in Appendix I

NOTES: $LgDR = 4.224 - (1{,}091.611 \times IT) - (0.0933 \times pCO_3) - (0.345 \times pO_2) + (0.0523 \times pH)$
N = 67; R = 0.754; R sqr = 0.568; Adj R sqr = 0.541; Standard Error of Estimate = 0.347

Table 6-6. Nonlinear Regression Model: Combined CSNF and UO_2 Data

Model Term	Parameter	Standard Error	Significance
a_0	5.825	1.866	0.003
a_1	-1,444.2	594.65	0.018
a_2	-1.891	0.672	0.007
a_3	0.259	0.596	0.665
a_5	-119.08	191.15	0.536
a_6	498.7	214.79	0.024

Source: CSNF MR REV2.xls, Spreadsheets A1 and A2 contain the derived values for the model variables that were used for this regression analysis; SigmaPlot regression file CSNF-UO2.JNB is in Appendix I

NOTES: $LgDR = 5.825 - (1{,}444.2 \times IT) - (1.891 \times pO_2) + (0.259 \times pCO_3) - (119.08 \times pCO_3 \times IT) + (498.7 \times pO_2 \times IT)$
R sqr = 0.598

Table 6-7. Linear Regression Model: CSNF Data

Model Term	Parameter	Standard Error	Significance
Constant	3.424	0.508	<0.001
IT	-776.683	157.894	<0.001
pO_2	-0.279	0.0441	<0.001
pCO_3	-0.0378	0.0395	0.344

Source: CSNF MR REV2.xls, Spreadsheet A2 contains the derived values for the model variables that were used for this regression analysis; SigmaPlot regression file CSNF-UO2.JNB is in Appendix I

NOTES: $LgDR = 3.424 - (776.683 \times IT) - (0.279 \times pO_2) - (0.0378 \times pCO_3)$
N = 45; R = 0.769; Rsqr = 0.592; Adj Rsqr = 0.562
Standard Error of Estimate = 0.244

Table 6-8. Linear Regression Model: UO_2 Data

Model Term	Parameter	Standard Error	Significance
Constant	7.618	1.313	<0.001
IT	-1,777.525	410.042	<0.001
pO_2	-0.473	0.108	<0.001
pCO_3	-0.286	0.103	0.013

Source: CSNF MR REV2.xls, Spreadsheet A1 contains the derived values for the model variables that were used for this regression analysis; SigmaPlot regression file CSNF-UO2.JNB is in Appendix I

NOTES: $LgDR = 7.618 - (1{,}777.525 \times IT) - (0.473 \times pO_2) - (0.286 \times pCO_3)$
N = 22; R = 0.854; Rsqr = 0.729; Adj Rsqr = 0.684
Standard Error of Estimate = 0.411

The standard error given in Tables 6-4, 6-5, 6-6, 6-7, and 6-8 provides a measure of the uncertainty of the coefficient estimate in the same units as the estimate. The fourth column provides statistics related to the test of the hypothesis that the coefficient being estimated is zero. A high significance value indicates the coefficient is zero and the term can be dropped from the model. Conversely, the closer the significance value is to zero, the more important the term. The significance statistic in Tables 6-4, 6-5, and 6-7 indicates that carbonate concentration has little effect. However, as shown in Table 6-8, it does have a bigger effect (indicated by a smaller value of the significance statistic) when the regression analysis is performed using the UO_2 data alone. The footnotes to the tables also provide some statistics to help assess the fit. First, the number of cases or testing data sets (N) is given. The "Rsqr" and "Adj Rsqr" are numbers that indicate how well the fitted model can account for the variability in the measured values. The results in Table 6-5 show that pH is not a big contributor to dissolution rate for the combined CSNF and UO_2 data set under alkaline conditions. It was removed in the regression to produce the model shown in Table 6-4 with little change in the Rsqr and Adj Rsqr values. Temperature and oxygen fugacity have the biggest effect on dissolution as indicated by their low significance values in Tables 6-4 and 6-5. Based on these results, the model shown in Table 6-4 was selected as the base-case model for alkaline conditions. The comparison between the base-case model and the CSNF and UO_2 data set is shown in Figure 6-3. The covariance matrix corresponding to the regression analysis in Table 6-4 is provided in the Mathcad analysis documented in Appendix II. This covariance matrix is required for the TSPA-LA models to implement uncertainty in the regression coefficients, in a way that accounts for the correlation between parameters and is consistent with the range of the dissolution rates and other data used to obtain

the regressed values. The Mathcad sheet also calculates the Cholesky decomposition of the covariance matrix (Appendix II). The Cholesky decomposition facilitates implementation of regression coefficient uncertainty in the TSPA-LA model file.

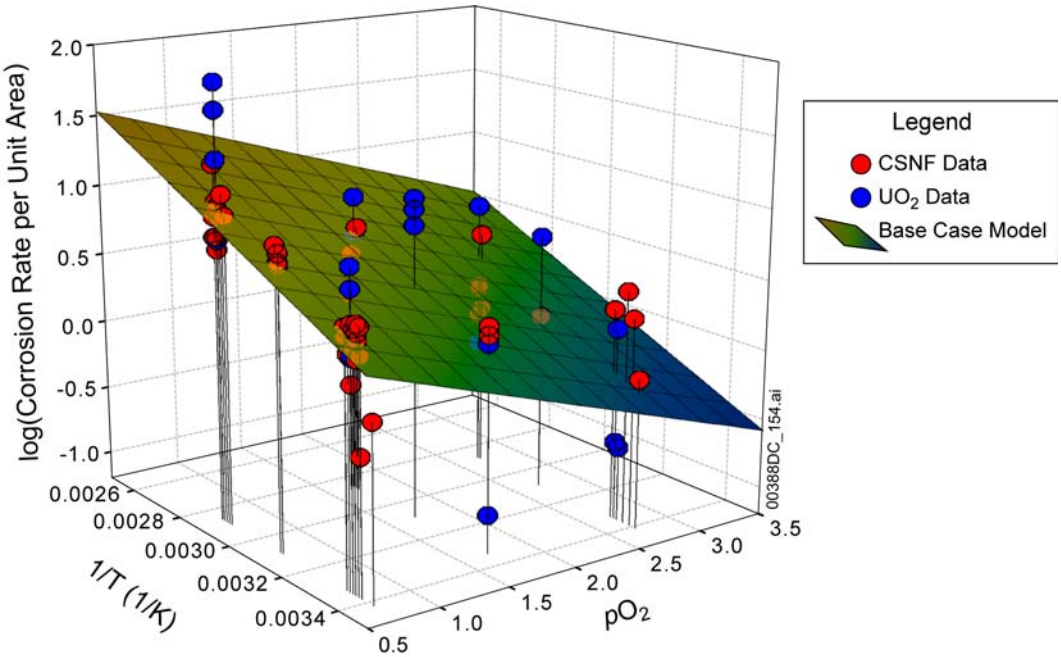

Figure 6-3. Comparison of the Base-Case Model (pCO_3 = 2.7) to the Input CSNF and UO_2 Data

For comparison to the base-case model (i.e., the model shown in Table 6-4), Table 6-6 shows a nonlinear model that includes cross product terms between temperature and oxygen fugacity and between temperature and total carbonate concentration. This regression analysis shows a weak interaction between temperature and oxygen fugacity. However, this nonlinear model provides only a slightly better fit to the data than the linear base-case model. This is shown by the comparing the Rsqr values for Tables 6-4 and 6-6, which indicate that other effects (i.e., effects other than chemisorption) are likely to be important in explaining the parts of the data variance that is not explained by the simpler linear models. Other effects that may influence the rate of the oxidative dissolution process include solution feedback, preferential dissolution at reactive surface sites, and mass transport of reactants and reaction products through surface alteration and insoluble residue layers. Because the slightly improved Rsqr values are achieved at the expense of ease of comparison of regression parameter values with literature data (literature data commonly expresses the dependence on the independent variables using the same mathematical form for the oxidative dissolution rate as that used in the base-case mode), more complex nonlinear models (Table 6-6) are not adopted for use in TSPA-LA.

Table 6-7 shows the regression analysis of the CSNF data alone (i.e., the data in Table 4-2) and Table 6-8 shows the results of regression analysis of the UO_2 data alone (i.e., the data in Table 4-3). The results in these tables indicate that the UO_2 data depends more strongly on temperature, oxygen fugacity, and carbonate concentration than the CSNF data. This point is illustrated in Figure 6-4. The Rsqr values for these regressions show that the simple linear model can explain a significantly larger fraction of the variability in the UO_2 data than in the CSNF data. This result is consistent with the expectation that factors peculiar to CSNF (e.g., formation

of insoluble residue layers on the corroding surface) may influence the CSNF corrosion rate and this uncontrolled experimental factor may account for some of the variability in the CSNF data set shown in Table 4-2. Also, as pointed out in Section 6.2.2.3, there is some evidence that different reaction steps may control the rate of the oxidative dissolution process in different regions of the experimental factor space over which the regression analyses were performed. Because of this, no single model can explain the variability over the experimental factor space. Also, the fact that worldwide data on the oxidative dissolution rates of UO_2 and CSNF exhibit broad variability attributed to uncontrolled experimental factors (Section 6.4.1.1) may account for some of the data variability not accounted for by the regression models.

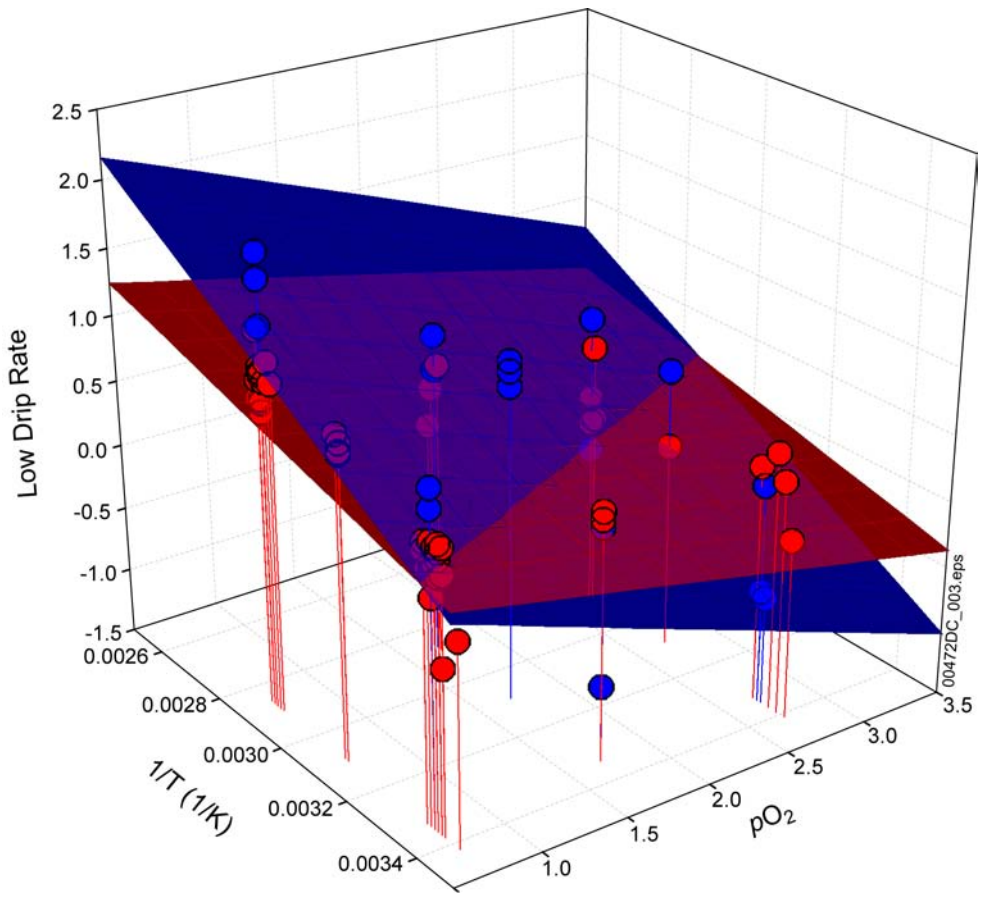

Figure 6-4. Comparison of Models (pCO_3 = 2.7) Obtained when the CSNF Data (Red) and the UO_2 Data (Blue) are Regressed Separately

6.4.1.3 Model for the Specific Dissolution Rate Under Acidic Conditions

The model for CSNF dissolution under acidic conditions was developed using the data in Table 4-4 and the model mathematical form shown in Section 6.4.1.2, Equation 10.

The data set in Table 4-4 shows the pH dependence of the dissolution rate at an average temperature of about 26°C, oxygen partial pressure of 0.2 atmospheres, and approximately zero carbonate concentrations (the test solutions were sparged with carbonate-free air). Comparison of the dissolution rate data for test Y6-A7B in Table 4-4 to the dissolution rate data for runs number 30 and 27 in Table 4-2 shows that the effect of total carbonate molar concentration

variation over the range of 0 to 2×10^{-2} is negligible in neutral to slightly alkaline solutions. However, because this result is based on one data set conditions, a value of 2×10^{-4} molar is to be used to conservatively model CSNF degradation under alkaline conditions when the in-package chemistry model calculates a concentration less than 2×10^{-4} molar. The total carbonate concentrations will decrease rapidly as the pH decreases in the acidic regime (BSC 2003 [DIRS 161962], Figure 39). Also, as described in Section 6.2.2.3, the U(VI) complexation and dissolution steps prompted by carbonate ions are unlikely to control the reaction rate under acidic conditions. The carbonate dependence term is, therefore, not included in the acid-side model. The same temperature and oxygen terms, with their associated uncertainties, were assumed (Assumption 5.3) in the acid model as were used in the alkaline model. Justification for this modeling assumption is given below.

The Equation 11 expression was regressed to dissolution rate data, from Table 4-4, using the alkaline-side values for the parameters a_1 and a_3:

$$\mathrm{LgDR} = a_0 \cdot 1 + a_1 \cdot \mathrm{IT} + a_3 \cdot pO_2 + a_4 \cdot \mathrm{pH} \qquad \text{(Eq. 11)}$$

This regression analysis is documented in Appendix II. The following equation (with Rsqr = 0.703) was obtained:

$$\text{Adjusted LgDR} = 6.60 \pm 0.446 - (0.340 \pm 0.110 \times \mathrm{pH}) \qquad \text{(Eq. 12)}$$

The resulting acid-side model has the form shown in Equation 11 where the parameter values are as follows: $a_o = 6.60 \pm 0.446$, $a_1 = -1093.826$, $a_3 = -0.338$, and $a_4 = -0.340 \pm 0.110$. Because the uncertainties determined for the temperature and oxygen fugacity dependence are assumed to be the same as those determined for alkaline conditions (Assumption 5.3), $a_1 = -1093.826 \pm 186.829$ and $a_3 = -0.338 \pm 0.0506$.

The basis for using the same temperature and oxygen fugacity dependence under alkaline and acidic conditions is that the same redox reaction steps are likely to be involved under acidic and alkaline conditions. As discussed in Section 6.2.2.3, the effects of low pH are to promote dissolution of the partially oxidized $UO_{2.33}$ surface layer, which is also the effect of carbonate under alkaline conditions. This indicates that the rate controlling steps under acidic conditions are probably similar to those in alkaline carbonate solutions when the dissolution of the $UO_{2.33}$ surface layer does not control the overall reaction rate. Also, the oxygen dependence for the rate of oxidative dissolution of UO_2 under acidic conditions (Torrero et al. 1997 [DIRS 114439]; Shoesmith 2000 [DIRS 162405], Section 3.1.2), which shows an oxygen concentration exponent value of 0.31, is similar to oxygen concentration exponent value of 0.338 in the base-case model for alkaline conditions (Section 6.4.1.2). This also indicates that the processes controlling the oxidative dissolution rate under acidic conditions are similar to those controlling the rate under alkaline carbonate conditions.

To determine the pH domains over which the models for alkaline and acidic conditions should be applied, the pH at which the alkaline and acidic conditions models give the same value of the specific dissolution rate was determined. The pH at which the acid-side model gives the same value for the log of the specific dissolution rate as the alkaline-side model is dependent on the carbonate concentration. This results in an inconsequential discontinuity if a specific pH is used

to identify the boundary between the acid and alkaline model domains. Because the total carbonate concentration has been calculated to be approximately 1×10^{-4} molar at near-neutral conditions in CSNF waste packages (BSC 2003 [DIRS 161962], Figure 39), the pH boundary between the domains of application of the acid and alkaline models was calculated using this carbonate concentration. At a total carbonate concentration of 1×10^{-4} molar, the acid-side and alkaline-side models are equal at a pH of 6.8. The acid-side model is therefore used for pH less than 6.8; the alkaline side model is used for pH $\geq$ 6.8. The Microsoft Excel spreadsheet used for the acid-side model calculations is attached (Appendix I, CSNF MR REV2.xls, Spreadsheet A3).

6.4.1.4 Input Data and Uncertainties for Scaling the Specific Dissolution Rate

As discussed in Section 1, the fractional radionuclide release rate from the CSNF matrix is obtained by multiplying the dissolution rate per unit area of the matrix by the specific surface area of the corroding fuel. The input data in Section 4.1.3 on the geometric surface area of CSNF was used to estimate the CSNF specific surface area results presented in Table 6-9.

Table 6-9. Summary of Geometric-Specific Surface Area Estimates

Fuel/(Section)	Data Source	Specific Surface Area (cm^2/g)
HBR/ATM-101(C5C-I)	Table 4-5	2.42[a]
TP/(F6-2B)	Table 4-5	2.23[a]
ATM-101 (N9C-C&F)	Table 4-6	2.22
ATM-101 (N9C-I&K)	Table 4-6	2.15
ATM-101 (N9C-O&M)	Table 4-6	2.00

NOTE: [a] Average of input data in Table 4-5

The specific surface area estimates for the HBR and TP fuels in Table 6-9 (data rows one and two) were obtained by averaging the estimates in Table 4-5 for each fuel type. The estimates for the ATM-101 fuel (in the third, fourth, and fifth data rows) were obtained by dividing the corresponding total surface area of the fuel fragments per millimeter length of fuel (i.e., the input data in the sixth column of Table 4-6) by the fuel mass per millimeter length of fuel. The latter was obtained by multiplying the volume of fuel per millimeter length ($\pi L(\text{diameter})^2/4$, where L, the length, is equal to one millimeter) by the fuel density; the input data for the fuel diameter and density are given in Table 4-6. These geometric-specific surface area data are likely to represent the geometric-specific surface area of CSNF in general because, as discussed in Section 6.2.1.1 and in Appendix V, the extent of CSNF pellet cracking is similar to that observed in these fuels and because the specific geometric surface area is not sensitive to the extent or cracking (Appendix V).

Section 6.2.2.1 discussed the likely evolution of the state of breached CSNF rods. The corrosion rate of the fuel in the repository will depend on the state of the fuel rods and the water contact scenarios because these will control the rate at which dissolved oxygen is transported to the corroding fuel surfaces. The plausible states of corroding fuel include fuel pellet fragments and short segments of fuel (Section 6.2.2.1). Data available for the fractional release rate of radionuclides from flow-through tests on fuel fragments (Gray and Wilson 1995 [DIRS 100758], Section 4.1.1, p 4.2) and from short fuel rod segments (DTN: MO0301ANLSF001.450

[DIRS 162384]) are used to estimate upper and lower bounds on the uncertainty range for the specific surface area of fuel rods in these degraded states.

The basis for using the specific surface area derived from flow-through tests on fuel fragments (Gray and Wilson 1995 [DIRS 100758], Section 4.1.1) to establish the high end of the uncertainty range for the specific surface area parameter is discussed in Section 6.4.1.5. The rod segment data (DTN: MO0301ANLSF001.450 [DIRS 162384]) are used to estimate the lower end of the uncertainty distribution range because the short length of the fuel rod segments used in the tests and the flow-through configuration are likely to conservatively bound the radionuclide release for fuel rod segments immersed or exposed to dripping groundwater or humid air, or both, in the repository. By using a test configuration in which water percolates through the test segment, these tests reasonably represent or overestimate the rate of dissolved oxygen supply to the corroding fuel when it is in the form of short fuel-rod segments. The conservative bias in the test results is due to the use of short fuel rod segments in the tests (longer pieces would have more oxygen depletion) and use of a flow-through configuration.

6.4.1.5 Scaling the Specific Dissolution Rate

The dependent variable for the models discussed in Sections 6.4.1.2 and 6.4.1.3 is the specific dissolution rate (i.e., the dissolution rate per unit area) of the CSNF matrix. To apply these models to calculating the fractional corrosion rate of the matrix, the specific dissolution rate must be multiplied by an estimate of the effective specific surface area (i.e., the effective surface area per unit mass) of the corroding fuel. The "effective surface area" is a scaling factor. The term "effective surface area" is used because it accounts not only for the specific geometric surface area of CSNF in plausible degraded states, but also for other factors that can influence the rate of oxidative dissolution of CSNF in the plausible degraded states (e.g., dissolved oxygen depletion and effects of alteration phases on the rate of mass transport of oxidants to, and reaction products away from, the corroding fuel surfaces).

When the model discussed in Section 6.4.1.2 is multiplied by an estimate of the effective specific surface area of the fuel (A), the fractional corrosion rate is given by the following equation:

$$\mathrm{Log}(F) = \mathrm{Log}(A) + 4.705 - (1093.826 \times \mathrm{IT}) - (0.102 \times pCO_3) - (0.338 \times pO_2) \quad \text{(Eq. 13)}$$

where

F = Fractional dissolution rate of the fuel (d^{-1}),

A = Estimate of the fuel effective specific surface area (m^2/mg).

Two approaches are available for estimating the effective specific surface area of the corroding fuel: (1) use estimates of the specific surface area of CSNF based on characterization of the geometric-specific surface area of the cracked fragments in irradiated fuel pellets, and (2) use the radionuclide fractional release rate data presented in Section 6.4.1.4, as summarized in Table 6-10, to estimate (F) and then solve the above equation for (A) using the fuel rod segment test conditions (T = 90°C, $pCO_3 = 2 \times 10^{-3}$ molar, and $pO_2 = 0.2$ atmospheres) (Goldberg 2003 [DIRS 162410], Tables 6, 7, 8, and 9).

The first of these two approaches is adopted to provide a best estimate of the effective surface area parameter A. The second is used with the rod segment data to estimate the lower end of the uncertainty distribution range for A. The upper end of the uncertainty distribution range is based on the input-specific surface area of fuel fragments estimated from SPFT data (Section 4.1.3).

Section 6.2.2.1 provides the basis for using fuel fragments and short fuel rod segments to represent plausible degraded states of fuel rods with breached cladding. Because the cladding in degraded fuel rods limits water and dissolved oxygen access to the fuel, the effective specific surface area of the fuel in fuel rod segments is lower than that of fuel exposed in the form of fuel pellet fragments. The SPFTs on fuel fragments maximize the effective specific surface area of the fuel fragments by minimizing deposition of alteration products on the corroding fuel and promoting effective mass transport of dissolved oxygen to the corroding fuel surfaces. As described in Section 4.1.3.2, the rod segment tests were conducted on short segments of fuel rods in a configuration in which water percolates through the rod segment and facilitates mass transport of dissolved oxygen to the corroding. The fractional radionuclide release rate results obtained from these tests are expected, therefore, to overestimate the fractional release rates from fuel rod segments in the repository. Use of data from these tests to estimate the effective specific surface area of the corroding fuel in fuel rod segments will give a conservative (i.e., biased toward the high side) estimate of the lower bound on the effective specific surface area parameter.

The best estimate for the specific surface area of CSNF is obtained by averaging the data in the third column of Table 6-9. This gives a specific surface area of 2.20 cm^2/g (i.e., 2.20×10^{-4} m^2/g or 2.20×10^{-7} m^2/mg). The corresponding value for the base ten log of the specific surface area is –6.66 when A is expressed in m^2/mg and the log is rounded to three significant figures; the value is -6.7 when rounded to two significant figures.

Table 6-10. Average Radionuclide Release Rates (d^{-1}) from Rod Segment Tests

Fuel	^{137}Cs	^{129}I	^{90}Sr	^{99}Tc
ATM-103, 1.5”	7.09E-7	8.94E-6	7.01E-7	4.01E-7
ATM-103, 2.6”	8.01E-7	1.52E-5	1.05E-6	5.17E-7
ATM-103, 3.7”	7.96E-7	1.37E-5	2.82E-7	6.31E-7
Average ATM-103	7.69E-7	1.26E-5	6.78E-7	5.16E-7
ATM-106, 1.4”	1.95E-6	1.03E-5	9.09E-7	1.93E-7
ATM-109, 3.2”	5.21E-7	5.07E-6	ND[a]	2.60E-8
Fuel Type Average[b]	1.08E-6	9.32E-6	7.94E-7	2.45E-7

Source: Appendix I, CSNF MR REV2.xls, Spreadsheet A6

NOTE: [a] Concentration not determined in test solution.
[b] Calculated by averaging the results for the ATM-103, ATM-106, and ATM-109 in rows 5, 6, and 7; the ATM-103 results in rows 2, 3, and 4 are used to calculate the ATM-103 average results in row 5.

The overall average fractional release rate (F), as calculated from the fuel rod segment data in Table 6-10, is used to estimate the effective specific surface area (A) based on the following equation:

$$\mathrm{Log}(A) = \mathrm{Log}(F) - 4.705 + 1093.826(IT) + 0.102(pCO_3) + 0.338(pO_2) \qquad \text{(Eq. 14)}$$

Because the ^{129}I data in Table 6-10 are likely to contain release contributions from the grain boundaries, these data were not included in calculating the overall fractional release rate of 7.06×10^{-7} d^{-1}. Substituting this value for F in Equation 14 and solving for log(A) gives the value of -7.33 (i.e., an effective specific surface area of the corroding fuel in the tests of 4.65×10^{-5} m^2/g). The Microsoft Excel spreadsheet used to perform these calculations is attached (Appendix I, CSNF MR REV2.xls, Spreadsheet A8).

As discussed in Appendix IV, estimates of the specific geometric surface areas of CSNF fragments are generally in agreement and consistent with the 2.2×10^{-4} m^2/g best-estimate value given above. However, the initial geometric-specific surface area may differ from the specific surface area of the reacting fuel since it does not take into account open porosity in the fuel fragments, roughness on the outside surface of the fragments, and opening of grain boundaries (Section 6.2.2.3). The effects of oxidative dissolution reactions on the specific surface area of CSNF were examined by Gray and Wilson (1995 [DIRS 100758], Sections 4.1.1 and 4.2.3). These authors estimated the specific surface area of the corroding fuel fragments to be about 3.9×10^{-3} m^2/g (Gray and Wilson 1995 [DIRS 100758], Section 4.1.1, p 4.2.

The effective specific surface area for the fuel rod segment tests is about a factor of five lower than the geometric-specific surface area. However, the effective specific surface area estimated for fuel fragments in flow-through tests (i.e., 3.9×10^{-3} m^2/g) is about a factor of five higher than that estimated for fuel fragments in the drip tests (see corroborating section below). This result is reasonable because flow-through tests minimize the accumulation of surface alteration layers and maximize mass transport of dissolved oxygen to the grain-boundary surfaces. This would maximize the effective surface area of the fragments under the single-pass flow-through conditions and is not expected in the repository. The 3.9×10^{-3} m^2/g effective specific area estimate is, therefore, used as the upper end of the plausible range. Additional arguments, presented in the next section, corroborate use of the effective specific surface area from flow-through tests conducted on CSNF fragments for the upper end of the effective specific surface area range.

Based on the above discussion, the effective specific surface area of the corroding fuel is treated as an uncertain parameter with the uncertainty represented by a distribution spanning 3.9×10^{-3} to 4.7×10^{-5} m^2/g. The upper limit is based on Gray and Wilson's (1995 [DIRS 100758], Sections 4.1.1 and 4.2.3) estimate of specific surface area of corroding fuel (3.9×10^{-3} m^2/g). The best estimate is based on using the average specific surface area (2.2×10^{-4} m^2/g) calculated in Table 6-9 from the input geometric surface area data. The lower end of the uncertainty range is based on the average of the rod segment tests, 4.7×10^{-5} m^2/g (DTN: MO0301ANLSF001.450 [DIRS 162384]). Rounding to two significant figures, the recommendation for the distribution of log(A) is triangular with a low of -7.3, apex of -6.7, and max of -5.4 (where A is in units of m^2/mg).

6.4.1.6 Corroborating Data for Estimating CSNF Specific Surface Areas

As discussed in Section 6.2.2.3, the corroding fuel fragments show a total surface area (Figure 6-2) that may be significantly different from the geometric surface area. Preferential corrosion at grain boundaries, and effects of the "wormy" texture that has been observed in

corroded SNF samples could increase the specific surface area while protective effects of the fuel alteration phases that precipitate onto the corroding CSNF surface could reduce the effective specific surface area (Section 6.2.2.3). Because the effective specific surface of CSNF may evolve as the fuel rods degrade and the fuel corrodes (Section 6.2.2.1), it is important to corroborate use of the geometric-specific surface area estimates to represent the effective specific surface area of corroding CSNF.

Fractional radionuclide release rate data from the unsaturated fuel fragment tests described in Section 6.2.2.2 are shown in Table 6-11. These data were obtained from six long-term tests conducted on CSNF pellet fragments exposed to a variety of hydraulically unsaturated test conditions (Thomas 2003 [DIRS 163048]). Four tests were begun in September 1992; one high drip-rate test and one low drip-rate test on each of two fuels (approved testing material ATM-103 and ATM-106). The remaining two tests, begun in late 1998, are high drip-rate tests, conducted on high-burnup fuels (designated ATM-109A and ATM-109C). As described in Section 6.2.2.2, the test configuration was designed to allow the injected water to drip onto the fuel fragments and to drain through holes in the bottom of the fuel holder (Thomas 2003 [DIRS 163048], p. 16). This test configuration exposed the fuel fragments to transient water flow associated with each injection and maintained exposure of the fuel to conditions of 100 percent relative humidity between injections.

Table 6-11 provides the average fractional release rates data for the soluble radionuclides, ^{137}Cs, ^{97}Mo, ^{99}Tc, and ^{90}Sr from these test data. Data through the approximately 4.8-year sampling are associated with DTN: LL991001251021.090 [DIRS 129285]. These data are summarized from data package submission (CRWMS M&O 2000 [DIRS 131861]). The interval fractional release rate data for these four elements for the subsequent sampling periods through approximately 8.7 years are associated with DTN: MO0301ANLSF001.451 [DIRS 162383]. The source of these data is the data package submission (Thomas 2003 [DIRS 163048]). The Microsoft Excel spreadsheets used to calculate the average fractional release results shown in Table 6-11 from the input data sources are included in Appendix I, CSNF MR REV2.xls, Spreadsheets A4 and A5 and summarized in Spreadsheet A7.

The data compiled in Table 6-11 show that the average fractional release rates of the individual radionuclides vary considerably and the radionuclide average for the high drip-rate tests is higher than that for the low drip-rate tests. The fractional radionuclide release rate data in Table 6-11 were used to calculate the effective specific surface area of corroding CSNF (i.e., the modeling parameter A) (Appendix I, CSNF MR REV2.xls, Spreadsheet A8). The uncertainties associated with the use of these input data for this purpose are described below.

Table 6-11. Average Fractional Release Rates (d^{-1}) in the Fuel Fragment Tests

Test (fuel/type)	Data Period*	^{90}Sr	^{137}Cs	^{99}Tc	^{97}Mo	Radionuclide Average
ATM-103 HDR	1.3 to 8.7 years	2.85E-07	3.08E-06	1.29E-05	1.12E-05	6.87E-06
ATM-106 HDR	1.3 to 8.7 years	7.66E-07	5.33E-06	1.49E-05	9.44E-06	7.60E-06
ATM-109A HDR	1 to 3 years	7.21E-08	2.33E-06	4.66E-05	8.82E-05	3.43E-05
ATM-109C HDR	1 to 3 years	2.39E-07	3.00E-06	4.12E-07	1.16E-06	1.20E-06
HDR Average		**3.41E-07**	**3.43E-06**	**1.87E-05**	**2.75E-05**	**1.25E-05**
ATM-103 LDR	1.6 to 5.7 years	3.37E-06	6.94E-07	1.16E-06	4.98E-08	1.32E-06
ATM-106 LDR	1.6 to 7.3 years	2.50E-07	4.22E-07	4.62E-06	3.00E-07	1.40E-06
LDR Average		**1.81E-06**	**5.58E-07**	**2.89E-06**	**1.75E-07**	**1.36E-06**

Source: Calculated in Appendix I CSNF MR REV2.XLS, Sheets A4 and A5, and summarized in Sheet A7

NOTES: HDR = High Drip Rate (unsaturated testing); LDR = Low Drip Rate (unsaturated testing)
*duration indicates elapsed time-in-test included among sampling data.

The uncertainties in the test conditions for the unsaturated fuel fragment tests are described elsewhere (Thomas 2003 [DIRS 163048], pp. 50 and 51). The uncertainties are associated with the test design (principally how the injected water contacts the fuel in the fuel holder and uncertainties in the dissolved oxygen concentration in this water) and with planned and unplanned operational occurrences (principally due to reconfiguration of the experimental setup, removal of corroded fuel samples, loss of water from the test vessels, and inadvertent dropping of pieces of fuel into the leachate).

Estimates of the oxygen partial pressure (fugacity) in the unsaturated fuel fragment tests are described in *Unsaturated Testing of Bare Spent UO_2 Fuel Fragments* (Thomas 2003 [DIRS 163048], p. 51). At the outset of each test interval, the oxygen partial pressure was estimated to be approximately 0.24 atmospheres and decreases rapidly between 0.05 and 0.04 atmospheres and persisted throughout most of the test cycle. Although the uncertainties in these estimates of the oxygen partial pressure in the tests are not known, the available estimates indicate that the oxygen partial pressure may be somewhat lower than the approximate 0.06 atmospheres oxygen partial pressure expected in the repository for 100 percent relative humidity air at 90°C and significantly lower than 0.2 atmospheres oxygen partial pressure expected at ambient temperatures.

The effects of other planned and unplanned operational occurrences (specifically, reconfiguration of the experimental set up, removal of corroded fuel samples, and inadvertent dropping of pieces of fuel into the leachate) on the fractional release of soluble radionuclides are discussed in *Unsaturated Testing of Bare Spent UO_2 Fuel Fragments* (Thomas 2003 [DIRS 163048], pp. 40 to 44). The data show these types of occurrences correlate with spikes in the fractional release data in the subsequent sampling. The effects of the disturbance then subside over time with the observed release fractions returning to approximately the same values that were observed prior to the disturbance. Because the data include these spikes, this source of uncertainty in the measured fractional release rates is likely to cause them to be unrealistically high and therefore somewhat conservative. The following discussion uses the overall average fractional release rate from the HDR and LDR test results in Table 6-11 (6.93×10^{-6} d^{-1}) to estimate the effective specific surface area using Equation 14. Solving this equation for log(A)

gives the value of -6.34 (i.e., an effective specific surface area of 4.56×10^{-4} m^2/g of the corroding fuel in the tests). The Microsoft Excel spreadsheet used to perform these calculations is attached (Appendix I, CSNF MR REV2.xls, Spreadsheet A8).

This result is about a factor of two higher than the best estimate for the specific surface area provided above in Section 6.4.1.5 indicating that the grain-boundary penetration and the wormy texture of the corroding CSNF do not greatly increase the effective specific surface area of corroding CSNF. In addition, the long-term fractional radionuclide release data in DTNs: MO0301ANLSF001.451 [DIRS 162383] and LL991001251021.090 [DIRS 129285] show a generally decreasing trend with time indicating, despite the development of grain-boundary penetration and the wormy texture in the grains, these effects do not result in an increase in the effective specific surface area of the corroding fuel. These results are consistent with the observations discussed in Section 6.2.2.3, which indicate that the general corrosion mode accounts for most of the matrix dissolution. Much of the grain-boundary area does not contribute effectively to the oxidative dissolution process, probably due to dissolved oxygen depletion in the water that penetrates the grain-boundary openings. This evidence indicates that effective surface areas much greater than the fragment's geometric surface areas are not likely in the repository. In particular, the $0.1 m^2/g$ specific surface area for individual fuel grains from Gray and Wilson (1995 [DIRS 100758], Section 4.1.1) is ruled out.

6.4.1.7 Summary of Model Input Data Uncertainties

Table 6-12 summarizes model input data and associated types of uncertainty.

6.4.2 Alternative Conceptual Models

Direct disposal of spent UO_2 nuclear fuel is being considered in geologic disposal programs being conducted by several countries other than the United States (Grambow et al. 2000 [DIRS 162391]; Johnson et al. 1996 [DIRS 162372]; Dehaudt 2001 [DIRS 164019]; Dehaudt 2001 [DIRS 164037]; Jegou et al. 2001 [DIRS 162397]; Pelletier 2001 [DIRS 164034]; Piron 2001 [DIRS 162396]). The models that have been developed in these programs to predict the long-term performance of the SNF are reviewed here to identify possible alternative conceptual models for CSNF corrosion in the repository.

Table 6-12. Summary of CSNF Waste Form Degradation Analysis Inputs

Input Name	Input Description	Input Source (DTN)	Value or Distribution	Type of Uncertainty
Gap/Grain Boundary Inventory	Data for the fraction (%) of the inventory of ^{137}Cs, ^{129}I, ^{99}Tc, and ^{90}Sr in the Gap and Grain-Boundary Regions of CSNF	MO0407SEPGGBID.000 [DIRS 170619]	Table 6-3	Mostly Aleatory (discussion in Section 6.3.1)
Average Radionuclide Release Rates	Data for fractional release rates of ^{137}Cs, ^{129}I, ^{99}Tc, and ^{90}Sr from CSNF rod segment tests	MO0301ANLSF001.450 [DIRS 162384]	Table 6-10	Aleatory and Epistemic (discussion in Section 6.4.1.4)
Flow-through Test Data	Data for the specific dissolution rate of CSNF and UO_2 as a function of pH, T, $[O_2]$, and $[HCO_3^-]$	MO0302PNLDUFTD.000 [DIRS 162385] MO0407SEPUDISR.000 [DIRS 170618] MO0304PNLLPHDD.000 [DIRS 163441]	Section 6.4.1	Epistemic (discussion in Section 6.4.1.1)
Surface areas for HBR and TP fuels	Estimated geometric-specific surface areas (cm^2/g) and estimated effective specific surface area of corroding CSNF	Wilson 1990 [DIRS 100793], Appendix E Barner 1985 [DIRS 109194], Tables 4.6 and 4.1 Gray and Wilson 1995 [DIRS 100758], Section 4.1.1, p 4.2	Table 6-9 And input value of 3.9×10^{-3} (m^2/g) for the effective specific surface area of corroding fuel	Aleatory (discussed in Section 6.4.1.4)

The long-term exposure scenarios for spent UO_2 nuclear fuel in repository development programs outside the United States generally involve contact by reducing groundwater. As a consequence, many of the models that have been developed internationally are based on modeling how the production, depletion and mass transport processes of oxidizing agents (e.g., dissolved O_2 and radiolysis products including H_2O_2 and radicals) limit their availability to support oxidative dissolution of the fuel. These modeling approaches are not applicable to Yucca Mountain because the rate of oxidative dissolution of CSNF in the repository will be limited by the kinetics of the oxidative dissolution process rather than by the availability of oxidizing agents. This is based on the fact that dissolved oxygen will be the principal oxidizing agent in the repository and an ample supply of atmospheric oxygen is expected to maintain the oxygen fugacity at or near 0.2 atmospheres in the repository void spaces (Section 6.2.2.3). Under these conditions, the rate of oxidative dissolution will be limited by the rate of the chemical reactions involved in the oxidative dissolution process. Exposure to humid air and air-saturated groundwater conditions have been considered in several international programs for evaluating fuel storage and possible exposure of the fuel in containers with early-life failures to oxidizing groundwaters.

The available experimental evidence from international studies shows that the overall oxidative dissolution process for UO_2 involves a complex set of adsorption, redox, surface complexation, and desorption reaction steps. Two important modeling approaches have been developed based on the kinetics of the redox reactions (electrochemical model) and the rates of surface complexation reactions (surface complexation model).

6.4.2.1 Electrochemical Model

The electrochemical approach for modeling the rate of the oxidative dissolution of unirradiated UO_2 and SNF is based on modeling the rates of the redox reactions involved in the fuel oxidation and dissolution (Shoesmith 2000 [DIRS 162405]; Johnson et al. 1996 [DIRS 162372]; Grambow et al. 2000 [DIRS 162391]; Dehaudt 2001 [DIRS 164019]; Dehaudt 2001 [DIRS 164037]; Jegou et al. 2001 [DIRS 162397]; Pelletier 2001 [DIRS 164034]; Piron 2001 [DIRS 162396]). For these reactions, the key variable is the corrosion potential and, as discussed below, is determined largely by the concentrations of oxidizing agents (e.g., dissolved O_2 and radiolysis products including H_2O_2 and radicals) at the fuel–solution interface.

An overall understanding of how the state of the corroding UO_2 fuel surfaces varies with the surface potential (a measure of the strength of the oxidizing conditions) and other water chemistry conditions were developed (Shoesmith 2000 [DIRS 162405]). For the surface potential regimes (greater than -100 mV saturated calomel electrode) of interest for the repository, the surface state can be described as follows:

1. In the potential (E) range -100 mV < E <+300 mV, saturated calomel electrode oxidation, dissolution, and accumulation of corrosion products on the surface occur with the balance between these processes depending on the local pH and solution composition as follows:

    A. In noncomplexing neutral and alkaline solutions, a layer of $UO_{2.33}$ forms at the surface and inhibits the fuel dissolution rate

    B. In solutions with pH ≤ 5, an observable surface $UO_{2.33}$ layer does not form and dissolution is rapid

    C. In neutral and alkaline solutions containing sufficient carbonate–bicarbonate ($\geq 10^{-3}$ mol/L), a surface layer of $UO_{2.33}$ does not form and dissolution is accelerated

    D. Calcium- and silicon-containing groundwaters enhance the formation of protective surface layers; low pH overrides this effect.

2. In the potential range above +300 mV, saturated calomel electrode rapid dissolution occurs and the associated hydrolysis of the released uranyl ions can lead to local pH decrease at the corroding surface.

Under neutral and basic conditions, the initial rate of surface oxidation is greater than the rate of dissolution of the oxidized surface layer resulting in the growth of the surface layer until a steady state is established in which the rate of growth matches the rate of dissolution. Under acidic and complexing conditions, the rate of dissolution is greater than the rate of oxidation resulting in the dissolution of the oxidized surface layer as it is formed.

When exposed to aqueous solutions, the potential of corroding UO_2 fuel will float to the potential (referred to as the corrosion potential E_{corr}), at which the anodic dissolution current is equal to the cathodic current at the corroding fuel–water interface. Because the corrosion rate is related to

the anodic dissolution current using Faraday's Law, the corrosion rate can be determined from the corrosion current (I_{corr}) as follows:

$$\frac{W}{t} = \frac{I_{corr} A_w}{nF} \qquad \text{(Eq. 15)}$$

where

W = Mass loss (g)
A_w = Molecular weight of UO_2
n = Number of electrons involved
F = Faraday constant
t = Duration of the corrosion period

The anodic corrosion current density I_A (i.e., the corrosion current per unit area; $I_{corr} = A\ I_A$ where A is the corroding surface area) is given by the following equation (Shoesmith and Sunder 1991 [DIRS 113366], p. 9):

$$I_A = k_{UO2}\, N\, [X]^m [Y]^P \exp(bE) \qquad \text{(Eq. 16)}$$

where

k_{UO2}	=	heterogeneous rate constant for oxidative dissolution
N	=	parameter that accounts for the UO_2 fuel reactivity
[X] and [Y]	=	concentrations of species X and Y (e.g., H^+ and HCO_3^-)
m and p	=	parameters that express the reaction orders for species X and Y
E	=	the potential
b	=	parameter that expresses the dependence of the rate on potential (referred to as the Tafel line slope, which is the slope of log I_A versus E plot)

Similar expressions can be developed for the cathodic current densities associated with reduction of various oxidants (e.g., dissolved O_2 and radiolysis products including H_2O_2 and radicals) (Shoesmith and Sunder 1991 [DIRS 113366], Section 3.3). Since the anodic and cathodic current densities are equal at $E = E_{corr}$, the expressions for the anodic and cathodic current densities could, in principle, be combined to give an expression for the corrosion potential and the corresponding corrosion current (dissolution rate) as a function of the parameters that control dissolution. However, because the expressions for the anodic and cathodic current densities are incompletely developed, a semi-empirical modeling approach has been developed based on the log I_A versus E relationships (Tafel plots) for anodic dissolution in repository-relevant solutions (Shoesmith 2000 [DIRS 162405]; Shoesmith and Sunder 1991 [DIRS 113366]; Shoesmith and Sunder 1992 [DIRS 113368]). The approach is based on the following three steps:

1. Measure the anodic corrosion current as a function of applied potential to determine the Tafel lines (i.e., the log of the current density versus applied potential) for repository-relevant water chemistry conditions

2. Measure the corrosion potential (E_{corr}) for repository relevant water chemistry conditions

3. Extrapolate the Tafel lines (determined in Step 1) to the corrosion potentials (determined in Step 2) to obtain the current density (and, hence, the corrosion rate) corresponding to the corrosion potentials measured in Step 2.

The following information is necessary to implement this approach:

1. Equations for the anodic dissolution Tafel lines under repository-relevant water chemistry conditions

2. Corrosion potential (E_{corr}) for repository relevant water chemistry conditions.

Extensive studies have been conducted in Canada (summarized in Shoesmith 2000 [DIRS 162405]) and in Europe (Grambow et al. 2000 [DIRS 162391]; Christensen and Sunder 2000 [DIRS 162387]) to determine the relationships between anodic corrosion current and applied potential for UO_2 and SNF under a broad range of water chemistry conditions. As discussed by Shoesmith (2000 [DIRS 162405]), the log current–potential relationships are sensitive to the carbonate–bicarbonate concentration. Carbonate concentration affects the shape of log current–potential relationships (and the Tafel line slopes) indicating that the mechanistic effects of carbonate are complex (Shoesmith 2000 [DIRS 162405], Figure 12). Even low carbonate concentrations (5 mmol l^{-1}) increase the corrosion current density for a given applied potential by more than two orders of magnitude when compared to noncomplexing solutions. Other groundwater species are known to increase or decrease the corrosion rate at a given potential depending on how they influence the dissolution of the UO_{2+x} surface layers (Shoesmith 2000 [DIRS 162405]). The corrosion rate increases dramatically with increasing hydrogen ion concentration [H^+] (decreasing pH) because the proton-mediated transfer of U(VI) species to solution is rapid. It is sufficiently rapid to prevent incorporation of O^{2-} into the UO_2 and the consequent formation of a detectable UO_{2+x} surface layer (Shoesmith 2000 [DIRS 162405], Section 3.1.2). On the other hand, calcium and silicon ions can decrease the corrosion rate by forming surface layers resistant to dissolution. When carbonate is present, it counterbalances the effects of Ca^{2+} and Si^{4+} (Shoesmith 2000 [DIRS 162405]). Despite the effects discussed above, it has been shown that a single log corrosion rate–potential relationship can be used for a variety of water chemistries (Grambow et al. 2000 [DIRS 162391], Figure I.6-32). The relationship between the corrosion rate and the corrosion potential for noncomplexing solutions is given by the following expression (Christensen and Sunder 2000 [DIRS 162387] Equation 6):

$$CR = 78 \times 10^{(-4.4+16E_{corr})} \qquad \text{(Eq. 17)}$$

where

CR = corrosion rate (μg cm^{-2} day^{-1})
E_{corr} = steady-state corrosion potential (volts saturated calomel electrode)

The effects of carbonate–bicarbonate concentrations on this relationship can be estimated approximately from the available data (Shoesmith 2000 [DIRS 162405], Figure 12). The steady state corrosion potential in air-saturated aqueous solutions is not sensitive to nonoxidizing aqueous species such as [HCO_3^-] (Shoesmith et al. 1989 [DIRS 162402]). However, it is influenced by the concentrations of oxidizing species (e.g., [O_2], [H_2O_2], and [radiolytic radicals]) that contribute to the cathodic reaction current (Shoesmith 2000 [DIRS 162405];

Christensen and Sunder 2000 [DIRS 162387]). The corrosion potentials appropriate for the repository conditions can be estimated approximately from the available literature data. The most direct approach is to use measured corrosion potential (E_{corr}) data for air-saturated water exposed to radiation field conditions (alpha, beta, and gamma) relevant to fuel corrosion in the repository (Shoesmith 2000 [DIRS 162405]; Christensen and Sunder 2000 [DIRS 162387]). An electrogeochemical modeling approach for estimating E_{corr} has been described by Grambow et al. (2000 [DIRS 162391], pp. 193 and 194). This approach involves calculating the location of the corrosion potential between the equilibrium potential for UO_2 dissolution and Eh of air-saturated water. Because the anodic and cathodic corrosion current-versus-potential relationships within this range are not known for Yucca Mountain conditions, the corrosion potential cannot be calculated precisely. However, published dissolution rate expressions based on the electrochemical modeling approach outlined above can be used. For example, the bicarbonate dependence of the oxidative dissolution rate at 25°C in air-saturated water can be expressed as (Shoesmith et al. 1998 [DIRS 162404], Figure 2; Shoesmith 2000 [DIRS 162405], Figure 30):

$$DR = 128 \times [HCO_3^-]^{0.38} \qquad \text{(Eq. 18)}$$

where

DR = dissolution rate (mg/m^2d)
$[HCO_3^-]$ = Bicarbonate concentration (mol/L)

This expression is used to estimate the CSNF oxidative dissolution rate based on the electrochemical model in Section 7.2.

6.4.2.2 Surface Complexation Model

A surface complexation model has been developed to predict the dissolution rates of unirradiated UO_2 and SNF based on a three-step bicarbonate-promoted oxidative dissolution mechanism (de Pablo et al. 1999 [DIRS 162388]). The three steps are: 1) initial oxidation of the UO_2 surface; 2) binding of bicarbonate ions at the U(VI) sites of the oxidized layer; and 3) detachment of the U(VI) –carbonate surface complex. The reactions and associated rate constants for these steps are found in Equations 19 through 20. Note that the notation used in the paper by de Pablo et al. (1999 [DIRS 162388]) is used here to show the surface reactions:

Step 1. Oxidation of the solid surface:

$$> UO_2 + \tfrac{1}{2} O_2 \underset{k_{-1}}{\overset{k_1}{\leftrightarrow}} > UO_3 \qquad \text{(Eq. 19)}$$

Step 2. Complexation of U(VI) by the HCO_3^-:

$$> UO_3 + HCO_3^- \xrightarrow{k_2} > UO_3 — HCO_3^- \qquad \text{(Eq. 20)}$$

Step 3. Dissolution (desorption) of the carbonate species created (considered to be rapid):

$$> UO_3 — HCO_3^- \xrightarrow{k_3} U(VI)_{aq} \qquad \text{(Eq. 21)}$$

This three-step mechanism has led to the following equation for the rate of dissolution (de Pablo et al. 1999 [DIRS 162388]):

$$r = \frac{k_1 k_2 \{>UO_2\}_{tot} [O_2][HCO_3^-]}{k_{-1} + k_1[O_2] + k_2[HCO_3^-]} \quad \text{(Eq. 22)}$$

where

r	= Dissolution rate (mol m^{-2} s^{-1}),
k_1, k_{-1}, and k_2	= Rate constants for the first two reaction steps
$\{>UO_2\}$	= Density of surface sites (10^{-6} mol m^{-2})
$[O_2]$	= Dissolved oxygen concentration (mol/L)
$[HCO_3^-]$	= Bicarbonate concentration (mol/L)

The above model has four parameters (k_1, k_{-1}, k_2, and $\{>UO_2\}$) and two independent variables. The value of the $\{>UO_2\}$ parameter (10^{-6} mol m^{-2}) is based on the average site density in various oxides. Values for the model parameters k_1, k_{-1}, and k_2 are determined by regression analysis of a set of UO_2 dissolution rate data spanning a matrix of test conditions. The values are temperature dependent and the values determined at 10°C, 25°C, 45°C, and 60°C are tabulated in Table 4 of "The Oxidative Dissolution Mechanism of Uranium Dioxide. I. The Effect of Temperature in Hydrogen Carbonate Medium" (de Pablo et al. 1999 [DIRS 162388]).

Because this model is semi-empirical, its application is limited to the range of the experimental data from which the model parameters are derived (i.e., fO_2 = 0.2 atmospheres; pH > 7; 10 < T(°C) < 60; 0.1 mmol/L< $[HCO_3^-]$ < 50 mmol/L). Also, because the database from which the model parameters are derived is limited to tests conducted with unirradiated UO_2, it is not appropriate to incorporate this model into the TSPA-LA model. It will be used for validation of the base-case model in accordance with Section 5.4.1 of AP-SIII.10Q, *Models*.

6.4.2.3 Alternative Conceptual Model Screening

The electrochemical and the surface complexation models are screened out for the TSPA-LA model. This is because the data that would support their application can only be estimated approximately for repository conditions. However, these models provide mechanistic insight and, in turn, provide confidence in long-term predictions. By comparing them to the base-case model, they provide a basis for discussing the validity of the base-case model's use for long-term extrapolations (Section 7 addresses model validation in accordance with AP-SIII.10Q, Section 5.4.1 c) 2) "corroboration of results with alternative mathematical models"). The alternative conceptual models discussed above are more mechanistically based than the empirical approach used in the base-case model for CSNF corrosion in the repository. However, because the base-case approach spans the range of conditions expected, it provides the best available approach to estimating the rate of CSNF corrosion. Comparison of the base-case model with the mechanistically based alternative models provides confidence that the empirically based modeling approach is indeed appropriate for use in long-term predictions. Such comparisons of these models with some of the data used in development of the Yucca Mountain model have already been published (Shoesmith 2000 [DIRS 162405]; Shoesmith et al. 1998 [DIRS 162404]; de Pablo et al. 1999 [DIRS 162388]).

The alternative conceptual models considered above are summarized in Table 6-13.

Table 6-13. Alternative Conceptual Models Considered

Alternative Conceptual Models	Key Assumptions	Screening Assessment and Basis
Electrochemical	The anodic Tafel lines can be extrapolated to the corrosion potential. The long-term corrosion behavior of SNF is similar to that of unirradiated UO_2. Differences between the corrosion behavior of SNF and unirradiated UO_2 are due to water radiolysis.	Do not incorporate into the TSPA-LA model; data necessary to apply the model can only be estimated approximately. Use for base-case model validation, particularly for validation of long-term extrapolation.
Surface Complexation Model	The overall rate of CSNF corrosion is controlled by the rate of surface complexation reactions. The long-term corrosion behavior of spent is similar to that of unirradiated UO_2.	Do not incorporate into the TSPA-LA model; data necessary to apply the model can only be estimated approximately from open literature. Use for base-case model validation, particularly for validation of long-term extrapolation.

6.4.3 Description of Barrier Capability

The barrier function of the CSNF waste form is to limit mobilization of radionuclides. The capability of the CSNF to perform this barrier function is indicated by the degradation rates and the range of time to complete degradation.

The model developed here shows that the degradation rate of CSNF with breached cladding will depend on the temperature, oxygen fugacity, dissolved carbonate, and pH conditions to which it is exposed in the repository. The expected time trajectories of each of these independent variables will be considered in the TSPA-LA model estimates of the CSNF degradation rates and lifetimes in the repository.

7. VALIDATION

The purpose of the CSNF waste form degradation modeling effort is to develop models that can be used to calculate the rate of release of radionuclides from CSNF after the cladding is breached in the repository. The developed models include an instantaneous release fraction model (for modeling release of the combined gap and grain-boundary inventories) and models for the matrix inventory release under alkaline and acidic conditions. Validation of these models involves presenting technical evidence that these models predict the CSNF degradation rate and the associated radionuclide release rates at an adequate level of confidence.

Sensitivity analyses (BSC 2003 [DIRS 168796]) indicate that estimated dose at the regulatory compliance point is not sensitive to the CSNF model. Consequently, as stated in Table 2-1 of *Technical Work Plan for: Regulatory Integration Modeling and Analysis of the Waste Form and Waste Package* (BSC 2004 [DIRS 169944]), Level 1 model validation is specified for the CSNF models.

Confidence-Building During Model Development to Establish Scientific Basis and Accuracy for Intended Use—Section 2.2.1 of *Technical Work Plan for: Regulatory Integration Modeling and Analyses of the Waste Form and Waste Package* (BSC 2004 [DIRS 169944]) specifies the following steps for *Confidence Building During Model Development*: The model will contain documentation of decisions and activities implemented during the model development process to build confidence and verify a reasonable and credible technical approach using scientific and engineering principles. The development of the model should be documented in accordance with the requirements of Section 5.3.2(b) of AP-SIII.10Q. The development of the CSNF waste form degradation model was conducted according to the following criteria:

> *(1) Selection of input parameters and/or input data, and a discussion of how the selection process builds confidence in the model.* (AP-SIII.10Q 5.3.2(b)(1); AP-2.27Q, Attachment 3, Level I (a))

The bases for selecting the input data used to determine and develop the CSNF waste form model are documented Section 4.1. Additional bases and discussions regarding the selection and appropriateness of the data in Tables 4-5 and 4-6 are documented in Appendix V. Model assumptions have been described in Section 5. Detailed discussion about model concepts can be found in Section 6.2.1 and 6.2.2. Thus, this requirement can be considered satisfied.

> *(2) Description of calibration activities, and/or initial boundary condition runs, and/or run convergences, simulation conditions set up to span the range of intended use and avoid inconsistent outputs, and a discussion of how the activity or activities build confidence in the model. Inclusion of a discussion of impacts of any non-convergence runs.* ((AP-SIII.10Q 5.3.2(b)(2); AP-2.27Q, Attachment 3, Level I (e)).

Detailed discussion of the CSNF initial state (microstructure, physicochemical condition, and distribution of fission products and actinide elements) is discussed in 6.2.1.1. Model formulations for the CSNF degradation and radionuclide release rates under alkaline and acidic conditions are discussed in Sections 6.3.1, 6.3.2, 6.4.1.2, and 6.4.1.3. The CSNF degradation and radionuclide release modes span the range of intended use conditions for each of the factors (i.e.,

temperature, pH, dissolved oxygen concentration, and carbonate concentration) that influence the rates of the important CSNF degradation and radionuclide release processes. Thus, this requirement can also be considered satisfied.

> *(3) Discussion of the impacts of uncertainties to the model results including how the model results represent the range of possible outcomes consistent with important uncertainties.* ((AP-SIII.10Q 5.3.2(b)(3); AP-2.27Q, Attachment 3, Level 1 (d) and (f)).

Uncertainties associated with the data used to determine the model's parameter values are discussed in Sections 6.3.1 and 6.4.1.1. Regression analyses are documented in Sections 6.4.1.2 and 6.4.1.3, which discuss alkaline and acidic conditions to address the range of possible outcomes consistent with important uncertainties. Additional discussion of uncertainties related to scaling the model is in Section 6.4.1.4. A summary discussion on uncertainties and their impact is given in Section 8.2.

> *(4) Formulation of defensible assumptions and simplifications.* (AP-2.27Q, Attachment 3, Level I (b)).

Discussion of assumptions and simplifications and their rationale are provided in Section 5 and Section 6.2.

> *(5) Consistency with physical principles, such as conservation of mass, energy, and momentum.* (AP-2.27Q, Attachment 3, Level I (c)).

Sections 6.2.2.2 and 6.2.2.3 provide a summary of the pertinent physical phenomena and chemical reactions associated with the oxidation and oxidative dissolution process that occur when CSNF is exposed to air-saturated groundwater and humid air. The content of these sections specifically addresses pertinent observations on how CSNF corrodes as a result of oxidative dissolution under humid air and infiltrating groundwater conditions relevant to the repository and the factors that influence the process rate.

Confidence-Building After Model Development to Support the Scientific Basis of the Model—The specific validation activities to be applied to the CSNF model after model development are identified in the technical work plan (BSC 2004 [DIRS 169944], Table 2-1).

> *(1) Corroboration of model results with data acquired from the laboratory, field experiments, analog studies, or other relevant observations, not previously used to develop or calibrate the model.* (AP-SIII.10Q, Section 5.3.2).

> *(3) Corroboration with information published in refereed journals or literature* (AP-SIII.10Q, Section 5.3.2).

Confidence in the accuracy of the models is addressed by evaluating the consistency of the models with data from laboratory tests not used to develop the models and data published in refereed journals or industrial literature (Section 7.1). Section 7.1.2 establishes confidence in the developed instantaneous radionuclide release model by comparing the model to available project

data not used in model development. Section 7.1.3 establishes confidence in the developed models for radionuclide release from the CSNF matrix under alkaline and acidic conditions by:

- Comparing model-calculated radionuclide fractional release rates with experimental rates published in peer-reviewed or industrial literature for alkaline and acidic conditions
- Comparing model-calculated specific dissolution rate of the UO_2 fuel matrix to experimental rates in peer-reviewed or industrial literature for alkaline and acidic conditions.

In addition, comparison of experimental data with natural analogue studies is addressed in Section 7.3 to provide confidence that the results observed in laboratory tests are likely to occur in an actual repository setting.

2) Corroboration of results with alternative mathematical models (AP-SIII.10Q, Section 5.3.2).

Section 7.2 describes the comparison of the developed model for the specific dissolution rate of the CSNF matrix with alternative mathematical models. In this section, confidence in the model is established by comparing the specific dissolution rates calculated by the developed model applicable to alkaline conditions to the rates calculated by the alternative mathematical models for a set of nominal exposure conditions. This section also establishes confidence in the model by comparing the model parameters to the "reaction order," (i.e., exponents of a power law dependence) reported in the literature.

The criteria specified in Table 2-1 of *Technical Work Plan for: Regulatory Integration Modeling and Analysis of the Waste Form and Waste Package* (BSC 2004 [DIRS 169944]) for evaluating consistency between the CSNF models and the experimental data or modeling results with which they are to be compared in each of these validation activities are "corroborating data must match qualitatively and must be bounded by model predictions." As discussed in Section 2.2.5 of *Technical Work Plan for: Regulatory Integration Modeling and Analysis of the Waste Form and Waste Package* (BSC 2004 [DIRS 169944]), corroboration for Level 1 validation is indicated by agreement within one to two orders of magnitude.

Sections 7.1.2 and 7.2 use an "error metric" (EM) to compare the CSNF matrix models to the validation data and to alternative mathematical models. This is the ratio of the base 10 log of the model-calculated rate to the base 10 log of the rates in the data sets used for validation. The range of values for EM expected to result from such comparisons can be assessed by considering estimates of the standard errors in the modeling and the data sets to which the models are compared. As shown in the footnote to Table 6-4, the "standard error of estimate" (i.e., an estimate of the modeling error) from the regression analysis of the alkaline-side data is 0.347. The corresponding 2σ error is 0.694 or 0.7 when rounded to one significant figure. Only approximate estimates are available for the errors in the validation data. As discussed in Section 6.4.1.1, the range of variability in the nominally comparable worldwide data is ±10 (i.e., an approximate order of magnitude). The corresponding range for the base-ten log of the dissolution rate data is 0 ±1. Propagating these errors (using the square root of the sum of the squares error propagation rule) to estimate the error in EM, results in ±1.2 as the expected range

of values for EM. Hence, agreement between the model and the validation data is indicated by a value of the EM in the range 0±1.2. Positive values for the EM within this range indicate a conservative modeling bias.

The data and alternative model sources used for validation are listed in Table 7-1.

Table 7-1. Data and Alternative Model Sources Used for Validation

Data/Alternative Model	Data Source	Validation Use
Instantaneous fractional release rate data from rod segment tests (DTN: MO0301ANLSF001.450 [DIRS 162384])	Goldberg 2003 [DIRS 162410]	Validate instantaneous fractional release model for gap and grain-boundary inventories.
CSNF radionuclide fractional release rate data in Table 7-2, Table 7-3, and Table 7-5 (alkaline conditions) and Table 7-6	Wilson 1990 [DIRS 100793], Test Series 3	Validate base-case model for radionuclide fractional release rate – alkaline conditions
CSNF radionuclide fractional release rate data in Table 7-7 – alkaline conditions	Forsyth 1997 [DIRS 123134]	
CSNF radionuclide fractional release rate data in Table 7-8 – acidic conditions	Forsyth 1997 [DIRS 123134]	Validate base-case model for radionuclide fractional release rate – acidic conditions
Exponent for CSNF corrosion rate dependence on pH under acidic conditions	Röllin et al. 2001 [DIRS 162398]	Comparison of the acid-side model's pH dependence to literature data
UO_2 dissolution rate per unit area data in Table 7-9 – alkaline conditions	Tait and Luht 1997 [DIRS 114435]	Validate base-case model for the specific rate of oxidative dissolution of the fuel matrix – alkaline conditions
UO_2 dissolution rate per unit area data in Table 7-10 – alkaline conditions	de Pablo et al. 1999 [DIRS 162388]	
UO_2 dissolution rate per unit area data in Table 7-11 – acidic conditions	Torrero et al.1997 [DIRS 114439]	Validate base-case model for the specific rate of oxidative dissolution of the fuel matrix – acidic conditions
Alternative electrochemical model – Eq. 20	Shoesmith 2000 [DIRS 162405]	Validate base-case model for the specific rate of oxidative dissolution of the fuel matrix – alkaline conditions
Alternative surface complexation model – Eq. 24	de Pablo et al. 1999 [DIRS 162388]	

7.1 COMPARISON OF BASE-CASE MODEL TO EXPERIMENTAL DATA

7.1.1 Comparison of the Instantaneous Release Model to CSNF Instantaneous Release Data

Instantaneous fractional release rates of ^{137}Cs, ^{129}I, ^{90}Sr, and ^{99}Tc from CSNF rod segment tests are shown in Table 7-2. The CSNF rod segment tests are described in Section 4.1.3. The instantaneous release fraction data from fuel rod segments are compared to the instantaneous fractional release model for the gap and grain-boundary inventories in Table 7-3. Note that although the fractional release rate data from these tests were used to estimate the lower end of the range for the effective specific surface area of corroding CSNF (Section 6.4.1.5), the instantaneous fractional release data were not used for model development and are, therefore, appropriate for use in validation. The first three rows in the table show the instantaneous release fraction data (Goldberg 2003 [DIRS 162410], Tables 6, 7, 8, and 9). For comparison, the model's average release fractions and the ranges used for the uncertainty distributions are shown in rows four and five of Table 7-3.

The data summarized in Table 7-3 show that the instantaneous release fractions measured in the fuel rod segment tests are within the instantaneous release model's uncertainty range for cesium and technetium and lower than the model's range for iodine and strontium. Table 7-2 is the source for the data in the first three rows of Table 7-3. A qualitative comparison of the model's uncertainty distribution range in Table 7-3 to worldwide data on instantaneous release fractions (Jegou et al. 2001 [DIRS 162397], Section 8.2.2.4 and Table 27) also shows that the model gives generally conservative results. These worldwide data for light water reactor fuel are summarized in Table 7-4. In this table, the $t_{cumulative}$(d) column shows the test time in days. Examination of these results shows that they are generally consistent with the applicable validation criterion that the model must match the validation data qualitatively. A conspicuous exception is that some of the ^{90}Sr and ^{99}Tc data from the longer-term results shown in Table 7-4 are significantly higher than the upper end of the model's distribution range. This is probably because these experimental results are influenced by corrosion of the fuel matrix. In general, this comparison indicates that the model provides a reasonably conservative representation of the instantaneous release fractions when compared to the available instantaneous release fraction data.

Table 7-2. Instantaneous Fractional Release - Rod Segment Tests

Fuel	^{137}Cs	^{129}I	^{90}Sr	^{99}Tc
ATM-103, 1.5"	4.81E-3	6.002E-3	4.01E-5	7.40E-5
ATM-103, 2.6"	4.68E-3	1.34E-3	9.16E-5	2.21E-5
ATM-103, 3.7"	5.22E-3	7.02E-3	3.89E-5	2.83E-5
Average ATM-103	4.84E-3	4.79E-3	5.69E-5	4.15E-5
ATM-106, 1.4"	7.18E-2	1.18E-2	1.51E-5	1.68E-4
ATM-109, 3.2"	4.36E-2	1.52E-2	ND	4.95E-6

Source: DTN: MO0301ANLSF001.450 [DIRS 162384]

NOTE: ND = Concentration not determined in test solution; ATM = Approved Testing Material

Table 7-3. Comparison of Instantaneous Release Fraction Data from Rod Segment Tests to Model Distribution Ranges for the Gap and Grain-Boundary Inventories

	Release Fraction (%)			
Fuel Type	^{137}Cs	^{129}I	^{90}Sr	^{99}Tc
ATM-103[a]	0.48	0.48	0.006	0.004
ATM-106[a]	7.18	1.18	0.002	0.017
ATM-109[a]	4.36	1.52	ND	0.0005
Model's Average Release Fraction (from Table 6-3)	3.63	11.24	0.09	0.06
Model's Uncertainty Distribution Range (from Table 6-3)	0.39 to 11.06	2.04 to 26.75	0.02 to 0.25	0.00 to 0.26

NOTE: [a] Table 7-2 is the source of the data in these rows.

Table 7-4. Literature Data - Combined Gap and Grain-Boundary Inventories

Burnup, GWd/t	FG (%)	$t_{cumulative}$ (d)	Percent of Inventory in Fuel			
			^{137}Cs (%)	^{129}I (%)	^{90}Sr (%)	^{99}Tc (%)
22	0.14	3	0.13	<5.41	9.74×10^{-3}	$<4.08 \times 10^{-2}$
		62	0.27	—	3.23×10^{-2}	<0.17
37	0.23	3	0.48	<3.09	1.70×10^{-2}	2.87×10^{-2}
		62	0.62	—	2.97×10^{-2}	<0.1
47	0.41	3	1.51	<2.41	6.96×10^{-2}	$<1.93 \times 10^{-2}$
		62	2.22	—	0.14	$<7.76 \times 10^{-2}$
62.8	2.59	3	0.33	<0.09	8.72×10^{-3}	$<4.03 \times 10^{-2}$
		62	0.93	—	3.48×10^{-2}	<0.22
62.8	2.59	2	0.37	<0.26	4.98×10^{-3}	—
		23	1.69	<2.54	1.07×10^{-2}	—
47	0.41	2	0.93	—	0.8	0.12
		97	3.5	—	2.8	0.54
62.8	2.59	1	0.53	—	2.70×10^{-2}	$<5.3 \times 10^{-2}$
		140	0.83	—	0.13	0.24
30	—	315	0.3	0.03	6×10^{-3}	—
50	—	315	0.3 to 1	0.1	6×10^{-3}	—
50.4	—	31	1.40 to 1.71	—	0.0843 to 0.311	$<6.68 \times 10^{-3}$ to 6.89×10^{-3}
		76	1.97 to 2.18	—	0.11 to 0.335	$<6.89 \times 10^{-3}$ to $<1.34 \times 10^{-2}$
		513 to 750	2.85 to 3.06	—	0.212 to 0.382	$<8.04 \times 10^{-3}$ to 4.06×10^{-2}
50.4	—	30 to 32	0.95 to 1.06	—	0.0211 to 0.0362	$<6.51 \times 10^{-3}$ to $<7.02 \times 10^{-3}$
		71 to 74	1.15 to 1.63	—	0.0241 to 0.0436	$<6.59 \times 10^{-3}$ to $<7.02 \times 10^{-3}$
		511 to 752	2.59 to 3.89	—	0.0456 to 0.0599	$<6.51 \times 10^{-3}$ to $<4.70 \times 10^{-2}$
50.4	—	63	3.48	—	0.25	1.27×10^{-4}
		173	3.66	—	0.27	$<3.65 \times 10^{-4}$
50.4	—	33	1.22	—	0.28	6.12
		76	1.34	—	0.3	>6.12
		516	2.55	—	0.66	>6.12
50.4	—	0.014	2.71	—	6.43×10^{-2}	$<2.59 \times 10^{-3}$
		40	2.85	—	9.16×10^{-2}	—
		449 to 657	4.73 to 6.71	—	0.89 to 1.23	0.12 to 0.22

Source: Jegou et al. 2001 [DIRS 162397], Table 27; the CANDU and MOX data in this source are not used here because they are not directly applicable.

7.1.2 Validation of CSNF Matrix Radionuclide Release Models for Alkaline and Acidic Conditions

Two sets of published literature data on the fractional release rates of radionuclides measured under air-saturated dissolution conditions are used in this assessment. First, the developed model for alkaline conditions is compared to the Nevada Nuclear Waste Storage Investigations (NNWSI) Series 3 batch test data (Wilson 1990 [DIRS 100793]). Then the developed models for alkaline and acidic conditions are compared to the extensive CSNF test results published by the Swedish SNF corrosion program (Forsyth 1997 [DIRS 123134]; Röllin et al. 2001 [DIRS 162398]).

To facilitate comparison of the fractional release rate models with experimental data, an "error metric" is used. The error metric is equal to the log of the ratio of the calculated to measured values for the fractional release and matrix dissolution rates. Stated mathematically, the error metric is equal to $\log_{10}(F_c / F_m)$, where F_c is the calculated fractional release rate and F_m is the measured fractional release rate. The absence of systematic modeling bias is indicated by values of the error metric centered at zero. An approximate order of magnitude agreement between the model and the data is indicated when most of the value of the error metric are expected to be in the range 0 ± 1. The Microsoft Excel spreadsheets showing the validation calculations are attached (Appendix I, CSNF MR REV2.XLS, sheets A9 to A12).

7.1.2.1 Comparison with Batch (Semi-Static) Test Data

Batch or semi-static dissolution tests were performed over a decade ago on SNF samples (Wilson 1990 [DIRS 100793]). The tests involved placing a few grams of SNF in various configurations in less than a liter of synthetic J-13 groundwater and periodically sampling and analyzing the solution for various radionuclides. The results include data on the fraction of radionuclide released per unit time.

Data from the Series 3 semi-static leaching tests by Wilson (1990 [DIRS 100793]) provide a basis for comparing modeling fractional radionuclide release rates to experimental data from batch immersion tests. The Series 1 tests described (Stout and Leider 1998 [DIRS 111047], p. 2-213) were the first of three series of batch or semi-static tests conducted to characterize potential radionuclide release from, and behavior of, spent fuel stored under YMP conditions. In the Series 1 tests, specimens prepared from Turkey Point Reactor Unit 3 fuel were tested in deionized distilled water in unsealed fused silica vessels under ambient hot cell air and temperature conditions. Four specimen configurations were tested: (1) intact fuel rod segments with water-tight end fittings; (2) fuel rod segments containing small (approximately 200-µm diameter) laser-drilled holes through the cladding and with water-tight end fittings; (3) fuel rod segments with a machined slit through the cladding and water-tight end fittings; and (4) bare-fuel particles removed from the cladding plus the cladding hulls. A "semi-static" test procedure was developed in which periodic solution samples were taken with the sample volume replenished with fresh deionized water. A test "cycle" was used to refer to a testing period, where samples are taken at its conclusion, the test vessels are stripped and cleaned or replaced, and the next testing period is initiated. Series 1 and 2 tests were similar except (1) Series 2 tests were run in reference J-13 well water, (2) each of the four specimen configurations was duplicated using the Turkey Point Reactor and H. B. Robinson Reactor pressurized water reactor CSNF types, and (3) a vessel and specimen rinse procedure was added to the cycle termination procedures.

The Series 3 tests (Wilson 1990 [DIRS 100793]) were run for three cycles. For this test series, the tests were run in sealed vessels made of Stainless Steel Types 304 and 304L; the tests used the same four-specimen configurations used in Series 1 and Series 2. Five specimens (one for each of the four configurations using H. B. Robinson reactor fuel, plus an additional bare fuel specimen using Turkey Point reactor fuel) were tested at 85°C, and a sixth specimen (H. B. Robinson bare fuel) was run at 25°C.

The Series 3 tests were chosen for this analysis because they were performed in stainless steel containers and with J-13 well water. The previous Series 1 and 2 tests were conducted in silica

vessels from which leached silica components could affect the results. The bare fuel tests were chosen because they offered full exposure of the fuel to water. The final test period, Cycle 3, was selected because the originally unwashed fuel samples had been exposed to two separate batches of J-13 well water for almost a year. Easily removed radionuclides that had segregated to the surface or left in unremoved fines would have likely dissolved by the time Cycle 3 had started. Cycle 3, therefore, would most likely represent radionuclide release from the fuel matrix. The unfiltered sample-concentration data for the very soluble radionuclides, ^{90}Sr, ^{99}Tc, ^{129}I, and ^{137}Cs, in the bare fuel tests were used and taken respectively from Tables A.2 through A.4 provided by Wilson (1990 [DIRS 100793], Series 3) for the HBR/BF-25, TP/BF-85, and HBR/BF-85 samples.

Sample-specific data are at the top in the analysis Tables 7-5, 7-6, and 7-7. These data include experimental vessel volume, fuel specific area and isotope inventories, and sample weight, as well as tables referenced by Wilson (1990 [DIRS 100793]). Isotope specific data in the analysis tables are organized by isotope at the bottom. For each isotope, the sample time and volume, and sample isotope concentration are listed. The fraction released, fraction released per day, and equivalent specific dissolution rates are calculated values using Equations 23 through 25.

$$F_r = (C_i \cdot V_V)/(I_i \cdot m_s \cdot 1{,}000{,}000) \qquad \text{(Eq. 23)}$$

$$F_{rd} = F_r/t_s \qquad \text{(Eq. 24)}$$

$$R_d = [F_{rd} \cdot 1{,}000]/A_S \qquad \text{(Eq. 25)}$$

where

(A_S)	=	Sample specific surface area (m^2/g)
(t_s)	=	Sampling time (days)
(C_i)	=	Sample isotope concentration (pCi/mL)
(F_r)	=	Fraction released (#)
(F_{rd})	=	Fraction released per day (d^{-1})
(I_i)	=	Radionuclide inventory (µCi/g)
(m_s)	=	Sample mass (g)
(R_d)	=	Equivalent UO_2 dissolution rate (mgU/($m^2 \times$ d))
(FW_i)	=	Chemical formula weight (g)
(V_V)	=	Vessel volume (mL)

The following is a detail of a calculation using the above equations. The calculation is taken from Table 7-5 for test HBR/BF-25 with ^{137}Cs at a sampling time of 97 days.

$$F_r = (1.92 \times 10^6 \cdot 250) \div (6.37 \times 10^4 \cdot 83.66 \cdot 1{,}000{,}000) = 9.01 \times 10^{-5} \qquad \text{(Eq. 26)}$$

The factor of 1,000,000 accounts for microcurie to picocurie conversion.

$$F_{rd} = 9.01 \times 10^{-5} \div 97 = 9.29 \times 10^{-7}\ d^{-1} \qquad \text{(Eq. 27)}$$

$$R_d = (9.29 \times 10^{-4} \times 1{,}000) \div (2.4 \times 10^{-4} \times 3) = 1.29 \qquad \text{(Eq. 28)}$$

The factor of 1,000 accounts for gram-to-milligram conversion. The factor of three in the surface area is the roughness factor by Gray and Wilson (1995 [DIRS 100758], p. 2.7).

The NNWSI fractional release rate data from the last sampling period are summarized in Table 7-8. The fifth row in this table shows the calculated release rates for the test conditions using the base-case model for alkaline conditions. Comparisons of the model-calculated results to the experimental data show that the agreement is good and well within an order of magnitude. Specifically, the calculated error metric values in the last row of Table 7-6 are all positive (indicating that the model-calculated fractional release rates may be somewhat conservatively biased). The error metric values are all much less than 1.0, indicating better than order of magnitude agreement, which satisfies the applicable validation criterion.

Table 7-5. Calculations of Equivalent Intrinsic Dissolution Rates of H. B. Robinson Fuel at 25°C

Table A.2:	Table 2.1:	Table 2.3:	
Vessel volume (mL) [Figure 2.1] = 250 mL	Cycle 3 Sample Weight (g) = 83.66	RN Inventories (μCi/g) [a] (HB Robinson ORIGEN-2)	
Specific Surface Area (Geometric) = 2.40×10^{-4} m^2/g [Table E.3, Col. 2]		^{137}Cs	6.37E+04
Specific Surface Area (x3 Roughness) = 7.20×10^{-4} m^2/g		^{99}Tc	10.5
		^{90}Sr	4.17E+04
		^{129}I	0.0265

		^{137}Cs					^{99}Tc				
					Dissolution Rate (Cesium)					Dissolution Rate (Technetium)	
Time (Days)	Sampling Volume (mL)	pCi/mL	Fraction Released	FracRel/d	Geo. SA mgU/(m^2·d)	Rough SA mgU/(m^2·d)	pCi/mL	Fraction Released	FracRel/d	Geo. SA mgU/(m^2·d)	Rough SA mgU/(m^2·d)
0											
20	25	1.19E+06	5.58E-05	2.79E-06	1.16E+01	3.88E+00	6.76E+01	1.92E-05	9.62E-07	4.01E+00	1.34E+00
55	25	1.58E+06	7.41E-05	1.35E-06	5.62E+00	1.87E+00	1.26E+02	3.59E-05	6.52E-07	2.72E+00	9.06E-01
97	250	1.92E+06	9.01E-05	9.29E-07	3.87E+00	1.29E+00	2.34E+02	6.66E-05	6.87E-07	2.86E+00	9.54E-01

		^{90}Sr					^{129}I				
					Dissolution Rate (Strontium)					Dissolution Rate (Iodine)	
Time (Days)	Sampling Volume (mL)	pCi/mL	Fraction Released	FracRel/d	Geo. SA mgU/(m^2·d)	Rough SA mgU/(m^2·d)	pCi/mL	Fraction Released	FracRel/d	Geo. SA mgU/(m^2·d)	Rough SA mgU/(m^2·d)
0											
20	25	4.73E+05	3.39E-05	1.69E-06	7.06E+00	2.35E+00					
55	25	6.53E+05	4.68E-05	8.51E-07	3.55E+00	1.18E+00	6.04E-02	6.81E-06	1.24E-07	5.16E-01	1.72E-01
97	250	7.84E+05	5.62E-05	5.79E-07	2.41E+00	8.04E-01	8.26E-02	9.31E-06	9.60E-08	4.00E-01	1.33E-01

Source: Wilson 1990 [DIRS 100793]

NOTE: [a] 1,000,000 pCi = 1 μCi
SA = surface area

Table 7-6. Calculations of Equivalent Intrinsic Dissolution Rates of H. B. Robinson Fuel at 85°C

Table A.4			Table 2.1:		Table 2.3	
Vessel volume (mL) [Figure 2.1]=	250	mL	Cycle 3 Sample Weight (g)		RN Inventories (μCi/g)[a] (H. B. Robinson ORIGEN-2)	
Specific Surface Area (Geometric) =	2.40E-04	m^2/g [Table E.3, Col. 2]	HBR/BF-85	78.67	^{137}Cs	6.37E+04
Specific Surface Area (x3 Roughness) =	7.20E-04	m^2/g			^{99}Tc	10.5
					^{90}Sr	4.17E+04
					^{129}I	0.0265

		^{137}Cs					^{99}Tc				
					Dissolution Rate					Dissolution Rate	
Time (Days)	Sampling Volume (mL)	pCi/mL	Fraction Released	FracRel/ day	Geo. SA mgU/(m^2·d)	Rough SA mgU/(m^2·d)	pCi/mL	Fraction Released	FracRel/ day	Geo. SA mgU/(m^2·d)	Rough SA mgU/(m^2·d)
0											
20	25	5.86E+05	2.92E-05	1.46E-06	6.09E+00	2.03E+00	2.34E+02	7.08E-05	3.54E-06	1.48E+01	4.92E+00
55	25	1.25E+06	6.24E-05	1.13E-06	4.72E+00	1.57E+00	5.41E+02	1.64E-04	2.98E-06	1.24E+01	4.13E+00
97	250	2.09E+06	1.04E-04	1.07E-06	4.48E+00	1.49E+00	9.91E+02	3.00E-04	3.09E-06	1.29E+01	4.29E+00

		^{90}Sr					^{129}I				
					Dissolution Rate					Dissolution Rate	
Time (Days)	Sampling Volume (mL)	pCi/mL	Fraction Released	FracRel/ day	Geo. SA mgU/(m^2·d)	Rough SA mgU/(m^2·d)	pCi/mL	Fraction Released	FracRel/d	Geo. SA mgU/(m^2·d)	Rough SA mgU/(m^2·d)
0											
20	25	5.59E+05	4.26E-05	2.13E-06	8.87E+00	2.96E+00					
55	25	5.72E+05	4.36E-05	7.93E-07	3.30E+00	1.10E+00	8.15E-01	9.77E-05	1.78E-06	7.40E+00	2.47E+00
97	250	6.13E+05	4.67E-05	4.82E-07	2.01E+00	6.69E-01	1.24E+00	1.49E-04	1.53E-06	6.39E+00	2.13E+00

Source: Wilson 1990 [DIRS 100793]

NOTE: [a] 1,000,000 pCi = 1 μCi
SA = surface area

Table 7-7. Calculations of Equivalent Intrinsic Dissolution Rates of Turkey Point Fuel at 85°C

Table A.3	Table 2.1	Table 2.3	RN Inventories (μCi/g)[a]
Vessel volume (mL) [Figure 2.1]= 250 mL	Cycle 3 Sample Weight (g)		Turkey Point ORIGEN-2
Specific Surface Area (Geometric) = 2.21E-04 m^2/g [Table E.3, Col. 2]	Turkey Point /BF-85 83.64	^{137}Cs	6.04E+04
		^{99}Tc	9.74
Specific Surface Area (x3 Roughness) = 6.63E-04 m^2/g		^{90}Sr	4.03E+04
		^{129}I	0.0242

		^{137}Cs					^{99}Tc				
					Dissolution Rate					Dissolution Rate	
Time (Days)	Sampling Volume (mL)	pCi/mL	Fraction Released	FracRel/ day	Geo. SA mgU/(m^2·d)	Rough SA mgU/(m^2·d)	pCi/mL	Fraction Released	FracRel/ day	Geo. SA mgU/(m^2·d)	Rough SA mgU/(m^2·d)
0											
20	25	5.36E+05	2.65E-05	1.33E-06	6.00E+00	2.00E+00	1.49E+02	4.57E-05	2.29E-06	1.03E+01	3.45E+00
55	25	1.16E+06	5.74E-05	1.04E-06	4.72E+00	1.57E+00	3.24E+02	9.94E-05	1.81E-06	8.18E+00	2.73E+00
97	250	1.70E+06	8.41E-05	8.67E-07	3.92E+00	1.31E+00	5.41E+02	1.66E-04	1.71E-06	7.74E+00	2.58E+00

		^{90}Sr					^{129}I				
					Dissolution Rate					Dissolution Rate	
Time (Days)	Sampling Volume (mL)	pCi/mL	Fraction Released	FracRel/ day	Geo. SA mgU/(m^2·d)	Rough SA mgU/(m^2·d)	pCi/mL	Fraction Released	FracRel/ day	Geo. SA mgU/(m^2·d)	Rough SA mgU/(m^2·d)
0											
20	25	4.41E+05	3.27E-05	1.64E-06	7.40E+00	2.47E+00					
55	25	5.63E+05	4.18E-05	7.59E-07	3.44E+00	1.15E+00	5.95E-01	7.35E-05	1.34E-06	6.05E+00	2.02E+00
97	250	6.26E+05	4.64E-05	4.79E-07	2.17E+00	7.22E-01	9.15E-01	1.13E-04	1.17E-06	5.27E+00	1.76E+00

Source: Wilson 1990 [DIRS 100793]

NOTE: [a] 1,000,000 pCi = 1 μCi
SA = surface area

Table 7-8. Summary of the NNWSI Series 3 Fractional Release Rate (d^{-1}) Results for Last Sampling Period

Isotope	H. B. Robinson Fuel (25°C)	H. B. Robinson Fuel (85°C)	Turkey Point Fuel (85°C)
^{90}Sr	5.79E-07	4.82E-07	4.79E-07
^{137}Cs	9.29E-07	1.07E-06	8.67E-07
^{99}Tc	6.87E-07	3.09E-06	1.71E-06
Average	7.32E-07	1.55E-06	1.02E-06
Base-Case Model Calculated Fractional Release Rates (d^{-1})	7.32E-07	3.02E-06	3.02E-06
Error Metric	0.0	0.3	0.5

Source: Appendix I, CSNF MR REV2.xls. Spreadsheet A9

7.1.2.2 Comparison to the Swedish CSNF Data

An extensive series of experimental results on CSNF radionuclide fractional release rates have been reported under oxidizing conditions (Forsyth 1997 [DIRS 123134], Tables 6-11 and 6-12). The results for alkaline conditions are summarized in Table 7-9. The sixth row of numbers in this table shows the model-calculated fractional release rates for the test conditions involved. When these calculated results are compared to the average of the measured fractional release rates (d^{-1}) for strontium, cesium, molybdenum, and technetium, the agreement is seen to be excellent and well within an order of magnitude. The values for the error metric, as shown in the last row of Table 7-9, are all close to zero, which indicates a very good agreement between the model and these experimental data. The applicable validation criteria are satisfied with little indication of any systematic modeling bias.

Table 7-9. Average Fractional Release Rates (d^{-1}) Measured in the Series 11 Tests on Fuel Rod Segments with Different Burnups and in the Series 3 Tests on Fuel Fragments

	Rod Segments[a]			Fragments[b]
Element	Burnup Range (27 to 30 MWd/kgU)	Burnup Range (35 to 46 MWd/kgU)	Burnup Range (46 to 49 MWd/kgU)	Burnup (42 MWd/kgU)
Strontium	2.07E-07	3.19E-07	3.12E-07	2.03E-06
Cesium	5.61E-07	6.69E-07	7.90E-07	3.53E-06
Molybdenum	1.85E-06	2.25E-06	1.28E-06	3.82E-06
Technetium	1.61E-06	1.80E-06	1.35E-06	2.56E-06
Average	1.06E-06	1.26E-06	9.33E-07	2.99E-06
Base-Case Model Calculated Fractional Release Rates (d^{-1})	8.42E-07	8.42E-07	8.42E-07	8.42E-07
Error Metric	-0.1	-0.2	0.0	-0.5

Source: Appendix I, CSNF MR REV2.xls., Spreadsheet A9

NOTE: [a] Forsyth 1997 [DIRS 123134], Tables 6-11
[b] Data shown here are the average fractional release rates for the 3.23 and 3.24 tests (Forsyth 1997 [DIRS 123134], Tables 6-12).

Table 6-7 of *The SKB Spent Fuel Corrosion Program: An Evaluation of Results from the Experimental Programme Performed in the Studsvik Hot Cell Laboratory* (Forsyth 1997 [DIRS 123134]) also contains test data on the fractional radionuclide release rates (d^{-1}) measured under acidic conditions. These data are summarized in Table 7-10 and compared to the developed model for acidic conditions; the model-calculated results are shown in the eighth column of this table. The calculated error metric results, shown in the ninth column, show the acid-side model may have a small conservative bias (indicated by generally positive error metric values) and reproduces the experimental results within an order of magnitude as indicated by values for the error metric in the 0 ±1 range.

A recent article (Röllin et al. 2001 [DIRS 162398]) provides single-pass flow-through data on the oxidative dissolution rate of CSNF under acidic conditions. The results (Röllin et al. 2001 [DIRS 162398], Figure 9) show dissolution rates comparable to those calculated by the developed model for acidic conditions.

Table 7-10. Fractional Release Rates (d^{-1}) Measured Under Acidic Conditions in the SKB Series 3 and 11 Tests

Experiment Number	pH	^{90}Sr	^{137}Cs	^{97}Mo	^{99}Tc	Average	F_i Calc	Error Metric
3.2.5	2.3	1.37E-05	1.56E-05			1.47E-05	1.88E-05	0.1
3.5.8.91	3.65	8.47E-06	9.08E-06			8.78E-06	6.52E-06	-0.1
3.3.9	4.2	8.26E-07	1.56E-06			1.19E-06	4.24E-06	0.6
3.2.9	4.25	1.43E-06	2.68E-06			2.06E-06	4.08E-06	0.3
3.4.8.91	4.3	1.32E-05	1.70E-05			1.51E-05	3.92E-06	-0.6
3.3.5	4.75	3.38E-06	5.62E-06			4.50E-06	2.76E-06	-0.2
3.3.10	5.1	1.77E-06	3.03E-06			2.40E-06	2.10E-06	-0.1
3.2.10	6.6	6.04E-07	2.63E-06			1.62E-06	6.48E-07	-0.4
11.14.4	3.64	3.02E-06	6.13E-06	3.63E-07	6.29E-07	2.54E-06	6.58E-06	0.4
11.7.4	3.8	1.20E-06	1.66E-06	2.91E-07	5.33E-07	9.21E-07	5.80E-06	0.8
3.1.9	3.85	1.71E-06	3.08E-06			2.40E-06	5.58E-06	0.4
3.1.5	3.9	4.10E-06	6.24E-06			5.17E-06	5.36E-06	0.0
3.1.10	5.2	3.21E-06	3.76E-06			3.49E-06	1.94E-06	-0.3

Source: Appendix I, CSNF MR REV2.xls. Spreadsheet A9

NOTE: Results for the exposure terms of approximately twenty days to acidic conditions are not included because they are more likely to be influenced by the fuel-exposure conditions prior to exposure to acidic conditions.

The above comparisons show that the model-calculated fractional release rates are consistent, within an order of magnitude, with experimentally measured fractional release rates in the available literature for acidic and alkaline conditions. Thus, the applicable validation criterion is satisfied and the required level of confidence is indicated for acidic and basic conditions.

7.1.2.3 Comparison with UO_2 Data

Grambow (1989 [DIRS 113233]) and McKenzie (1992 [DIRS 131639]) provide reviews of the literature prior to 1992. There are three more-recent reports of particular interest for model validation. Tait and Luht (1997 [DIRS 114435]) summarizing UO_2 and CANDU SNF flow-through dissolution studies performed over an extended period of time at Atomic Energy of

Canada Limited, Whiteshell Laboratories is represented in Table 7-11. de Pablo et al. (1999 [DIRS 162388]) summarized flow-through oxidative dissolution studies of UO_2 in aqueous solutions as a function of temperature and carbonate concentration (Table 7-12). Torrero et al. (1997 [DIRS 114439]) measured uranium dioxide dissolution at various dissolved oxygen concentrations and pH at room temperature (Table 7-13). These results can be compared to the developed models for the dissolution rate per unit area under alkaline and acidic conditions. To facilitate this comparison, the error metric in this case is defined as $\log_{10}(DR_{calculated}/DR_{measured})$, where DR represents the specific dissolution rate (i.e., the dissolution rate per unit area).

As shown by the error metric results in column 7 of Table 7-11, the developed model for alkaline conditions predicts the various Tait and Luht (1997 [DIRS 114435]) results well over a range of temperature, oxygen, and water-chemistry conditions, providing a good confirmation of the model. The error metric values in Table 7-11 (all of which are less than 1.0) and the mix of positive and negative error metric values indicate little, if any, systematic modeling bias. This indicates model predictions are consistent with these experimental data within an approximate order of magnitude and applicable validation criteria are satisfied.

Table 7-11. Comparison of Data from Tait and Luht (1997 [DIRS 114435]) with the Alkaline Model

Sample	Water	T (°C)	From Tait and Luht (1997 [DIRS 114435])	DR_m (mgU/m^2d)	DR_c (mgU/m^2d)	Error Metric
UO_2	SC[b]	25	Figure 4	1.37	3.5	0.4
UO_2	SC[b]	25	Figure 9	1.4	3.5	0.4
UO_2 (CANDU)	SC[b]	35	Figure 13	10.2	4.6	-0.3
UO_2 (CANDU)	SC[b]	50	Figure 13	22	6.7	-0.5
UO_2 (CANDU)	SC[b]	50	Figure 13	25.6	6.7	-0.6
UO_2 (CANDU)	SC[b]	75	Figure 13	102	11.7	-0.9
Used (CANDU) Fuel[a]	SC[b]	25	Figure 17	13	3.5	-0.6
Used (CANDU) Fuel[a]	SC[b]	25	Figure 19	4	3.5	-0.1
Used (CANDU)Fuel[a]	SC[b]	35	Figure 21	20	4.6	-0.6
Used (CANDU) Fuel[a]	SC[b]	75	Figure 21	45	11.7	-0.6

Source: Appendix I, CSNF MR REV2.xls. Spreadsheet A10

NOTE: Experimental data in column DR_m are approximate; they were from figures in the source document. CANDU = Canada Deuterium Uranium; DRm = measured dissolution rate, in $mg/(m^2 \cdot d)$; DRc = calculated dissolution rate, in $mg/(m^2 \cdot d)$
[a] Used Fuel Burnup =10 MWd/kgU
[b] SC = Aerated 0.01*M* $NaHCO_3$/0.1 *M* NaCl (pH≅9.3)

Table 7-12 summarizes flow-through oxidative dissolution studies of UO_2 in aqueous solutions as a function of temperature and carbonate concentration (de Pablo et al. 1999 [DIRS 162388], Tables 1 and 2). In these tests, leaching solutions were in contact with air concentration (de Pablo et al. 1999 [DIRS 162388], p 3,098) (i.e., the oxygen fugacity was 0.2 atm). The data obtained at 10°C are not included in Table 7-12 because this temperature is outside the repository-relevant temperature range. These results were obtained using a continuous flow-through reactor with the flow rates adjusted to minimize the possibility of secondary reactions (including precipitation). The error metric results shown in column 7 show that there is generally good agreement (i.e., consistent within an approximate order of magnitude) between

the experimental data and the model-calculated results and that the applicable validation criteria are satisfied.

Table 7-12. Experimental UO_2 Dissolution Rates as a Function of Temperature and Bicarbonate Concentration

Temperature (°C)	$[HCO_3^-]$ (mmol/L)	pH (±0.1)	pO_2	Dissolution Rate (mg m^{-2} d^{-1})	Calculated Dissolution Rate (mg m^{-2} d^{-1})	Error Metric
25	0.1	8.1	0.7	2.10E-01	2.5E+00	1.1
25	0.1	8.1	0.7	2.22E-01	2.5E+00	1.0
25	0.1	8.1	0.7	2.36E-01	2.5E+00	1.0
25	0.1	8.1	0.7	2.36E-01	2.5E+00	1.0
25	0.1	8.1	0.7	2.38E-01	2.5E+00	1.0
25	1	8.3	0.7	9.26E-01	3.1E+00	0.5
25	1	8.3	0.7	9.33E-01	3.1E+00	0.5
25	1	8.3	0.7	9.33E-01	3.1E+00	0.5
25	1	8.3	0.7	9.52E-01	3.1E+00	0.5
25	10	8.3	0.7	6.88E+00	3.9E+00	-0.2
25	10	8.3	0.7	7.30E+00	3.9E+00	-0.3
25	10	8.3	0.7	7.60E+00	3.9E+00	-0.3
25	10	8.3	0.7	7.65E+00	3.9E+00	-0.3
45	0.1	7.8	0.7	3.15E-01	4.2E+00	1.1
45	0.1	7.8	0.7	3.41E-01	4.2E+00	1.1
45	0.1	7.8	0.7	3.36E-01	4.2E+00	1.1
45	1	8.1	0.7	1.88E+00	5.3E+00	0.5
45	1	8.1	0.7	1.97E+00	5.3E+00	0.4
45	1	8.1	0.7	1.99E+00	5.3E+00	0.4
45	1	8.1	0.7	2.01E+00	5.3E+00	0.4
45	1	8.1	0.7	1.99E+00	5.3E+00	0.4
45	1	8.1	0.7	1.84E+00	5.3E+00	0.5
45	1	8.1	0.7	2.05E+00	5.3E+00	0.4
45	1	8.1	0.7	1.85E+00	5.3E+00	0.5
45	10	8.2	0.7	1.86E+01	6.7E+00	-0.4
45	10	8.2	0.7	2.02E+01	6.7E+00	-0.5
45	10	8.2	0.7	1.93E+01	6.7E+00	-0.5
45	10	8.2	0.7	1.91E+01	6.7E+00	-0.5
45	10	8.2	0.7	1.94E+01	6.7E+00	-0.5
45	10	8.2	0.7	1.92E+01	6.7E+00	-0.5
60	0.1	7.6	0.7	6.63E-01	6.0E+00	1.0
60	0.1	7.6	0.7	6.00E-01	6.0E+00	1.0
60	0.1	7.6	0.7	5.93E-01	6.0E+00	1.0
60	1	8.0	0.7	2.92E+00	7.6E+00	0.4
60	1	8.0	0.7	2.80E+00	7.6E+00	0.4
60	1	8.0	0.7	2.68E+00	7.6E+00	0.5
60	1	8.0	0.7	2.66E+00	7.6E+00	0.5

Table 7-12. Experimental UO_2 Dissolution Rates as a Function of Temperature and Bicarbonate Concentration (Continued)

Temperature (°C)	$[HCO_3^-]$ (mmol/L)	pH (±0.1)	pO_2	Dissolution Rate (mg m^{-2} d^{-1})	Calculated Dissolution Rate (mg m^{-2} d^{-1})	Error Metric
60	1	8.0	0.7	2.75E+00	7.6E+00	0.4
60	1	8.0	0.7	2.73E+00	7.6E+00	0.4
60	10	8.1	0.7	6.63E+01	9.6E+00	-0.8
60	10	8.1	0.7	6.70E+01	9.6E+00	-0.8
60	10	8.1	0.7	6.67E+01	9.6E+00	-0.8
60	10	8.1	0.7	6.72E+01	9.6E+00	-0.8
60	10	8.1	0.7	6.79E+01	9.6E+00	-0.9
60	10	8.1	0.7	6.65E+01	9.6E+00	-0.8

Source: Appendix I, CSNF MR REV2.xls. Spreadsheet A11

Table 7-13 compares published acid-side UO_2 data (Torrero et al. 1997 [DIRS 114439]) to the developed model for acidic conditions. The error metric results in the sixth column show the developed acid side model often overpredicts the experimental UO_2 data by more than an order of magnitude (error metric is greater than 1), indicating a potentially conservative modeling bias. This systematic discrepancy between the acid-side model and these data is explained, in part, by the fact that the sample surface areas were measured by the BET method, which is known to overestimate the effective surface area for oxidative dissolution of UO_2 and CSNF (Gray and Wilson 1995 [DIRS 100758], Section 2.1.3). Dissolution rates by Torrero et al. (1997 [DIRS 114439]) under acidic conditions were low in general when compared to other work (Grambow 1989 [DIRS 113233]).

Table 7-13. Measured UO_2 Flow-Through Dissolution Data with Variation of Oxygen and pH

pH[a]	T(°C)[a]	O_2 Pressure (atmospheres)[a]	Dissolution Rate ($mgUO_2$ d^{-1} m^{-2})	Calculated Dissolution Rate ($mgUO_2$ d^{-1} m^{-2})	Error Metric
3.3	25	0.05	1.80E+00	23.4	1.1
3.6	25	0.05	1.25E+00	18.5	1.2
4.4	25	0.05	7.09E-01	9.9	1.1
4.8	25	0.05	5.51E-01	7.2	1.1
5.2	25	0.05	4.00E-01	5.3	1.1
5.6	25	0.05	2.77E-01	3.9	1.1
6.6	25	0.05	1.30E-01	1.8	1.1
3.2	25	0.21	3.44E+00	41.1	1.1
3.5	25	0.21	2.88E+00	32.5	1.1
4.1	25	0.21	1.93E+00	20.3	1.0
4.7	25	0.21	9.83E-01	12.7	1.1
5.2	25	0.21	5.38E-01	8.6	1.2
6.2	25	0.21	3.45E-01	3.9	1.1
6.5	25	0.21	2.46E-01	3.1	1.1
6.6	25	0.21	1.77E-01	2.9	1.2

Source: Appendix I, CSNF MR REV2.xls. Spreadsheet A12
[a] from Torrero et al. 1997 [DIRS 114439], Table 1

NOTE: Surface Area (BET) = 1.13E-02 m^2/g

The above comparisons show that the model-calculated specific dissolution rates of UO_2 are consistent, within an approximate order of magnitude, with experimentally measured specific dissolution rates in the available literature for alkaline and acidic conditions. Thus, the applicable validation criterion is satisfied and the required level of confidence is indicated.

7.1.3 Comparison with UO_{2+x} Data

Based on the discussion in Section 6.2.2.2, it is likely that CSNF will corrode by the oxidative dissolution process when exposed to humid air at temperatures less than 100°C. However, the possibility of oxidation of CSNF in the repository environment before it is contacted by water cannot be excluded (Section 6.2.2.2). Hence, dissolution studies of the higher oxides are discussed in this section.

The dependence of UO_{2+x} dissolution kinetics on pH, temperature, time, and carbon dioxide–carbonate–bicarbonate concentrations was investigated (Stout and Leider 1998 [DIRS 111047], p. 2-223). All tests in the higher oxide test series were run at 0.2 atmospheres oxygen partial pressure or 8 ppm dissolved oxygen. The flow-through tests were carried out in basic buffer solutions (pH of 8 to 10). Tests were done at three temperatures (25°C, 50°C, and 75°C), three carbonate–bicarbonate concentrations (2×10^{-4} to 2×10^{-2} mol/L), and three pHs (8, 9, 10) for the two compounds U_3O_8 and $UO_3{\cdot}xH_2O$. Stout and Leider (1998 [DIRS 111047], p. 2-224, Table 2.1.3.5-5, Part 1) list the uranium dissolution rates for the three oxides—UO_2, U_3O_8, and $UO_3{\cdot}xH_2O$—measured under atmospheric oxygen conditions and show the oxide state has, by far, the strongest effect on the uranium dissolution rate. The rate increase from UO_2 to U_3O_8 is small, but it increases dramatically from U_3O_8 to $UO_3{\cdot}xH_2O$. Increasing carbonate concentrations increase dissolution rates of U_3O_8 and $UO_3{\cdot}xH_2O$, as shown previously with UO_2. An increase in U_3O_8 dissolution rate with increasing temperature is seen as well. A similar temperature effect occurs on $UO_3{\cdot}xH_2O$. For example, raising the temperature to 75°C from room temperature increases the dissolution rate by a factor of two to four for the two higher oxides. Similar to the UO_2 results, alkaline pH does not have a significant role in changing the dissolution rate of the higher oxides.

Stout and Leider (1998 [DIRS 111047], p. 2-224) data indicate with higher oxides, unlike UO_2, carbonate concentration affects the dissolution rate to a greater extent than does temperature. The enhancement is particularly strong at the highest carbonate concentration. Shoesmith (2000 [DIRS 162405], Section 5.2) states this is consistent with the results seen in a dissolution study of soddyite, another fully oxidized uranium oxide. This strong dependence of U(VI) uranium-oxide dissolution on carbonate indicates that concentrated carbonate might prevent deposition of corrosion products during SNF dissolution.

Results were also reported from flow-through dissolution tests with oxidized specimens of SNF and unirradiated U_3O_7 and U_3O_8 (Stout and Leider 1998 [DIRS 111047], p. 2-225). Dissolution rates of CSNF samples oxidized to U_4O_{9+x} were measured for three CSNF types: ATM-104, ATM-105, and ATM-106. The surface area normalized dissolution rate of oxidized fuel grains was little or no higher than unoxidized (UO_2) grains for ATM-105. Oxidized ATM-106 fuel grains dissolved faster than unoxidized grains, but the difference was a factor of only about five.

Oxidation has the potential to change SNF intrinsic dissolution rates by increasing the effective surface area. The specific dissolution rates (i.e., dissolution rates per unit area) of ATM-104, ATM-105, and ATM-106 (data obtained using grain specimens) (Stout and Leider 1998 [DIRS 111047], p. 2-226) were not significantly affected by oxidation to U_4O_{9+x}. The data suggest that oxidation up to the U_4O_{9+x} stage does not have a large effect on specific dissolution rates (the largest increase was less than a factor of 6). However, data for some of the particle specimens suggest this degree of oxidation may markedly increase fractional dissolution rates of relatively intact fuel rods by opening the grain boundaries, thereby increasing the effective surface area available for contact by water. From a disposal viewpoint, this is the more important consideration (Stout and Leider 1998 [DIRS 111047], pp. 2-226 and 2-227). When ATM-106 fuel was oxidized to U_3O_8, its surface area-normalized dissolution rate was up to 10 times faster than unoxidized ATM-106 fuel grains and about twice as fast as ATM-106 fuel grains oxidized to U_4O_{9+x} (Gray and Wilson 1995 [DIRS 100758], Section 3.4.4 and Figure 68). A more important effect of oxidation to U_3O_8 was the very large increase in surface area compared to the particles used to prepare the U_3O_8. This resulted in a fractional dissolution rate (rate per unit specimen weight) of U_3O_8 equal to 150 times that of the unoxidized particles.

At O_2 overpressure of 0.2 atmospheres, the intrinsic dissolution rate of unirradiated U_3O_7 [approximately 3 mgU/(m^2·d)] was similar to UO_2 [approximately 2.5 mgU/(m^2·d)] and the intrinsic dissolution rate of unirradiated U_3O_8 [approximately 10-15 mgU/(m^2·d)] was about four to six times that of UO_2. At an O_2 overpressure of 0.003 atmospheres, the intrinsic dissolution rate of the U_3O_7 was two to three times that of UO_2 [0.5-1 mgU/(m^2·d)]. These estimates are based on a single test on each oxide at each condition) (Stout and Leider 1998 [DIRS 111047], p. 2-227).

In summary, for each supplemental test conducted with oxidized SNF, unirradiated U_3O_7, or U_3O_8, the intrinsic dissolution rate of the oxidized material was only moderately higher than the unoxidized (UO_2) material. The largest difference was a factor of 10 with CSNF U_3O_8. However, because of the potentially large increases in the specific surface area associated with oxidation of CSNF to higher oxides, an instantaneous radionuclide release rate model is used for any fuel that is exposed to humid air at temperatures greater than 100°C.

7.2 COMPARISON OF THE DEVELOPED MODEL TO ALTERNATIVE MODELS

This section addresses validation by comparing the developed model for the specific dissolution rate of the CSNF matrix for alkaline conditions to the rates calculated using the electrochemical and surface complexation models described in Sections 6.4.2.1 and 6.4.2.2.

As described in Section 6.4.2, alternative models were developed for the specific dissolution rate (i.e., the dissolution rate per unit area) of CSNF under alkaline conditions. The base-case alkaline model was compared to the alternative electrochemical (Equation 17) and surface complexation (Equation 22) models by evaluating the dissolution rates calculated by each model for a set of nominal repository conditions. The parameter values in the surface complexation model were taken from the paper by de Pablo et al. (1999 [DIRS 162388], Table 4) and the total density of surface sites (i.e., $\{>UO_2\}_{tot} = 10^{-6}$ mol m^{-2}). The nominal conditions used in this comparison are: oxygen fugacity = 0.2 atmospheres, total carbonate concentration equal to 2.00×10^{-3} mol/L, and T = 30°C. The results are shown in Table 7-14. Although the

Equation 20 form of the electrochemical model applies at 25°C, this difference from the nominal conditions is not significant.

Table 7-14. Comparison of the Base-Case Model to Alternative Models

Model	Calculated Dissolution Rate ($mg/m^2/d$)
Base-Case	3.8
Surface Complexation	2.4
Electrochemical	12.1

The results in Table 7-14 show excellent agreement between the base-case model and the surface complexation model. The dissolution rates calculated by the electrochemical model are about a factor of five larger than the rates calculated by the other two models. This result suggests that either the base-case and surface complexation models have a nonconservative bias or the electrochemical model is conservatively biased. The latter interpretation is more likely. As discussed in Section 6.2.2.3, the oxidative dissolution process consists of redox reaction steps [that convert U(IV) to U(VI)] followed by U(VI) dissolution steps promoted by carbonate complexation. In any such reaction process involving a sequence of steps, the slower steps will control the overall rate of the process. The electrochemical model is based on the rate of the redox reaction steps; and is therefore expected to overestimate the overall reaction rate for any reaction conditions where slower surface complexation, dissolution, or mass transfer steps, or both, influence the overall reaction rate. The likely conservative bias in the electrochemical model is apparent from the comparison with of the model with other data sources in the source documents for Equation 18 (Section 6.4.2.1). These comparisons between the base-case model and the surface complexation and electrochemical models, for a set of nominal repository conditions, show an adequate level of confidence is indicated for the developed model for the specific dissolution rate of the CSNF matrix under alkaline conditions and the applicable validation criteria are satisfied.

A recent article (Röllin et al. 2001 [DIRS 162398]) provides single-pass flow-through data on the oxidative dissolution rate of CSNF under acidic conditions. The results (Röllin et al. 2001 [DIRS 162398], Figure 9) show dissolution rates comparable to those calculated by the developed model for acidic conditions.

In comparing the developed models to alternative models, it is instructive to compare the developed model's parameter values to the corresponding coefficients (partial reaction orders and activation energy) in the published literature. As described by Jegou et al. (2001 [DIRS 162397], Section 8.2.2.3) the rate law commonly accepted for homogenous reaction kinetics has the same mathematical form as the base-case model. It is, therefore, appropriate to compare the base-case model's parameters with the activation energies and the partial reaction orders that have been reported in the literature for expressing the rate dependence on temperature, dissolved oxygen concentration, total carbonate, and pH. Shoesmith (2000 [DIRS 162405], Section 6) pointed out that there is evidence that different mechanisms control the rate for different regions of the data domain used in the base case model regression. Hence, only approximate agreement between the base-case model parameters and the partial reaction orders reported in the literature can be expected.

As shown by Shoesmith et al. (1998 [DIRS 162404], Figure 1), the coefficient for the dissolved oxygen concentration dependence of the SNF dissolution rate is 0.39, which compares well to the oxygen fugacity dependence of 0.338 in the base-case model. However, values from 1 to 0.1 for the partial order dependence on dissolved oxygen has been reported (Jegou et al. 2001 [DIRS 162397], Section 8.2.3.3; Shoesmith 2000 [DIRS 162405], Sections 5.4 and 6.2). Also, there is evidence that the partial order for oxygen dependence depends on temperature; it is very low at 25°C and increases as temperature increases (Shoesmith 2000 [DIRS 162405], Section 6.4; Jegou et al. 2001 [DIRS 162397], Section 8.2.3.3). Literature data show a weaker dependence of CSNF on dissolved oxygen concentration compared to UO_2 (Shoesmith 2000 [DIRS 162405], Section 5.4). This is probably due to the effects of radiolytic oxidants, which become more significant as the dissolved oxygen concentration is reduced and, as a result, cause a smaller apparent dependence on the dissolved oxygen concentration.

The dependence on carbonate concentration in the base-case model (coefficient of 0.102) is significantly weaker than the coefficient for carbonate dependence in the electrochemical model (i.e., 0.38). However, it is worth noting that the UO_2 carbonate dependence (total carbonate parameter value = 0.473 in Table 6-8) agrees more closely with the literature value. This is consistent with the fact that the literature values for the partial order dependence on total carbonate are based on UO_2.

The temperature dependence in the base-case model corresponds to an activation energy of 21 kJ/mol. This is at the low end of the range (20 to 60 kJ/mol.) reported by others for UO_2 (Jegou et al. 2001 [DIRS 162397], p. 481). Note that the value indicated for the UO_2-only model (Table 6-8) is 34 kJ/mol. The effects of temperature are known to be complex in carbonate solutions; the activation energies reported are lower for low carbonate concentrations that give apparent activation energies close to the value obtained for the base-case model (Shoesmith 2000 [DIRS 162405], Section 6.5). As discussed in Section 6.2.2.3, this is consistent with the interpretation that diffusion through surface alteration layers influences the rate of the oxidative dissolution process under conditions where these layers are formed. Under higher carbonate or acidic conditions that promote rapid dissolution of U(VI) alteration layers, these mass transport effects do not influence the rate and activation energies near the upper end of the range are observed (Shoesmith 2000 [DIRS 162405], Section 5.6). As discussed in Section 7.1.2, Table 7.1-5 results provide evidence that the model for the CSNF matrix radionuclide release rate is valid for temperatures up to 85°C. Uncertainty associated with extending the model's domain of application to 100°C can be assessed by examining how uncertainty in the applicable activation energy could influence the modeled rate. Using the model's activation energy of 21 kJ/mol the rate increases by approximately 20 percent between 85°C and 100°C. If an activation energy of 60 kJ/mol is used (i.e., the upper end of the activation energy range), the rate increases by a factor of about 2.2 between 85°C and 100°C. However, if a more likely activation energy of 40 kJ/mol (i.e., the middle of the activation energy range) is used, the rate increases by approximately 70 percent between 85°C and 100°C. These results indicate that extension of the model's temperature domain to 100°C introduces, at most, an uncertainty factor of two. Extension of the model domain of application to 100°C is justified because the uncertainty associated with this extension is small compared to the overall modeling uncertainties.

The lack of pH dependence of the rate under alkaline conditions is consistent with published data (Shoesmith 2000 [DIRS 162405], Section 6.3). For acidic conditions, Grambow (1989 [DIRS 113233]) calculated room-temperature acidic dissolution rates for boiling water reactor SNF types with data reported by Forsyth et al. (1986 [DIRS 120955]). Grambow (1989 [DIRS 113233], p. 11) in his Figure 2 plot of the converted Forsyth et al. (1986 [DIRS 120955]) acidic SNF dissolution rate data, gives a slope of about -0.5. In his review of the dependence of UO_2 corrosion rate in the pH regime $3<pH<6.7$, Shoesmith (2000 [DIRS 162405], Section 3.1.2) reports a power law dependence on pH with an exponent of 0.37. A recent article (Röllin et al. 2001 [DIRS 162398]) provides single-pass flow-through data on the oxidative dissolution rate of CSNF under acidic conditions. The results (Röllin et al. 2001 [DIRS 162398], Figure 9) show a coefficient of 0.6 for dependence on pH. Although this is a higher dependence on pH than the 0.34 coefficient (i.e., the value for the a_4 parameter determined in Section 6.4.1.3) in the base-case acid model the dissolution rates presented are comparable to those calculated by the base-case acid model. Although the base-case model parameters are generally consistent with literature data, this consistency constitutes weak validation because of the wide range of activation energies and reaction orders reported in the literature.

7.3 NATURAL ANALOGUES

7.3.1 Studies of Natural Analogue Sites

This section on natural analogues has been included to provide a qualitative overview of the uranium mineral phases seen at natural uranium-bearing sites around the world and to provide a comparison with corrosion products seen in laboratory tests. It does not provide data that can be used directly for validating the CSNF models. However, confidence can be gained in using the base-case model for modeling fuel corrosion over extended time periods by showing that secondary phase development in multiyear laboratory tests is similar to the alteration phase paragenesis determined at the uranium-bearing natural analogue sites. Similarities in the alteration phases observed in laboratory experiments to those observed in very long-term alteration of uraninite provides evidence that the overall alteration processes observed in the laboratory are similar to those likely to control alteration in the long term.

CSNF consists of uranium dioxide (UO_2) having a cubic fluorite crystalline structure. Uranium dioxide occurs in nature as the mineral uraninite, also exhibiting a fluorite structure. Numerous geologic sites contain uraninite, and studies of natural uraninite alteration cover a wide range of geologic conditions. Of the several extensively studied sites, only Nopal I, the uranium mining site at Pena Blanca, Mexico, has geologic, geochemical, and hydrogeologic characteristics similar to those at Yucca Mountain (Murphy 1995 [DIRS 100469]). The volcanic (tuffaceous) host rock at Nopal I, the youngest of the studied sites, has been exposed to oxygen for tens of thousands of years. Uraninite, containing U(IV), was originally formed several million years ago. Pearcy and Murphy (1991 [DIRS 130197]) discuss in some detail other natural analogue sites around the world. The oxidizing sites discussed are Koongarra in Australia, Pocos de Caldas in Brazil, the Shinkolobwe mine in the Congo, and the Krunkelbach mine in Germany. The other sites are either somewhat reducing or hydrologically saturated, or the mineralogy of the uraninite alteration is significantly affected by the presence of chemical elements not found in underground repositories or their environs (e.g., lead, phosphorus, or vanadium).

The process of uranium mineral formation and subsequent uranium transport at Nopal I have been extensively studied. Because the sites are geologically similar, it is anticipated that the uranium compound alteration and transport processes will be comparable to those that would occur at the repository.

The data in this section provide the basis for comparing the mineral phases and paragenesis seen at Nopal I, the natural geologic site, and the chronological progression of CSNF and UO_2 corrosion products seen in laboratory tests.

The uranium minerals found at Nopal I are listed in Table 7-15 with a qualitative illustration of their relative time sequence of formation and relative abundance. The compounds found are limited compared to other sites because of the simple chemistry of the Pena Blanca system.

Table 7-15. Paragenesis of Uranium Minerals at Nopal I

Mineral Group	Mineral	Time	Nominal Chemical Formula
Oxide	Uraninite	· · · · · · · ·	UO_{2+x}
Oxyhydroxides	Ianthinite	—	$U^{4+}(U^{6+}O_2)_5(OH)_{14}\cdot 3H_20$
	Schoepite/Dehydrated Schoepite	— · · · · ·	$UO_3\cdot 2H_20$ $UO_3\cdot nH_2O(n< 2)$
	Becquerelite	— · ·	$Ca(UO_2)_6O_4(OH)_6\cdot 8H_2O$
	Billietite(?)/Abernathyite(?)	· · · · · · ·	$Ba(UO_2)_6O_4(OH)_6\cdot nH_2O(n=4\text{-}8)$ $K(UO_2)(AsO_4)\cdot 4H_2O$
Silicates	Soddyite	—	$(UO_2)_2SiO_4\cdot 2H_2O$
	Weeksite and Boltwoodite	· · · · · · · · · ·	$K_2(UO_2)_2Si_6O_{15}\cdot 4H_2O$ $KH(UO_2)SiO_4\cdot 1.5H_2O$
	Uranophane: β-Uranophane	————	$Ca(UO_2)_2Si_2O_7\cdot 6H_2O$

Source: Pearcy et al. 1994 [DIRS 100486]

NOTES: · · · · · · · minor
— · · · · · abundant, then minor
———— abundant
———— very abundant
? indicates tentative identification

7.3.2 Comparison of Laboratory Corrosion Products to Nopal Minerals

Combined optical, scanning-electron microscope, energy dispersive x-ray spectroscope, and x-ray diffraction examinations of samples taken from unsaturated tests performed on the two CSNF types (ATM-103 and ATM-106) indicate that the time-dependent evolution of the alteration phases is strongly dependent on the rate at which the EJ-13 water contacts the spent UO_2 fuel (Stout and Leider 1998 [DIRS 111047], p. 2-250). The three tests (high drip rate, low drip rate, and vapor) show several similarities, including corroded grain boundaries, dissolution of fuel grains, and precipitation of alteration phases (Figure 6-2).

Analyses of the alteration phases were done by sampling the alteration phases and by analyzing the collected samples using a combination of methods, including x-ray diffraction, transmission electron microscopy, scanning electron microscopy, and light microscopy. Only a small fraction of the total volume of corrosion products that have formed on the surfaces of UO_2 and SNF

fragments have been removed and analyzed. The extent to which these samples are representative of the entire alteration phase assemblage is, therefore, uncertain. Of the analysis methods used, only transmission electron microscopy and x-ray diffraction provide positive identification of a crystal structure by diffraction. The transmission electron microscope provides additional information on chemical composition using x-ray energy dispersive spectrometry and electron energy loss spectrometry, plus magnified images that provide crystal domain size, shape, etc. The scanning electron microscope provides information on elemental composition using x-ray energy dispersive spectrometry, plus morphological information such as crystal shape and growth habit. Light microscopy, as used in these studies, provides only information about crystal growth patterns, some crystal shape, and color (for instance, many uranium (VI) phases are characteristically bright yellow). The composition of the alteration-phase assemblage remains uncertain; the techniques used and the extent of the analyses are not sufficient to ensure all of the phases formed have been identified and to establish a complete understanding of the phase paragenesis in these tests.

The available alteration phase identification results indicate that the alteration-phase assemblage depends strongly on water flux and its composition, with uranyl oxy-hydroxides predominating in vapor tests and alkali and alkaline earth uranyl silicates predominating in high drip-rate tests. Low drip-rate tests exhibit a complex assemblage of corrosion products, including phases identified in vapor and high drip-rate tests (Stout and Leider 1998 [DIRS 111047], Section 2.1.3.5).

The vapor tests display the simplest assemblage of alteration products. Samples from vapor tests display a relatively simple combination of uranyl oxy-hydroxide alteration phases dominated by dehydrated schoepite $(UO_2)O_{0.25-x}(OH)_{1.5+2x}$ ($0 \leq x \leq 0.15$) and metaschoepite. This assemblage is readily explained by the lack of added cations in the vapor and condensate that contacts the fuel surface. The only cations (except H^+) available for the precipitation of solids come from the dissolution of fuel. A Cs–Ba–Mo–uranate phase, which incorporates two fission products, cesium and molybdenum, was identified (Buck et al. 1997 [DIRS 112904]). The precipitation of dehydrated schoepite and metaschoepite in these tests indicates that the film of water that forms on the fuel surface is sufficiently corrosive to dissolve the fuel and form a thin corrosion rind of alteration products. Such a water film is likely present in the drip tests, as well as during those intervals that EJ-13 water is not being dripped onto the fuel. It seems likely that the corrosion processes important in the vapor tests remain important in the drip tests. Dehydrated schoepite or metaschoepite, or both, may also form in the drip tests between water injections. If these phases are present when contacted by EJ-13 water, they may be at least as susceptible to dissolution or replacement, or both, as the unoxidized fuel.

The drip tests display more chemically complex alteration phases, owing to the interaction of the fuel with EJ-13 water (rather than water vapor and condensate only). The most abundant elements in EJ-13 water are Na and Si, and the most abundant alteration products in the high drip-rate tests are Na- and Si-bearing U(VI) phases. Other U(VI) phases are also present, including metaschoepite and β-uranophane, indicating the importance of additional minor phases and elements to the overall corrosion process.

Fuel samples exposed to the higher drip-rates yield two uranophane-group silicates, β-uranophane $[Ca(UO_2)_2(SiO_3OH)_2(H_2O)_5]$ and Na-boltwoodite $(Na,K)(UO_2)(SiO_3OH)(H_2O)$,

compared to the complex alteration-phase assemblage seen in the low drip-rate tests. The simple phase assemblage in the high drip-rate tests reflects higher overall reaction progress for the spent fuel in these tests. Samples from low drip-rate tests possess a much more complex assemblage of U(VI) phases than observed in samples from either vapor or high drip-rate tests. This complexity may reflect the limited influx of EJ-13 water, which contributes Si, Na, Ca, and other cations. Common corrosion products from low-drip-rate tests include metaschoepite, an unidentified Na-uranyl oxy-hydroxide tentatively identified as "Na-compreignacite," and soddyite, a Cs–Ba–Mo–uranate phase that commonly occurs adjacent to dissolving fuel grains. In one sample from the ATM-103 low-drip-rate test at the 5.2-year interval, soddyite appears to replace Na-compreignacite. Also, a few isolated crystals of Na-boltwoodite were first detected in the ATM-103 low-drip-rate test at the 4.1-year interval. They were later abundant at the 5.2-year interval but less abundant than soddyite. These observations provide limited direct evidence for the replacement of uranyl oxy-hydroxides by uranyl silicates.

In Wilson's (1990 [DIRS 100793]) Series 3 tests using J-13 well water, the uranium silicate, soddyite, and calcium uranium silicates, β-uranophane (haiweeite, minor), were found using x-ray diffraction and scanning electron microscopy (Stout and Leider 1998 [DIRS 111047], p. 2-261).

The sequence of uraninite alteration at Nopal I is similar to that of CSNF and UO_2 in the laboratory tests. Uraninite is already partially oxidized (Pearcy et al. 1994 [DIRS 100486]). Spent fuel and UO_2 must first undergo that first surface oxidation to approach uraninite. The corrosion products observed in laboratory CSNF and UO_2 tests conform to the mineral phases seen at Nopal I. The general sequence is oxidation of the solid surface followed by hydration, thereby forming uranyl-oxide hydrates. Silicate in the groundwater is incorporated as soddyite. The silicate, in combination with alkali ions (e.g., calcium and sodium), forms various alkaline uranyl silicate hydrates, such as Na-boltwoodite and β-uranophane. The exact sequence and timing of formation depends significantly on local chemical environment, water flows, and time in the laboratory tests and at the Nopal I site. Simultaneous precipitation is indicated in laboratory and field tests. Some alteration phases, such as sklodowskite and compreignacite, are found in the laboratory tests but not at Nopal I. This may simply be a result of the small number of samples in all studies. Also, some phases, such as ianthanite, seen at the Nopal I site have not been reported in the laboratory tests. The fact that ianthanite was not observed does not preclude its possible presence in the tests. Ianthanite is an interesting phase, containing a mixture of U(VI) and U(IV) sites. The conditions under which it forms, thus, may reflect local redox conditions present in the natural system at Nopal, but not reproduced in the drip tests.

The groundwater at Nopal I is richer in calcium than J-13 well water (Pearcy et al. 1994 [DIRS 100486]), but poorer in sodium and potassium. This could explain the dominance of β-uranophane at the natural site, as well as the limited soddyite and weeksite occurrence. There is substantial calcite at Yucca Mountain. In time, this may make repository-alteration products conform more to the Nopal I sequence than that seen in the laboratory, which produces β-uranophane at long times.

In summary, the natural analog data builds confidence in using the base-case models for modeling fuel corrosion over extended time periods by showing that secondary-phase development in multiyear laboratory tests is similar to the alteration-phase paragenesis

determined at the uranium-bearing natural analogue sites. Similarities in the alteration phases observed in laboratory experiments to those observed in very long-term alteration of uraninite provides evidence that the overall alteration processes observed in the laboratory are similar to those likely to control alteration in the long term. Hence, the laboratory processes that provide the basis for the base-case models are likely to be relevant for describing CSNF degradation into the distant future.

7.4 VALIDATION SUMMARY

The CSNF model has been validated by applying acceptance criteria based on an evaluation of the model's relative importance to the potential performance of the repository system. All validation requirements defined in Section 2 of *Technical Work Plan for: Regulatory Integration Modeling and Analysis of the Waste Form and Waste Package* (BSC 2004 [DIRS 169944]) have been fulfilled, including corroboration of model results with experimental data, publications of refereed journals, and corroboration with alternative conceptual models. Activities required for confidence-building during model development have been satisfied. The model development activities and postdevelopment validation activities described establish the scientific basis for the CSNF models. The model validation exercises described in Sections 7.1 and 7.2 indicate the models developed for alkaline and acidic conditions are consistent with the data used for model validation and with the alternative conceptual models, although a somewhat conservative modeling bias is indicated. However, the conservative modeling bias may be larger than indicated by the validation because the CSNF data used for validation also include the radiolytic effects of short-lived β and γ radiation and because the test configurations may cause the effective surface area in the tests to be unrealistically high. Also, long-term weathering rates of minerals in general, as measured in laboratory tests, greatly exceed rates observed under natural weathering conditions (White and Brantley 2003 [DIRS 168088]). This general observation has been attributed to factors such as progressive depletion of the more energetically reactive sites, weathering conditions that approach equilibrium (i.e., minimize solution undersaturation), and effects of secondary-phase precipitates and alteration residues on the rate of mass transport to and from the corroding surfaces. These effects will also decrease the long-term oxidative dissolution rate of CSNF in the repository, but the extent of the conservative bias introduced by their omission is uncertain.

Based on this, the CSNF models used in this model report are sufficiently accurate and adequate for their intended purpose. The level of confidence required by the model's relative importance to the performance of the repository system has been met.

8. CONCLUSIONS

8.1 DEVELOPED OUTPUT - THE MODEL PARAMETER VALUES

The developed outputs from this model report are models for the instantaneous release fractions (f_i) and for the matrix fractional release rates (F_i) under acidic and basic conditions. The output also includes the model parameter values and the associated distributions that capture the assessed uncertainty in these parameters.

This report developed models, associated model parameter values, and uncertainty distributions for release of:

- Gap and grain-boundary inventory fractions of cesium, iodine, technetium, and strontium
- Fuel matrix inventory under basic and acidic conditions. An instantaneous radionuclide release rate model is to be used for any fuel that is exposed to humid air at temperatures greater than 100°C and is subsequently contacted by water.

These outputs are described below.

Model for Release of Gap and Grain-Boundary Inventory

The release of the gap and grain-boundary inventories of cesium, iodine, technetium, and strontium is modeled as an instantaneous release of the fraction (f_i) of the total inventory of each of these elements estimated to be in the gap and grain-boundary regions. The instantaneous fractional releases for ^{137}Cs, ^{129}I, ^{99}Tc, and ^{90}Sr are modeled as triangular distributions with the apex of the triangular probability distribution function located at the average release fractions shown in Table 8-1 and spanning the range shown in the last row of this table for each element.

Table 8-1. Characteristic Values of the Triangular Probability Distribution Functions for Instantaneous Fractional Releases of Cesium, Iodine, Technetium, and Strontium

	^{137}Cs	^{129}I	^{99}Tc	^{90}Sr
Average Release Fraction (%)	3.63	11.24	0.10 [a]	0.09
Range (%)	0.39 to 11.06	2.04 to 26.75	0.01[b] to 0.26	0.02 to 0.25

NOTE: [a] This value was rounded up from Table 6-2. This roundup is conservative and reasonable based on the measurement uncertainties in these very small fractions (Section 4.1.1)
[b] This value was changed to provide a nonzero minimum. This is reasonable because it is consistent with the measurement results (Section 4.1.1) and because a zero value is not physically plausible; some diffusion out of the fuel grains is expected.

Model for Release of Fuel Matrix Inventory - Alkaline Conditions

The radionuclide release rate from the CSNF matrix under alkaline conditions (pH ≥ 6.8, Section 6.4.1.3) is modeled as the fractional matrix dissolution rate (d^{-1}) with the following mathematical form:

$$\text{Log (F)} = \text{Log (A)} + a_0 + a_1 \times \text{IT} + a_2 \times pCO_3 + a_3 \times pO_2$$

This model has one dependent variable (Log (F)), three independent variables (IT, pCO_3, and pO_2), and five parameters (Log (A), a_0, a_1, a_2, and a_3) defined as follows:

Dependent Variable:

Log (F) = Base 10 log of the fractional dissolution rate of the fuel (d^{-1})

Independent Variables:

IT = Inverse temperature (K^{-1}) (i.e., IT = 1/T)
pCO_3 = Negative base 10 log of total carbonate (molar) (i.e., $pCO_3 = -\log_{10}([HCO_3^-] + [CO_3^{2-}])$)
pO_2 = Negative base 10 log of oxygen pressure (atmospheres) (i.e., $pO_2 = -\log_{10}(O_2)$)

Parameters:

Log (A) = Base 10 log of the fuel effective specific surface area (m^2/mg)
a_0, a_1, a_2, a_3 = Regression parameters for the dissolution rate per unit area

The best-estimate values and the corresponding characteristic values of the uncertainty distributions for each of the five model parameters are given in Table 8-2.

Table 8-2. Parameter Values and Associated Characteristic Values of the Uncertainty Distributions for the Alkaline Conditions Model

Model Parameter	Parameter Value	Uncertainty Distribution Characteristic Values
Log(A)	- 6.7	Triangular Distribution [a]
a_0	4.705	0.601 [b]
a_1	-1,093.826	186.829 [b]
a_2	-0.102	0.0471 [b]
a_3	-0.338	0.0506 [b]

NOTES: [a] Distribution minimum = -7.3; distribution maximum = -5.4; distribution apex = -6.7.
[b] Estimated standard errors. The uncertainties in the regression coefficients are also related through the covariance matrix provided in Appendix II.

Model for Release of Fuel Matrix Inventory - Acidic Conditions

The radionuclide release rate from the CSNF matrix under acidic conditions (pH < 6.8) is modeled as the fractional matrix dissolution rate (d^{-1}) in the following mathematical form:

$$\text{Log (F)} = \text{Log (A)} + a_0 + a_1 \cdot \text{IT} + a_3 \cdot pO_2 + a_4 \cdot \text{pH}$$

This model has one dependent variable (Log (F)), three independent variables (IT, pO_2, and pH), and five parameters (Log (A), a_0, a_1, a_3, and a_4) are defined as follows:

Dependent Variable:
Log (F) = Base 10 log of the fractional dissolution rate of the fuel (d^{-1})

Independent Variables:
IT = Inverse temperature (K^{-1}) (i.e., IT = 1/T)
pO_2 = Negative base 10 log of oxygen pressure (atmospheres) (i.e., $pO_2 = -\log_{10}(O_2)$)
pH = Negative base 10 log of the hydrogen ion concentration (molar)

Parameters:
Log (A) = Base 10 log of the fuel effective specific surface area (m^2/mg)
a_0, a_1, a_2, a_3 = model parameters

The model parameter values and the corresponding uncertainties for each of the five model parameters are given in Table 8-3.

Table 8-3. Parameter Values and Associated Characteristic Values of the Uncertainty Distribution for the Acidic Conditions Model

Model Parameter	Parameter Value	Uncertainty Distribution Characteristic Values
Log(A)	- 6.7	Triangular Distribution [a]
a_0	6.60	0.446 [b]
a_1	-1,093.826	186.829[b]
a_3	-0.338	0.0506[b]
a_4	-0.340	0.110 [b]

NOTES: [a] Distribution minimum = -7.3; distribution maximum = -5.4; distribution apex = -6.7.
[b] Estimated standard errors. The uncertainties in the regression coefficients are also related through the covariance matrix provided in Appendix II. Values for parameters a_1 and a_3 have been taken from the analysis for the alkaline conditions model and have no associated standard errors in the context of the acid conditions analysis; the standard errors obtained from the alkaline side regression analysis are used. a1 and a3 are to be considered as independent parameters (i.e., no covariance).

Model for the Radionuclide Release Rate from Fuel Exposed to Humid Air at Temperatures Greater than 100°C

An instantaneous radionuclide release-rate model is to be used for any fuel exposed to humid air at temperatures greater than 100°C and is subsequently contacted by water after the temperature drops below 100°C.

8.2 UNCERTAINTY IN THE DEVELOPED PARAMETER VALUES

As summarized in Section 8.1, this report developed values for two sets of parameters: 1) instantaneous release fractions (f_i) for cesium, iodine, technetium, and strontium, and 2) acidic and alkaline conditions (A, a_0, a_1, a_2, a_3, and a_4) used in the CSNF matrix fractional release rate models.

As described in Section 6.3.3, the instantaneous release fractions for cesium, iodine, technetium, and strontium are uncertain parameters. The uncertainty is mostly aleatory uncertainty associated with factors such as linear power history, grain size, and burnup that influence the gap and grain-boundary inventories of these elements. The available data are analyzed (Section 6.3) to determine ranges, and plausible probability distribution functions within these ranges, for the gap and grain-boundary inventory fractions (f_i). Uncertainty is represented by a probability distribution function spanning the range of the available data set (Section 6.3.3).

Uncertainties in the developed parameter values for the base-case model for the CSNF matrix fractional release rate include: those in the mathematical form of the model that may influence the validity of long-term extrapolations, those in the model's parameter values derived from uncertainties in the empirical data from which these parameters are taken (i.e., epistemic uncertainties), and those associated with the variability in the properties of CSNF and the extent to which these are adequately represented by the test materials from which the input data (Section 4.1) are obtained (i.e., aleatory uncertainties).

Uncertainties in the mathematical form of the base-case model and in its validity over the extended time domain of application are addressed by discussing the model's consistency with current understanding of the mechanism for the process (referred to as oxidative dissolution) that degrade the fuel under the range of plausible exposure conditions. Comparison of the base-case model with the mechanistically based alternative models provides confidence that the empirically based modeling approach is indeed appropriate for use in long-term predictions.

As discussed in Section 1, the parameters in the base-case model for the radionuclide fractional release rate from the CSNF matrix are: (1) effective specific surface area (i.e., the surface area per unit mass) of the fuel (A); and (2) parameters a_0, a_1, a_2, a_3, and a_4, which express the dependence of the CSNF matrix oxidative dissolution rate on environmental factors (temperature, dissolved oxygen concentration, carbonate–bicarbonate concentration, and pH). Uncertainties in a_0, a_1, a_2, a_3, and a_4 are represented as characteristic values of probability distributions associated with the parameter values obtained from the regression analyses described in Sections 6.4.1.2 and 6.4.1.3, and summarized in Tables 8-2 and 8-3. The values and associated uncertainties for the CSNF-specific surface-area parameter (A) are discussed in Section 6.4.1.5.

The developed parameter values and the associated uncertainty distributions are summarized in Table 8-4. The model validation exercises described in Sections 7.1 and 7.2 indicate that the models developed for alkaline and acidic conditions are consistent with the data used for model validation and with the alternative conceptual models, although a somewhat conservative modeling bias is indicated. However, the conservative modeling bias may be larger than indicated by the validation because the CSNF data used for validation also include the radiolytic effects of short-lived β and γ radiation and because the test configurations may cause the effective surface area in the tests to be unrealistically high. Also, long-term weathering rates of minerals in general, as measured in laboratory tests, greatly exceed rates observed under natural weathering conditions (White and Brantley 2003 [DIRS 168088]). This general observation has been attributed to factors such as progressive depletion of the more energetically reactive sites, weathering conditions that approach equilibrium (i.e., minimize solution undersaturation), and effects of secondary phase precipitates and alteration residues on the rate of mass transport to and from the corroding surfaces. These effects will also decrease the long-term oxidative dissolution rate of CSNF in the repository.

Because the models developed in this report are largely empirical, the domain of application should be restricted to the range of qualified experimental data used for the model development and validation. The range of the input data spans CSNF with burnup from 15 to 65 MWd/kgU and percent fission gas release from 1 percent to 18 percent. It also spans pH values down to 2 and up to 10.3, temperatures from 25°C to 90°C, oxygen partial pressure from 0.002 to 0.2 atmospheres, and carbonate–bicarbonate concentrations from 0 to 2×10^{-2} molar. Based on the discussion in Section 6.4.1.3, a value of 2×10^{-4} molar is to be used for modeling CSNF degradation under alkaline conditions when the in-package chemistry model calculates a total carbonate molar concentration less than 2×10^{-4} molar. Because the temperature dependence of the rate is adequately described by the Arrhenius form of the temperature dependence used in the base-case model and because it is unlikely that the mechanism controlling the rate of the oxidative dissolution process will change between 90°C and 100°C, the upper end of the temperature range can be extended to 100°C. An instantaneous radionuclide release rate model is to be used for any fuel exposed to humid air at temperatures greater than 100°C and is subsequently contacted by water after the temperature drops below 100°C.

Table 8-4. Summary of Output Developed in This Model Report

Output Name	Output Description	Output Uncertainty		
		Sources of Uncertainty	Uncertainty Distribution	Characteristic Values
Instantaneous release fractions (f_i)	Probability distribution functions for the instantaneous release fractions for ^{137}Cs, ^{129}I, ^{99}Tc, and ^{90}Sr	Principally variability (aleatory uncertainty) in the input data	Triangular centered at the data mean and spanning the range of the input data	Table 8-1 for average and range maximum and minimum values
(F) Fractional radionuclide release rate from the CSNF matrix – alkaline conditions; parameters (a_0, a_1, a_2, a_3)	Values and standard errors for each of these parameters	Uncertainties in the input flow-through data set (Sections 4.1.2 and 6.4.1.1) and in the form of the model	Normal	Standard errors in Table 8-2 Covariance matrix in Appendix II
(F) Fractional radionuclide release rate from the CSNF matrix – acidic conditions; parameters (a_0, a_1, a_3, a_4)	Values and standard errors for each of these parameters	Uncertainties in the input flow-through data for acidic conditions (Sections 4.1.2 and 6.4.1.1) and in the form of acid-side model	Normal	Standard errors Table 8-3 Covariance matrix in Appendix II
Effective specific surface area of corroding CSNF (A)	Probability distribution function for the log of the estimated specific surface area (A)	Uncertainties in the input data set (Sections 4.1.3) and evolution of (A) as CSNF corrodes (Section 6.4.1.5)	Triangular	Characteristic values of the triangular distribution in Tables 8-2 and 8-3

NOTE: All data in this table is contained in Output DTN: MO0404ANLSF001.001.

8.3 YUCCA MOUNTAIN REVIEW PLAN ACCEPTANCE CRITERIA

Yucca Mountain Review Plan, Final Report (YMRP) (NRC 2003 [DIRS 163274]) contains acceptance criteria intended to establish the basis for the review of the material contained in the license application. As this model report serves, in part, as the basis for the license application, it is important to show how the information contained herein addresses each of the applicable YMRP acceptance criteria.

YMRP acceptance criteria applicable to this report are identified in *Technical Work Plan for: Regulatory Integration Modeling and Analysis of the Waste Form and Waste Package* (BSC 2004 [DIRS 169944], Table 3-1). Each applicable criterion is quoted in italics, followed by pointers to where within the report the information addressing the criterion can be found. In some cases, the criterion is only partially addressed. A demonstration of full compliance requires a review of multiple reports.

8.3.1 System Description and Demonstration of Multiple Barriers

The CSNF waste form meets the definition of a barrier in 10 CFR 63.2 [DIRS 156605]. The following Acceptance Criteria can be found in Section 2.2.1.1.3 of *Yucca Mountain Review Plan, Final Report* (NRC 2003, [DIRS 163274]).

Acceptance Criterion 1—Identification of Barriers Is Adequate

> *Barriers relied on to achieve compliance with 10 CFR 63.113(b), as demonstrated in the total system performance assessment, are adequately identified, and are clearly linked to their capability.*

The CSNF barrier functions of limiting radionuclide release are addressed throughout this document and, more specifically, in Section 6.4.3.

Acceptance Criterion 2—Description of Barrier Capability to Isolate Waste Is Acceptable

> *The capability of the identified barriers to prevent or substantially reduce the rate of movement of water or radionuclides from the Yucca Mountain repository to the accessible environment, or prevent the release or substantially reduce the release rate of radionuclides from the waste is adequately identified and described:*
>
> *(1) The information on the time period over which each barrier performs its intended function, including any changes during the compliance period, is provided;*
>
> *(2) The uncertainty associated with barrier capabilities is adequately described;*
>
> *(3) The described capabilities are consistent with the results from the total system performance assessment; and*
>
> *(4) The described capabilities are consistent with the definition of a barrier at 10 CFR 63.2.*

The capability of CSNF to reduce radionuclide release rate after a hypothetical failure of the waste package and fuel rod cladding is identified and described throughout this report; the models developed to describe this capability are summarized in Section 8.1. Uncertainties associated with the CSNF barrier's capabilities to perform its intended function are addressed in Sections 8.1 and 8.2. The CSNF models and their associated uncertainties are consistent with the models used in TSPA-LA.

Acceptance Criterion 3—Technical Basis for Barrier Capability Is Adequately Presented

> *The technical bases are consistent with the technical basis for the performance assessment. The technical basis for assertions of barrier capability is commensurate with the importance of each barrier's capability and the associated uncertainties.*

The technical bases for the CSNF's capabilities to perform its intended function of limiting radionuclide release are addressed throughout this document and, more specifically, in Section 6.2. The technical bases are consistent with the corresponding technical bases in performance assessment because the CSNF models are used as input to TSPA-LA.

8.3.2 Degradation of Engineered Barriers

The following Acceptance Criteria can be found in Section 2.2.1.3.1.3 of *Yucca Mountain Review Plan, Final Report* (NRC 2003, [DIRS 163274]).

Acceptance Criterion 1—System Description and Model Integration are Adequate

> *(1) TSPA adequately incorporates important design features, physical phenomena and couplings and uses consistent assumptions throughout the degradation of engineered barriers abstraction process;*

The appropriate design features and applicable physical phenomena, as well as environmental factors and their coupling are addressed in Section 6.2.

> *(2) Abstraction uses assumptions, technical bases, data and models that are appropriate and consistent with [those used] in other abstractions.*

Throughout this report, the performed analyses use assumptions, technical bases, input data, and models that appropriately reflect the design and contents of the waste form and the humid-air and groundwater media that may come in contact with the waste form. The assumptions are addressed in Section 5. The data, technical bases, and models are addressed in Sections 4.1 and 6. This information is used in a manner that is consistent with other abstractions of processes associated with the degradation of the CSNF waste form.

> *(3) The descriptions of the engineered barriers, design features, degradation processes, physical phenomena, and couplings that may affect the degradation of the engineered barriers are adequate.*

Detailed descriptions of the relevant CSNF design features and degradation processes (Sections 6.2.1 and 6.2.2), and the physical phenomena and their couplings that may affect the CSNF degradation (Sections 6.2.2 and 6.2.3) are provided.

> *(4) Initial and boundary conditions are propagated consistently throughout the abstraction process.*

The CSNF initial (Section 6.2.1) and relevant environmental boundary conditions for the performed analyses (Section 6.2) are described and used in developing the CSNF degradation and radionuclide release models.

> *(5) Sufficient technical basis for the inclusion and exclusion of FEPs are provided;*

The features, events, and processes (FEPs) relevant to assessing CSNF degradation and radionuclide release are identified and discussed in Section 6.2. The technical bases for the included FEPs are described in Sections 6.2.1 and 6.2.2. Section 6.2.3 indicates that two FEPs are included and Table 6-1 provides an explanation of this decision. A listing of excluded FEPs, including the technical bases for the exclusion decisions, is provided in *Miscellaneous Waste Form FEPs* (BSC 2004 [DIRS 163116]).

> *(6) ...*

Not applicable to this report.

> *(7) Guidance in NUREG 1297 and NUREG 1298 [re: Expert Elicitation] are followed.*

Not applicable to this report because expert elicitation is not used.

Acceptance Criterion 2—Data Are Sufficient for Model Justification

> *(1) Parameters used to evaluate the degradation of EBS are adequately justified;*

The input data and parameters used for the performance of the CSNF waste form degradation model come, primarily, from laboratory experiments and tests performed for the project (Section 4.1), and technical or scientific reports and papers (Sections 6 and 7).

Justification for the use of specific data is typically provided in the section in which the data are initially discussed (Section 4.1) and used (Sections 6.2, 6.3, and 7.1).

> *(2) Sufficient data have been collected to establish initial and boundary conditions;*

Extensive scientific investigations and experiments have been performed by the project to develop the data necessary to support the analyses provided in this report (Sections 4.1 and 6.2). All initial and boundary conditions are adequately and appropriately established and justified.

> *(3) Data on the degradation of the engineered barriers (e.g. – general and localized corrosion, microbially induced corrosion, galvanic interactions, hydrogen embrittlement and phase stability) are based on laboratory measurements, site-specific field measurements, industrial and/or natural analogs and tests designed to replicate anticipated conditions. As appropriate, sensitivity or uncertainty analyses are provided and are shown to be adequate.*

Data related to the various potential degradation modes for the CSNF waste form are discussed in detail in Section 6.2.2.

> *(4) Degradation models for the applicable processes are adequate. For example, general and localized corrosion, microbially induced corrosion, galvanic interactions, hydrogen embrittlement and phase stability are given appropriate consideration and treatment.*

The various models related to the potential degradation modes for the CSNF waste form are discussed in detail throughout this report. Specifically, the conceptual basis for assessing the progression of fuel rod degradation following initial breaching of the cladding is discussed in Section 6.2, modeling of the instantaneous release fractions is discussed in Section 6.3, and modeling of the CSNF matrix fractional release rates is addressed in Sections 6.4.1 and 6.4.2.

Acceptance Criterion 3—Data Uncertainty is Characterized and Propagated through the Model Abstraction

> *(1) Models use parameter values, assumed ranges, probability distributions and/or bounding assumptions that are technically defensible, reasonably account for uncertainties and variabilities, and do not result in under-representation of the risk estimate.*

Each of the models developed in this report use parameter values, assumed ranges, probability distributions or bounding, or both assumptions that are technically defensible, reasonably account for uncertainties and variabilities, and do not result in underrepresentation of the risk estimate. In each situation, discussion and consideration of the uncertainties associated with specific data are addressed in detail. The effects of data uncertainties on the parameter ranges and uncertainty distributions in the instantaneous radionuclide release and matrix release rate models are discussed in Sections 6.3 and 6.4, respectively.

> *(2) Appropriate parameters, based on techniques that may include laboratory experiments, field measurements, and industrial analogs are used.*

The various models addressed in this report use data and parameters that were developed based on laboratory experiments (Sections 4.1, 6.3.1, and 6.4.1). Sections 7.1 and 7.3 use peer-reviewed and industrial literature and relevant natural analog data for model validation.

> *(3) Assumed range of values and probability distributions for parameters used in conceptual and process-level models are not likely to underestimate the actual degradation and failure of engineered barriers.*

In those instances where uncertainties exist regarding the range of values and probability distributions, care is taken to choose values anticipated to provide conservative results (Sections 6.3 and 6.4). As discussed in Section 8.2, model validation results indicate a conservative modeling bias.

> *(4) ...*

Not applicable; no NDE of CSNF waste form materials was involved with the development of this model report.

> *(5) Where sufficient data do not exist, the definition of parameter values and conceptual models is based on appropriate use of other sources, such as expert elicitation.*

The available data is generally sufficient to support the definition of parameter values and CSNF conceptual models. As described in Section 5, appropriate and conservative assumptions are used in a few instances where sufficient data are not available.

Acceptance Criterion 4—Model Uncertainty is Characterized and Propagated Through the Model Abstraction

> *(1) Alternative modeling approaches are considered and are consistent with available data and current scientific understanding.*

Alternative modeling approaches consistent with available data and current scientific understanding are considered and discussed in Section 6.4.2. Although these alternative models are screened out for use in TSPA-LA (Section 6.4.2.3), they are used for model validation in Section 7.2.

> *(2) Consideration of conceptual model uncertainty is consistent with available site characterization data, laboratory experiments, ... and the treatment of uncertainty does not result in under-estimation of the risk estimate.*

Consideration of uncertainties in the models used in this report is an integral part of the model development and validation processes. Conceptual model uncertainty is consistent with the information that has been developed through laboratory experiments (Sections 6 and 7). Care to ensure the treatment of uncertainty does not result in underestimation of the risk estimate is taken. As discussed in Section 8.2, model validation results indicate a somewhat conservative modeling bias.

> *(3) Alternative modeling approaches, consistent with available data and current scientific understanding, are used and the modeling results are evaluated using tests that are sensitive to the processes modeled.*

Alternative modeling approaches, consistent with available data and current scientific understanding, are considered (Section 6.4.2). In all instances, it is determined that the base case model provides a more credible modeling basis than would be achieved by using the alternative models. Thus, although due consideration is given to the use of alternative modeling approaches, no alternative models are used in TSPA-LA. Model validation includes comparison with the alternative models (Section 7.2).

Acceptance Criterion 5—Model Abstraction Output Is Supported By Objective Comparisons

> *(1) Models implemented in this total system performance assessment abstraction provide results consistent with output from detailed process-level models and or empirical observations (laboratory and field testing, and/or natural analogs).*

Results of CSNF degradation models implemented in this total system performance assessment abstraction are compared with empirical observations (laboratory and natural analogs) as part of the model validation (Sections 7.1 and 7.3).

(2) ...

Not applicable; this report includes no numerical models.

(3) Evidence is sufficient to show that models will not underestimate the actual degradation and failure of engineered barriers.

In those instances where there is doubt about the appropriateness or accuracy of the models or data, care is taken to select a conservative approach or conservative data that would result in an overestimation of risk. Model validation results indicate that this approach results in a somewhat conservative modeling bias (Section 8.2).

(4) Mathematical degradation models are based on the same environmental parameters, material factors, assumptions and approximations shown to be appropriate for closely analogous applications.

The testing of irradiated spent fuel samples for degradation mechanisms and effects has a long history that has led to the establishment of well-accepted methodologies and understanding of the processes that control the CSNF degradation and radionuclide release processes. As a result, models are based on the same environmental parameters, material factors, assumptions, and approximations appropriate for closely analogous applications (Section 6.2).

(5) Accepted and well documented procedures are used to construct and test the numerical models that simulate the EB chemical environment and degradation of EB;

The development and testing of the models used to simulate the CSNF degradation and radionuclide release, is performed in accordance with previously established well-documented Yucca Mountain project procedures based on industry established norms. These procedures also establish the appropriate Quality Assurance requirements for such activities and appropriate checking, auditing, and other activities performed to ensure the adequacy and appropriateness of the models (Section 2).

(6) ...

Not applicable to the scope of this model report.

8.3.3 Radionuclide Release Rates and Solubility Limits

The following Acceptance Criteria can be found in Section 2.2.1.3.4.3 of *Yucca Mountain Review Plan, Final Report* (NRC 2003, [DIRS 163274]).

Acceptance Criterion 1—System Description and Model Integration Are Adequate

(1) ...

Not Applicable.

(2) The abstraction of radionuclide release rates and solubility limits uses assumptions, technical bases, data, and models that are appropriate and consistent with other related U.S. Department of Energy abstractions. For example, the assumptions used for this model abstraction are consistent with the abstractions of "Degradation of Engineered Barriers" (Section 2.2.1.3.1); "Mechanical Disruption of Waste Packages" (Section 2.2.1.3.2); "Quantity and Chemistry of Water Contacting Waste Packages and Waste Forms" (Section 2.2.1.3.3); "Climate and Infiltration" (Section 2.2.1.3.5); and "Flow Paths in the Unsaturated Zone" (Section 2.2.1.3.6). The descriptions and technical bases provide transparent and traceable support for the abstraction of radionuclide release rates and solubility limits;

The CSNF degradation rate abstraction model is developed in Sections 6.3 and 6.4 from inputs in Section 4.1.

(3) The abstraction of radionuclide release rates and solubility limits provides sufficient, consistent design information on waste packages and engineered barrier systems. For example, inventory calculations and selected radionuclides are based on the detailed information provided on the distribution (both spatially and by compositional phase) of the radionuclide inventory, within the various types of high-level radioactive waste;

The CSNF degradation model reflects detailed information on distribution of radionuclide inventory within the CSNF in Sections 4.1.1, 6.2, and 6.3.

(4) The U.S. Department of Energy reasonably accounts for the range of environmental conditions expected inside breached waste packages and in the engineered barrier environment surrounding the waste package. For example, the U.S. Department of Energy should provide a description and sufficient technical bases for its abstraction of changes in hydrologic properties in the near field, caused by coupled thermal-hydrologic-mechanical-chemical processes;

The CSNF degradation model considers dripping and humid-air conditions within the breached waste package. It covers the expected range of pH, temperature, and carbonate concentrations as described in Sections 1 and 6.

(5) The description of process-level conceptual and mathematical models is sufficiently complete, with respect to thermal-hydrologic processes affecting radionuclide release from the emplacement drifts. For example, if the U.S. Department of Energy uncouples coupled processes, the demonstration that uncoupled model results bound predictions of fully coupled results is adequate;

The CSNF degradation model is temperature dependent and coupled to the thermal-hydrologic processes within the TSPA-LA model.

(6) Technical bases for inclusion of any thermal-hydrologic-mechanical-chemical couplings and features, events, and processes in the radionuclide release rates and solubility limits model abstraction are adequate. For example, technical

bases may include activities, such as independent modeling, laboratory or field data, or sensitivity studies;

The CSNF degradation model is temperature and chemistry dependent and coupled to these processes within the TSPA-LA model. The thermal and chemistry dependence of the model is based on laboratory testing described in Section 4 and validated with testing described in Section 7.

(7-8) ...

Not Applicable.

Acceptance Criterion 2—Data Are Sufficient for Model Justification

(1) Geological, hydrological, and geochemical values used in the license application are adequately justified. Adequate description of how the data were used, interpreted, and appropriately synthesized into the parameters is provided;

The CSNF degradation model receives hydrologic and geochemical information from other models where that information is justified. The CSNF degradation model is designed to cover the full range of hydrologic and geochemical conditions to which it is sensitive.

(2) Sufficient data have been collected on the characteristics of the natural system and engineered materials to establish initial and boundary conditions for conceptual models and simulations of thermal-hydrologic-chemical coupled processes. For example, sufficient data should be provided on design features, such as the type, quantity, and reactivity of materials, that may affect radionuclide release for this abstraction;

Extensive data have been collected to develop and validate the semi-empirical model for the CSNF degradation model, as described in Sections 4 and 7.

(3) ...

Not Applicable.

(4) The corrosion and radionuclide release testing program for high-level radioactive waste forms intended for disposal provides consistent, sufficient, and suitable data for the in-package and in-drift chemistry used in the abstraction of radionuclide release rates and solubility limits. For expected environmental conditions, the U.S. Department of Energy provides sufficient justification for the use of test results, not specifically collected from the Yucca Mountain site, for engineered barrier components, such as high-level radioactive waste forms, drip shield, and backfill.

The first sentence in this criterion, which addresses in-package and in-drift chemistry, is not applicable to this modeling report. The CSNF degradation model does not directly use any test results not specifically collected for the YMP.

Acceptance Criterion 3—Data Uncertainty Is Characterized and Propagated Through the Model Abstraction

> *(1) Models use parameter values, assumed ranges, probability distributions, and bounding assumptions that are technically defensible, reasonably account for uncertainties and variabilities, and do not result in an under-representation of the risk estimate;*

Data uncertainty is described in Sections 4.1, 6.3.1, and 6.3.3. Propagation of this uncertainty is discussed in Section 6.4.1. Section 7 discusses how the model is reasonable or conservative, or both.

> *(2) Parameter values, assumed ranges, probability distributions, and bounding assumptions used in the abstractions of radionuclide release rates and solubility limits in the total system performance assessment are technically defensible and reasonable based on data from the Yucca Mountain region, laboratory tests, and natural analogs. For example, parameter values, assumed ranges, probability distributions, and bounding assumptions adequately reflect the range of environmental conditions expected inside breached waste packages;*

The CSNF degradation model receives hydrologic and geochemical information from other models where that information is justified. As stated in Section 1, the CSNF degradation model is designed to cover the full range of hydrologic and geochemical conditions to which it is sensitive: pH 2 to 10.3, oxygen partial pressure from 0.002 to 0.2 atmospheres, and carbonate–bicarbonate concentrations from 0 to 2×10^{-2} molar. The model is based on laboratory data collected for the Yucca Mountain Project as described in Section 4.1.

> *(3) The U.S. Department of Energy uses reasonable or conservative ranges of parameters or functional relations to determine effects of coupled thermal-hydrologic-chemical processes on radionuclide release. These values are consistent with the initial and boundary conditions and the assumptions for the conceptual models and design concepts for natural and engineered barriers at the Yucca Mountain site. If any correlations between the input values exist, they are adequately established in the total system performance assessment. For example, estimations are based on a thermal loading and ventilation strategy; engineered barrier system design (including drift liner, backfill, and drip-shield); and natural system masses and fluxes that are consistent with those used in other abstractions;*

The CSNF degradation model receives hydrologic and geochemical information from other models where that information is justified. As stated in Section 1, the CSNF model is designed to cover the full range of hydrologic and geochemical conditions to which it is sensitive: pH 2 to 10.3, oxygen partial pressure from 0.002 to 0.2 atmospheres, and carbonate–bicarbonate concentrations from 0 to 2×10^{-2} molar.

> *(4) Uncertainty is adequately represented in parameter development for conceptual models, process models, and alternative conceptual models*

considered in developing the abstraction of radionuclide release rates and solubility limits, either through sensitivity analyses or use of bounding analyses;

Uncertainty is addressed in Sections 8.2 and 8.3.

(5-7) ...

Not Applicable.

(8) The U.S. Department of Energy adequately considers the uncertainties, in the characteristics of the natural system and engineered materials, such as the type, quantity, and reactivity of material, in establishing initial and boundary conditions for conceptual models and simulations of thermal-hydrologic-chemical coupled processes that affect radionuclide release; and

Uncertainty is addressed in Sections 8.2 and 8.3.

(9) ...

Not Applicable.

Acceptance Criterion 4—Model Uncertainty Is Characterized and Propagated Through the Model Abstraction

(1) Alternative modeling approaches of features, events, and processes are considered and are consistent with available data and current scientific understanding, and the results and limitations are appropriately considered in the abstraction;

Alternative modeling approaches are discussed in Section 6.4.2 and compared to the base-case modeling approach in Section 7.2.

(2) In considering alternative conceptual models for radionuclide release rates and solubility limits, the U.S. Department of Energy uses appropriate models, tests, and analyses that are sensitive to the processes modeled for both natural and engineering systems. Conceptual model uncertainties are adequately defined and documented, and effects on conclusions regarding performance are properly assessed. For example, in modeling flow and radionuclide release from the drifts, the U.S. Department of Energy represents significant discrete features, such as fault zones, separately, or demonstrates that their inclusion in the equivalent continuum model produces a conservative effect on calculated performance; and

In the consideration of alternative conceptual models (Section 6.4.2), appropriate models, tests, and analyses sensitive to the processes modeled for natural and engineering systems are used. Conceptual model uncertainties are adequately defined and documented, and effects on conclusions regarding performance are properly assessed. Although alternative conceptual models are considered, it is determined that the baseline model is more appropriate and the considered alternative conceptual models are not used in TSPA-LA (Section 6.4.2). Comparison of the base-case model to the alternative models in Section 7.2 shows good agreement.

(3) Consideration of conceptual model uncertainty is consistent with available site characterization data, laboratory experiments, field measurements, natural analog information and process-level modeling studies; and the treatment of conceptual model uncertainty does not result in an under-representation of the risk estimate; and

The good agreement between the CSNF degradation rate results obtained using different conceptual models (Section 7.2) indicates that conceptual model uncertainty does not result in underrepresentation of the CSNF contribution to risk estimates.

(4) The effects of thermal-hydrologic-chemical coupled processes that may occur in the natural setting, or from interactions with engineered materials, or their alteration products, on radionuclide release, are appropriately considered.

Appropriate consideration is given to the effects of thermal-hydrologic-chemical coupled processes that may occur in the natural setting, or from interactions with engineered materials, or their alteration products, on radionuclide release. Related features, events, and processes are discussed in Section 6.2.3. Alternative conceptual models are discussed in Section 6.4.2.

Acceptance Criterion 5—Model Abstraction Output Is Supported by Objective Comparisons

(1) The models implemented in this total system performance assessment abstraction provide results consistent with output from detailed process-level models and/or empirical observations (laboratory and field testings and/or natural analogs);

Comparison with laboratory testing, other process-level models, and natural analogs are described in Sections 7.1, 7.2, and 7.3.

(2) ...

Not Applicable.

(3) The U.S. Department of Energy adopts well-documented procedures that have been accepted by the scientific community to construct and test the numerical models, used to simulate coupled thermal-hydrologic-chemical effects on radionuclide release. For example, the U.S. Department of Energy demonstrates that the numerical models used for high-level radioactive waste degradation and dissolution, and radionuclide release from the engineered barrier system, are adequate representations; include consideration of uncertainties; and are not likely to underestimate radiological exposures to the reasonably maximally exposed individual and releases of radionuclides into the accessible environment; and

The CSNF degradation model is developed using ASTM C1174-97 [DIRS 105725].

(4) ...

Not Applicable.

INTENTIONALLY LEFT BLANK

9. INPUTS AND REFERENCES

9.1 DOCUMENTS CITED

101530 Aagaard, P. and Helgeson, H.C. 1982. "Thermodynamic and Kinetic Constraints on Reaction Rates Among Minerals and Aqueous Solutions. I. Theoretical Considerations." *American Journal of Science*, *282*, (3), 237-285. New Haven, Connecticut: Yale University. TIC: 225516.

117653 Aronson, S. 1958. "Oxidation of UO_2 in Water Containing Oxygen." In *Bettis Technical Review, Reactor Metallurgy*. 14th Edition. WAPD-BT-10. TID-4500. Pittsburgh, Pennsylvania: Westinghouse Electric Corporation, Bettis Atomic Power Division. ACC: NNA.19911025.0062.

109194 Barner, J.O. 1985. *Characterization of LWR Spent Fuel MCC-Approved Testing Material–ATM-101*. PNL-5109, Rev. 1. Richland, Washington: Pacific Northwest Laboratory. TIC: 240883.

163824 BSC (Bechtel SAIC Company) 2003. *CSNF Waste Form Degradation: Summary Abstraction.* ANL-EBS-MD-000015 REV 01. Las Vegas, Nevada: Bechtel SAIC Company. ACC: DOC.20030708.0004.

161962 BSC 2003. *In-Package Chemistry Abstraction*. ANL-EBS-MD-000037 REV 02. Las Vegas, Nevada: Bechtel SAIC Company. ACC: DOC.20030723.0003.

168796 BSC 2003. *Risk Information to Support Prioritization of Performance Assessment Models*. TDR-WIS-PA-000009 REV 01 ICN 01, with errata. Las Vegas, Nevada: Bechtel SAIC Company. ACC: MOL.20021017.0045; DOC.20031014.0003.

163116 BSC 2004. *Miscellaneous Waste-Form FEPs*. ANL-WIS-MD-000009 REV 01. Las Vegas, Nevada: Bechtel SAIC Company. ACC: DOC.20040421.0005.

169944 BSC 2004. *Technical Work Plan for: Regulatory Integration Modeling and Analysis of the Waste Form and Waste Package*. TWP-WIS-MD-000009 REV 00. Las Vegas, Nevada: Bechtel SAIC Company. ACC: DOC.20040616.0006.

112904 Buck, E.C.; Wronkiewicz, D.J.; Finn, P.A.; and Bates, J.K. 1997. "A New Uranyl Oxide Hydrate Phase Derived from Spent Fuel Alteration." *Journal of Nuclear Materials, 249*, (1), 70-76. Amsterdam, The Netherlands: Elsevier. TIC: 234844.

166275 Canori, G.F. and Leitner, M.M. 2003. *Project Requirements Document*. TER-MGR-MD-000001 REV 02. Las Vegas, Nevada: Bechtel SAIC Company. ACC: DOC.20031222.0006.

162386 Casas, I.; Giménez, J.; Martí, V.; Torrero, M.E.; and de Pablo, J. 1994. "Kinetic Studies of Unirradiated UO_2 Dissolution Under Oxidizing Conditions in Batch and Flow Experiments." *Radiochimica Acta, 66/77*, 23-27. München, Germany: R. Oldenbourg Verlag. TIC: 254041.

162387 Christensen, H. and Sunder, S. 2000. "Current State of Knowledge of Water Radiolysis Effects on Spent Nuclear Fuel Corrosion." *Nuclear Technology, 131*, (1), 102-123. La Grange Park, Illinois: American Nuclear Society. TIC: 254040.

131861 CRWMS M&O (Civilian Radioactive Waste Management System Management and Operations) 2000. *Commercial Spent Nuclear Fuel Degradation in Unsaturated Drip Tests*. Input Transmittal WP-WP-99432.T. Las Vegas, Nevada: CRWMS M&O. ACC: MOL.20000107.0209.

149230 CRWMS M&O 2000. *Clad Degradation - Dry Unzipping*. ANL-EBS-MD-000013 REV 00. Las Vegas, Nevada: CRWMS M&O. ACC: MOL.20000503.0200.

162406 Cunnane, J.; Ebert, W.; Goldberg, M.; Finch, R.; and Mertz, C. 2003. *Yucca Mountain Project Report, Waste Form Testing Work*. Argonne, Illinois: Argonne National Laboratory, Chemical Technology Division. ACC: MOL.20030630.0418.

164019 Dehaudt, P. 2001. "Physical and Chemical State of the Nuclear Spent Fuel After Irridiation." Section 5.2 of *Synthesis on the Long Term Behavior of the Spent Nuclear Fuel*. Poinssot, C., ed. CEA-R-5958(E). Volume I. Paris, France: Commissariat à l'Énergie Atomique. TIC: 253976.

164037 Dehaudt, P. 2001. "State of the Art of the Oxidation of Spent Nuclear Fuel." Section 7.2 of *Synthesis on the Long Term Behavior of the Spent Nuclear Fuel*. Poinssot, C., ed. CEA-R-5958(E). Volume II. Paris, France: Commissariat à l'Énergie Atomique. TIC: 253976.

162388 de Pablo, J.; Casas, I.; Giménez, J.; Molera, M.; Rovira, M.; Duro, L.; and Bruno, J. 1999. "The Oxidative Dissolution Mechanism of Uranium Dioxide. I. The Effect of Temperature in Hydrogen Carbonate Medium." *Geochimica et Cosmochimica Acta, 63,* (19-20), 3097-3103. New York, New York: Pergamon. TIC: 254443.

171386 DOE (U.S. Department of Energy) 2004. *Quality Assurance Requirements and Description.* DOE/RW-0333P, Rev. 16. Washington, D.C.: U.S. Department of Energy, Office of Civilian Radioactive Waste Management. ACC: DOC.20040823.0004.

126446 Einziger, R.E.; Marschman, S.C.; and Buchanan, H.C. 1991. "Spent-Fuel Dry-Bath Oxidation Testing." *Nuclear Technology, 94*, 383-393. Hinsdale, Illinois: American Nuclear Society. TIC: 246459.

127332 Finch, R.J.; Buck, E.C.; Finn, P.A.; and Bates, J.K. 1999. "Oxidative Corrosion of Spent UO_2 Fuel in Vapor and Dripping Groundwater at 90°C." *Scientific Basis for Nuclear Waste Management XXII, Symposium held November 30-December 4, 1998, Boston, Massachusetts, U.S.A*. Wronkiewicz, D.J. and Lee, J.H., eds. *556*, 431-438. Warrendale, Pennsylvania: Materials Research Society. TIC: 246426.

123134 Forsyth, R. 1997. *The SKB Spent Fuel Corrosion Program. An Evaluation of Results from the Experimental Programme Performed in the Studsvik Hot Cell Laboratory*.

SKB TR-97-25. Stockholm, Sweden: Svensk Kärnbränsleförsörjning A.B. TIC: 246406.

120955 Forsyth, R.S.; Werme, L.O.; and Bruno, J. 1986. "The Corrosion of Spent UO_2 Fuel in Synthetic Groundwater." *Journal of Nuclear Materials, 138*, 1-15. Amsterdam, The Netherlands: Elsevier. TIC: 246407.

162410 Goldberg, M. 2003. *Rod Segment Test Data Report, CSNF Degradation Model: Q Data Input from ANL Testing*. Task Number: PAWC1M5. Argonne, Illinois: Argonne National Laboratory, Chemical Engineering Division. ACC: MOL.20030627.0221.

113233 Grambow, B. 1989. *Spent Fuel Dissolution and Oxidation: An Evaluation of Literature Data*. SKB TR-89-13. Stockholm, Sweden: Svensk Kärnbränsleförsörjning A.B. TIC: 208579.

162391 Grambow, B.; Loida, A.; Martinez-Esparza, A.; Diaz-Arocas, P.; de Pablo, J.; Paul, J.L.; Marx, G.; Glatz, J.P.; Lemmens, K.; Ollila, K.; and Christensen, H. 2000. "Long-Term Safety of Radioactive Waste Disposal: Source Term for Performance Assessment of Spent Fuel as a Waste Form, Final Report." *Forchungszentrum Karlsruhe, Technik und Umwelk, FZKA 6420*. Karlsruhe, Germany: Forschungszentrum Karlsruhe GmbH. TIC: 254058.

113255 Grandstaff, D.E. 1976. "A Kinetic Study of the Dissolution of Uraninite." *Economic Geology and the Bulletin of The Society of Economic Geologists, 71*, (8), 1493-1506. El Paso, Texas: Economic Geology Publishing. TIC: 246339.

121407 Gray, W.J. 1999. "Inventories of Iodine-129 and Cesium-137 in the Gaps and Grain Boundaries of LWR Spent Fuels." *Scientific Basis for Nuclear Waste Management XXII, Symposium held November 30-December 4, 1998, Boston, Massachusetts, U.S.A*. Wronkiewicz, D.J. and Lee, J.H., eds. *556*, 487-494. Warrendale, Pennsylvania: Materials Research Society. TIC: 246426.

170109 Gray, W.J.;Steward, S.A.;Tait, J.C.;Shoesmith, D.W. 1994. "Interlaboratory Comparison of UO_2 Dissolution Rates" International Conference on High Level Radioactive Waste Management (5th : 1994 : Las Vegas, Nev.), UCRL-JC-115356. TIC: 210975

162393 Gray, W.J.; Strachan, D.M.; and Wilson, C.N. 1992. "Gap and Grain-Boundary Inventories of Cs, Tc and Sr in Spent LWR Fuel." *Scientific Basis for Nuclear Waste Management XV, Symposium held November 4-7, 1991, Strasbourg, France*. Sombret, C.G., ed. *257*, 353-360. Pittsburgh, Pennsylvania: Materials Research Society. TIC: 204618.

100758 Gray, W.J. and Wilson, C.N. 1995. *Spent Fuel Dissolution Studies FY 1991-1994*. PNL-10450. Richland, Washington: Pacific Northwest Laboratory. ACC: MOL.19960802.0035.

101671 Grenthe, I.; Fuger, J.; Konings, R.J.M.; Lemire, R.J.; Muller, A.B.; Nguyen-Trung, C.; and Wanner, H. 1992. *Chemical Thermodynamics of Uranium*. Volume 1 of *Chemical Thermodynamics*. Wanner, H. and Forest, I., eds. Amsterdam, The Netherlands: North-Holland Publishing Company. TIC: 224074.

109206 Guenther, R.J.; Blahnik, D.E.; Campbell, T.K.; Jenquin, U.P.; Mendel, J.E.; and Thornhill, C.K. 1988. *Characterization of Spent Fuel Approved Testing Material—ATM-106*. PNL-5109-106. Richland, Washington: Pacific Northwest Laboratory. ACC: NNA.19911017.0105.

109205 Guenther, R.J.; Blahnik, D.E.; Campbell, T.K.; Jenquin, U.P.; Mendel, J.E.; Thomas, L.E.; and Thornhill, C.K. 1988. *Characterization of Spent Fuel Approved Testing Material—ATM-103*. PNL-5109-103. Richland, Washington: Pacific Northwest Laboratory. ACC: NNA.19911017.0104.

162397 Jegou, C.; Paul, J.L.; and Lucchini, J.F. 2001. "State of the Art of the Leaching and RN Release from Spent Fuel." Section 8.2 of *Synthesis on the Long Term Behavior of the Spent Nuclear Fuel*. Poinssot, C., ed. CEA-R-5958(E). Voume II. [Paris], France: Commissariat à l'Énergie Atomique. TIC: 253976.

162372 Johnson, L.H.; LeNeveu, D.M.; King, F.; Shoesmith, D.W.; Kolar, M.; Oscarson, D.W.; Sunder, S.; Onofrei, C.; and Crosthwaite, J.L. 1996. *Vault Model*. Volume 2 of *The Disposal of Canada's Nuclear Fuel Waste: A Study of Postclosure Safety of In-Room Emplacement of Used CANDU Fuel in Copper Containers in Permeable Plutonic Rock*. AECL-11494-2. Pinawa, Manitoba, Canada: Atomic Energy of Canada Limited. TIC: 226733.

127125 Johnson, L.H. and Taylor, P. 1998. *Alteration of Spent CANDU Fuel in Aerated Steam at 150°C*. Draft. Pinawa, Manitoba, Canada: Atomic Energy of Canada Limited. ACC: MOL.19981118.0337.

125636 Kansa, E.J.; Hanson, B.D.; and Stout, R.B. 1998. *Grain Size and Burnup Dependence of Spent Fuel Oxidation: Geological Repository Impact*. UCRL-JC-131592. Livermore, California: Lawrence Livermore National Laboratory. ACC: MOL.19990420.0128.

126191 Kohli, R.; Stahl, D.; Pasupathi, V.; Johnson, A.B.; and Gilbert, E.R. 1985. "The Behavior of Breached Boiling Water Reactor Fuel Rods on Long-Term Exposure to Air and Argon at 598 K." *Nuclear Technology, 69*, 186-197. La Grange Park, Illinois: American Nuclear Society. TIC: 245332.

168087 Lasaga, A.C. and Luttge, A. 2003. "A Model for Crystal Dissolution." *European Journal of Mineralogy*, *15*, (4), 605-615. Stuttgart, Germany: E. Schweizerbart'sche Verlagsbuchhandlung. TIC: 255729.

106466 Lasaga, A.C.; Soler, J.M.; Ganor, J.; Burch, T.E.; and Nagy, K.L. 1994. "Chemical Weathering Rate Laws and Global Geochemical Cycles." *Geochimica et*

Cosmochimica Acta, *58*, (10), 2361-2386. New York, New York: Pergamon. TIC: 237441.

168991 Leenaers, A.; Sannen, L.; Van den Berghe, S.; Verwerft, M. 2003. "Oxidation of Spent UO_2 Fuel Stored in Moist Environment." *Journal of Nuclear Material, 317*, 226-233. Amsterdam, The Netherlands: Elsevier. TIC: 256014.

113270 McEachern, R.J. and Taylor, P. 1998. "A Review of the Oxidation of Uranium Dioxide at Temperatures Below 400°C." *Journal of Nuclear Material, 254*, 87-121. Amsterdam, The Netherlands: Elsevier. TIC: 246427.

131639 McKenzie, W.F. 1992. *UO_2 Dissolution Rates: A Review*. UCRL-ID-111663. Livermore, California: Lawrence Livermore National Laboratory. TIC: 246408.

100469 Murphy, W.M. 1995. "Natural Analogs for Yucca Mountain." *Radwaste Magazine, 2*, (6), 44-50. La Grange Park, Illinois: American Nuclear Society. TIC: 237929.

163274 NRC (U.S. Nuclear Regulatory Commission) 2003. *Yucca Mountain Review Plan, Final Report*. NUREG-1804, Rev. 2. Washington, D.C.: U.S. Nuclear Regulatory Commission, Office of Nuclear Material Safety and Safeguards. TIC: 254568.

125562 Olander, D.R.; Kim, Y.S.; Wang, W-E.; and Yagnik, S.K. 1999. "Steam Oxidation of Fuel in Defective LWR Rods." *Journal of Nuclear Materials, (270)*, 11-20. New York, New York: Elsevier. TIC: 246527.

170078 Olander, D.R. 1986. "Oxidation of UO_2 by High-Pressure Steam" *Nuclear Technology, 74*, 215-217. La Grange Park, Illinois: American Nuclear Society. TIC: 256246.

163420 Oversby, V.M. 1999. *Uranium Dioxide, SIMFUEL, and Spent Fuel Dissolution Rates - A Review of Published Data*. SKB TR-99-22. Stockholm, Sweden: Svensk Kärnbränsleförsörjning A.B. TIC: 246954.

162412 Pan, Y.-M.; Brossia, C.S.; Cragnolino, G.A.; Jain, V.; Pensado, O.; and Sridhar, N. 2001. *Effects of In-Package Chemistry on the Degradation of Vitrified High-Level Radioactive Waste and Spent Nuclear Fuel Cladding*. CNWRA 2002-01. San Antonio, Texas: Center for Nuclear Waste Regulatory Analyses. TIC: 254197.

130197 Pearcy, E.C. and Murphy, W.M. 1991. *Geochemical Natural Analogs Literature Review*. CNWR 90-008. San Antonio, Texas: Center for Nuclear Waste Regulatory Analyses. TIC: 213164.

100486 Pearcy, E.C.; Prikryl, J.D.; Murphy, W.M.; and Leslie, B.W. 1994. "Alteration of Uraninite from the Nopal I Deposit, Pena Blanca District, Chihuahua, Mexico, Compared to Degradation of Spent Nuclear Fuel in the Proposed U.S. High-Level Nuclear Waste Repository at Yucca Mountain, Nevada." *Applied Geochemistry, 9*, 713-732. New York, New York: Elsevier. TIC: 236934.

164034 Pelletier, M. 2001. "State of the Art on the Potential Migration of Species." Section 5.4 of *Synthesis on the Long Term Behavior of the Spent Nuclear Fuel*. Poinssot, C., ed. CEA-R-5958(E). Volume I. [Paris], France: Commissariat à l'Énergie Atomique. TIC: 253976.

162396 Piron, J.P. 2001. "Presentation of the Key Scientific Issues for the Spent Nuclear Fuel Evolution in a Closed System." Section 5.1 of *Synthesis on the Long Term Behavior of the Spent Nuclear Fuel*. Poinssot, C., ed. CEA-R-5958(E). Volume I. Paris, France: Commissariat à l'Énergie Atomique. TIC: 253976.

113577 Reed, D.T. and Bowers, D.L. 1990. "Alpha Particle-Induced Formation of Nitrate in the Cm-Sulfate Aqueous System." *Radiochimica Acta, 51*, 119-125. München, Germany: R. Oldenbourg Verlag. TIC: 245894.

162398 Röllin, S.; Spahiu, K.; and Eklund, U.-B. 2001. "Determination of Dissolution Rates of Spent Fuel in Carbonate Solutions Under Different Redox Conditions with a Flow-Through Experiment." *Journal of Nuclear Materials, 297*, (3), 231-243. Amsterdam, The Netherlands: North-Holland. TIC: 254044.

162399 Serrano, J.A.; Rondinella, V.V.; Glatz, J.P.; Toscano, E.H.; Quiñones, J.; Diaz-Arocas, P.P.; and Garcia-Serrano, J. 1998. "Comparison of the Leaching Behaviour of Irradiated Fuel, SIMFUEL, and Non-irradiated UO_2 Under Oxic Conditions." *Radiochimica Acta, 82*, (1-4), 33-37. München, Germany: R. Oldenbourg Verlag. TIC: 254195.

162405 Shoesmith, D.W. 2000. "Fuel Corrosion Processes Under Waste Disposal Conditions." *Journal of Nuclear Materials, 282*, (1), 1-31. Amsterdam, The Netherlands: North-Holland. TIC: 254043.

162402 Shoesmith, D.W.; Sunder, S.; Bailey, M.G.; and Wallace, G.J. 1989. "The Corrosion of Nuclear Fuel (UO_2) in Oxygenated Solutions." *Corrosion Science, 29,* (9), 1115-1128. New York, New York: Pergamon Press. TIC: 254042.

113366 Shoesmith, D.W. and Sunder, S. 1991. *An Electrochemistry-Based Model for the Dissolution of UO_2*. SKB TR-91-63. Stockholm, Sweden: Svensk Kärnbränsleförsörjning A.B. TIC: 206581.

113368 Shoesmith, D.W. and Sunder, S. 1992. "The Prediction of Nuclear Fuel (UO_2) Dissolution Rates Under Waste Disposal Conditions." *Journal of Nuclear Materials, 190*, 20-35. Amsterdam, The Netherlands: Elsevier. TIC: 246431.

162404 Shoesmith, D.W.; Sunder, S.; and Tait, J.C. 1998. "Validation of an Electrochemical Model for the Oxidative Dissolution of Used CANDU Fuel." *Journal of Nuclear Materials, 257*, (2), 89-98. New York, New York: Elsevier. TIC: 243109.

111047 Stout, R.B. and Leider, H.R. 1998. *Waste Form Characteristics Report, CD-ROM Version*. UCRL-ID-132375. Livermore, California: Lawrence Livermore National Laboratory. TIC: 246106.

113639 Stroes-Gascoyne, S. 1996. "Measurements of Instant-Release Source Terms for ^{137}Cs, ^{90}Sr, ^{99}Tc, ^{129}I and ^{14}C in Used CANDU Fuels." *Journal of Nuclear Materials, 238*, 264-277. Amsterdam, The Netherlands: Elsevier. TIC: 245893.

100829 Stumm, W. and Morgan, J.J. 1981. *Aquatic Chemistry, An Introduction Emphasizing Chemical Equilibria in Natural Waters*. 2nd Edition. New York, New York: John Wiley & Sons. TIC: 208448.

126463 Sunder, S. and Miller, N.H. 1996. "Oxidation of CANDU Uranium Oxide Fuel by Air in Gamma Radiation at 150 degrees C." *Journal of Nuclear Materials, 231*, 121-131. Amsterdam, The Netherlands: Elsevier. TIC: 246429.

114435 Tait, J.C. and Luht, J.L. 1997. *Dissolution Rates of Uranium from Unirradiated UO_2 and Uranium and Radionuclides from Used CANDU Fuel Using the Single-Pass Flow-Through Apparatus*. 06819-REP-01200-0006 R00. Toronto, Ontario, Canada: Ontario Hydro. TIC: 243164.

125792 Taylor, P.; Wood, D.D.; Duclos, A.M.; and Owen, D.G. 1989. "Formation of Uranium Trioxide Hydrates on UO_2 Fuel in Air-Steam Mixtures Near 200°C." *Journal of Nuclear Materials, 168*, (1&2), 70-75. Amsterdam, The Netherlands: Elsevier. TIC: 246601.

125815 Taylor, P.; Wood, D.D.; and Owen, D.G. 1995. "Microstructures of Corrosion Films on UO_2 Fuel Oxidized in Air–Steam Mixtures at 225ºC." *Journal of Nuclear Materials*, *223*, (3), 316-320. New York, New York: Elsevier. TIC: 256013.

163048 Thomas, E. 2003. "Transmittal of Unsaturated Testing of Bare Spent UO_2 Fuel Fragments: Data Report, Argonne National Laboratory." Interoffice memorandum from E. Thomas (BSC) to J.C. Cunnane, July 2, 2003, 0702037939, with attachment. ACC: MOL.20030702.0116; MOL.20030311.0097.

114439 Torrero, M.E.; Baraj, E.; De Pablo, J.; Gimenez, J.; and Casas, I. 1997. "Kinetics of Corrosion and Dissolution of Uranium Dioxide as a Function of pH." *International Journal of Chemical Kinetics, 29*, (4), 261-267. New York, New York: John Wiley & Sons. TIC: 246160.

125710 Wasywich, K.; Hocking, W.H.; Shoesmith, D.W.; and Taylor, P. 1993. "Differences in Oxidation Behavior of Used CANDU Fuel During Prolonged Storage in Moisture-Saturated Air and Dry Air at 150°C." *Nuclear Technology, 104*, (3), 309-329. La Grange Park, Illinois: American Nuclear Society. TIC: 246598.

168088 White, A.F. and Brantley, S.L. 2003. "The Effect of Time on the Weathering of Silicate Minerals: Why do Weathering Rates Differ in the Laboratory and Field?." *Chemical Geology*, *202*, (3-4), 479-506. New York, New York: Elsevier. TIC: 255730.

100793 Wilson, C.N. 1990. *Results from NNWSI Series 3 Spent Fuel Dissolution Tests*. PNL-7170. Richland, Washington: Pacific Northwest Laboratory. ACC: NNA.19900329.0142.

122032 Woodley, R.E.; Einzeger, R.E.; and Buchanan, H.C. 1989. "Measurement of the Oxidation of Spent Fuel Between 140 and 225 Degrees C." *Nuclear Technology, 85*, (1), 74-88. La Grange Park, Illinois: American Nuclear Society. TIC: 243577.

102047 Wronkiewicz, D.J.; Bates, J.K.; Wolf, S.F.; and Buck, E.C. 1996. "Ten-Year Results from Unsaturated Drip Tests with UO_2 at 90°C: Implications for the Corrosion of Spent Nuclear Fuel." *Journal of Nuclear Materials, 238*, (1), 78-95. Amsterdam, The Netherlands: North-Holland Publishing Company. TIC: 243361.

9.2 CODES, STANDARDS, REGULATIONS, AND PROCEDURES

156605 10 CFR 63. Energy: Disposal of High-Level Radioactive Wastes in a Geologic Repository at Yucca Mountain, Nevada. Readily available.

AP-2.27Q, Rev. 1, ICN 4. *Planning for Science Activities*. Washington, D.C.: U.S. Department of Energy, Office of Civilian Radioactive Waste Management. ACC: DOC.20040610.0006.

AP-SIII.2Q, Rev. 1, ICN 2. *Qualification of Unqualified Data.* Washington, D.C.: U.S. Department of Energy, Office of Civilian Radioactive Waste Management. ACC: DOC.20040127.0008

AP-SIII.10Q, Rev. 2, ICN 5. *Models*. Washington, D.C.: U.S. Department of Energy, Office of Civilian Radioactive Waste Management. ACC: DOC.20040615.0003.

105725 ASTM C1174-97. 1998. *Standard Practice for Prediction of the Long-Term Behavior of Materials, Including Waste Forms, Used in Engineered Barrier Systems (EBS) for Geological Disposal of High-Level Radioactive Waste.* West Conshohocken, Pennsylvania: American Society for Testing and Materials. TIC: 246015.

LP-SI.11Q-BSC, Rev. 0, ICN 0. *Software Management.* Washington, D.C.: U.S. Department of Energy, Office of Civilian Radioactive Waste Management. ACC: DOC.20040225.0007.

9.3 SOURCE DATA, LISTED BY DATA TRACKING NUMBER

135012 LL000107951021.107. Radionuclide Inventory in Spent Fuel. Submittal date: 01/12/2000.

129285 LL991001251021.090. Draft - CSNF Waste Form Degradation: Unsaturated Drip Tests - G2020 Analysis and Modeling Report. Submittal date: 10/04/1999.

162384 MO0301ANLSF001.450. Initial Release Fractions and Fractional Release Rates (Per Day) for Rod Segment Tests (BSC Test Plan: SITP-02-WF-001, REV 0). Submittal date: 01/15/2003.

162383 MO0301ANLSF001.451. Summary of Fractional Release Rate Data (Per Day) for Fuel Fragment Tests (BSC Test Plan: SITP-02-WF-001, REV 0). Submittal date: 01/15/2003.

162385 MO0302PNLDUFTD.000. Flowthrough Dissolution Data. Submittal date: 02/28/2003.

163441 MO0304PNLLPHDD.000. Low pH Dissolution Data. Submittal date: 04/09/2003.

170619 MO0407SEPGGBID.000. Gap and Grain Boundary Inventory Data for Commercial Spent Nuclear Fuel

170618 MO0407SEPUDISR.000. Conversion of Uranium Dissolution Rates from Spent Fuel and Uranium Dioxide.

170760 MO0407SEPFEPLA.000. LA FEP List. Submittal date: 7/20/2004

9.4 OUTPUT DATA, LISTED BY DATA TRACKING NUMBER

MO0404ANLSF001.001. CSNF Radionuclide Release Model. Submittal date: 04/09/2004.

INTENTIONALLY LEFT BLANK

APPENDIX I
MICROSOFT EXCEL SPREADSHEETS AND SIGMA PLOT REGRESSION ANALYSES (WITH CD-ROM)

INTENTIONALLY LEFT BLANK

APPENDIX II

MATHCAD REGRESSION ANALYSIS OF ALKALINE AND ACID DATA

APPENDIX II

II.1 MATHCAD REGRESSION ANALYSIS OF ALKALINE DATA

Alkaline-Side Model

$rY := Dat^{\langle 4 \rangle}$ log Degradation Rate (LDR)

$rX^{\langle 0 \rangle} := Dat^{\langle 0 \rangle}$ Dummy column of 1's - used to get constant in model

$rX^{\langle 1 \rangle} := Dat^{\langle 1 \rangle}$ IT

$rX^{\langle 2 \rangle} := Dat^{\langle 2 \rangle}$ pCO3

$rX^{\langle 3 \rangle} := Dat^{\langle 3 \rangle}$ pO2

Regression Coefficients

$$rb := \left(rX^T \cdot rX\right)^{-1} \cdot rX^T \cdot rY \qquad rb^T = (4.705 \;\; -1093.826 \;\; -0.102 \;\; -0.338)$$

Covariance

$$r\Sigma := \left| \frac{\left(rY^T \cdot rY - rb^T \cdot rX^T \cdot rY\right)}{(\mathrm{length}(rY) - \mathrm{cols}(rX))} \right| \cdot \left(rX^T \cdot rX\right)^{-1} \qquad \sqrt{r\Sigma_{0,0}} = 0.601$$

$$r\Sigma = \begin{pmatrix} 0.36114 & -108.86521 & -0.00501 & -0.00499 \\ -108.86521 & 34904.98147 & -0.24973 & 0.47255 \\ -0.00501 & -0.24973 & 0.00222 & 0.00002 \\ -0.00499 & 0.47255 & 0.00002 & 0.00256 \end{pmatrix}$$

Cholesky Decomposition of $r\Sigma$

$$L := \text{cholesky}(r\Sigma)$$

$$L = \begin{pmatrix} 0.60095 & 0 & 0 & 0 \\ -181.15646 & 45.68717 & 0 & 0 \\ -0.00834 & -0.03852 & 0.02586 & 0 \\ -0.00831 & -0.0226 & -0.03574 & 0.02659 \end{pmatrix}$$

Standard Error

$$StErr := \begin{pmatrix} \sqrt{r\Sigma_{0,0}} \\ \sqrt{r\Sigma_{1,1}} \\ \sqrt{r\Sigma_{2,2}} \\ \sqrt{r\Sigma_{3,3}} \end{pmatrix} \qquad StErr = \begin{pmatrix} 0.6009 \\ 186.8287 \\ 0.0471 \\ 0.0506 \end{pmatrix}$$

Other Statistics

$$SSreg := \sum (rX \cdot rb - \text{mean}(rY))^2 \qquad SSreg = 9.694$$

Sum of Squares regression or "Explained SS"

$$SStot := \sum (rY - \text{mean}(rY))^2 \qquad SStot = 17.283$$

Sum of Squares total

$$Rsq := \frac{SSreg}{SStot} \qquad Rsq = 0.561$$

Coefficient of determination, R^2 This is the fraction of the total squared error that is explained by the model. R^2 measures the relative predictive power of a model.

$$SSres := \sum (rY - rX \cdot rb)^2$$ $SSres = 7.59$ Sum of Squares residual

$$s_e := \sqrt{\frac{SSres}{length\left(rX^{\langle 1 \rangle}\right) - cols(rX)}}$$ $s_e = 0.347$ Standard Error of Estimate This statistic measures the spread around the regression line.

Table II-1. Data for Alkaline-Side Regression Analysis

Constant	IT	pCO_3	pO_2	LDR
1.00000	0.00310	2.70000	0.70000	0.88000
1.00000	0.00309	2.70000	0.70000	0.93000
1.00000	0.00310	2.70000	0.70000	0.80000
1.00000	0.00337	1.70000	0.70000	0.62000
1.00000	0.00289	1.70000	0.70000	1.14000
1.00000	0.00286	1.70000	0.70000	1.33000
1.00000	0.00287	3.70000	0.70000	1.02000
1.00000	0.00290	3.70000	0.70000	1.00000
1.00000	0.00338	3.70000	0.70000	-0.24000
1.00000	0.00342	3.70000	0.70000	0.03000
1.00000	0.00337	1.70000	0.70000	0.51000
1.00000	0.00337	2.70000	0.70000	0.39000
1.00000	0.00334	3.70000	1.70000	0.33000
1.00000	0.00285	3.70000	1.70000	0.25000
1.00000	0.00334	1.70000	1.70000	0.39000
1.00000	0.00286	1.70000	1.70000	0.55000
1.00000	0.00337	1.70000	2.70000	0.47000
1.00000	0.00288	1.70000	2.70000	-0.02000
1.00000	0.00287	3.70000	2.70000	0.15000
1.00000	0.00341	3.70000	2.70000	-0.12000
1.00000	0.00309	1.70000	2.70000	0.08000
1.00000	0.00339	2.70000	2.70000	0.29000
1.00000	0.00288	1.70000	1.70000	0.75000
1.00000	0.00310	2.70000	0.70000	0.82000
1.00000	0.00335	1.70000	0.70000	0.21000
1.00000	0.00338	1.70000	0.70000	0.61000
1.00000	0.00286	1.70000	0.70000	0.97000
1.00000	0.00338	3.70000	0.70000	0.42000
1.00000	0.00287	3.70000	0.70000	1.04000
1.00000	0.00337	1.70000	0.70000	0.56000
1.00000	0.00336	1.70000	0.70000	0.58000
1.00000	0.00287	1.70000	0.70000	0.84000
1.00000	0.00336	3.70000	0.70000	0.45000
1.00000	0.00288	3.70000	0.70000	0.98000
1.00000	0.00287	1.70000	2.70000	0.13000
1.00000	0.00333	3.70000	2.70000	0.31000
1.00000	0.00288	3.70000	2.70000	0.54000
1.00000	0.00333	1.70000	0.70000	0.51000

Table II-1. Data for Alkaline-Side Regression Analysis (Continued)

Constant	IT	pCO_3	pO_2	LDR
1.00000	0.00287	1.70000	0.70000	1.08000
1.00000	0.00333	3.70000	0.70000	0.57000
1.00000	0.00335	1.70000	0.70000	0.60000
1.00000	0.00287	1.70000	0.70000	0.75000
1.00000	0.00334	3.70000	0.70000	0.40000
1.00000	0.00286	3.70000	0.70000	0.83000
1.00000	0.00287	1.70000	2.70000	-0.07000
1.00000	0.00335	1.70000	0.70000	0.38400
1.00000	0.00287	1.70000	0.70000	1.88900
1.00000	0.00287	3.70000	0.70000	1.03700
1.00000	0.00335	3.70000	0.70000	0.40700
1.00000	0.00335	1.70000	0.70000	0.82700
1.00000	0.00335	2.70000	0.70000	0.97000
1.00000	0.00334	3.70000	1.70000	-0.92100
1.00000	0.00287	3.70000	1.70000	0.96400
1.00000	0.00334	1.70000	1.70000	0.27200
1.00000	0.00287	1.70000	1.70000	0.70800
1.00000	0.00335	1.70000	2.70000	-0.65800
1.00000	0.00287	1.70000	2.70000	0.74900
1.00000	0.00287	3.70000	2.70000	-0.29200
1.00000	0.00334	3.70000	2.70000	-0.63800
1.00000	0.00309	1.70000	2.70000	0.66300
1.00000	0.00334	2.70000	2.70000	0.18200
1.00000	0.00309	2.70000	1.70000	1.09000
1.00000	0.00309	2.70000	1.70000	0.90100
1.00000	0.00309	2.70000	1.70000	1.01700
1.00000	0.00287	3.70000	0.70000	0.81200
1.00000	0.00287	2.70000	0.70000	1.36700
1.00000	0.00287	1.70000	0.70000	1.73200

DTN: MO0302PNLDUFTD.000 [DIRS 162385];
MO0407SEPUDISR[DIRS 170618]

NOTES: Data for IT has been rounded to 3 significant figures.
Data for LDR, pCO_3, and pO_2 has been rounded to 2 significant figures.

II.2 MATHCAD REGRESSION ANALYSIS OF ACID DATA

Acid-Side Model

$$DatA := \begin{pmatrix} 1 & 2.02 & 5.5812 \\ 1 & 3.01 & 5.4183 \\ 1 & 3.25 & 5.9547 \\ 1 & 3.8 & 5.6121 \\ 1 & 5.07 & 4.7488 \\ 1 & 5.82 & 4.4725 \end{pmatrix}$$

$rYA := DatA^{\langle 2 \rangle}$ Adjusted LDR

$rXA^{\langle 0 \rangle} := DatA^{\langle 0 \rangle}$ Dummy column of 1's - used to get constant in model

$rXA^{\langle 1 \rangle} := DatA^{\langle 1 \rangle}$ pH

Regression Coefficients

$$rbA := \left(rXA^T \cdot rXA\right)^{-1} \cdot rXA^T \cdot rYA \qquad rbA^T = (6.599 \;\; -0.34)$$

Covariance Matrix

$$r\Sigma A := \left| \frac{\left(rYA^T \cdot rYA - rbA^T \cdot rXA^T \cdot rYA\right)}{(\mathrm{length}(rYA) - \mathrm{cols}(rXA))} \right| \cdot \left(rXA^T \cdot rXA\right)^{-1} \qquad r\Sigma A = \begin{pmatrix} 0.19869 & -0.0467 \\ -0.0467 & 0.0122 \end{pmatrix}$$

Cholesky Decomposition of Covariance Matrix

$$LA := \mathrm{cholesky}(r\Sigma A) \qquad LA = \begin{pmatrix} 0.44575 & 0 \\ -0.10478 & 0.03495 \end{pmatrix}$$

Standard Error

$$StErr := \begin{pmatrix} \sqrt{r\Sigma A_{0,0}} \\ \sqrt{r\Sigma A_{1,1}} \end{pmatrix} \qquad StErr = \begin{pmatrix} 0.446 \\ 0.11 \end{pmatrix}$$

Other Statistics

$$SSregA := \sum (rXA \cdot rbA - mean(rYA))^2 \qquad SSregA = 1.13$$

Sum of Squares regression or "Explained SS"

$$SStotA := \sum (rYA - mean(rYA))^2 \qquad SStotA = 1.608$$

Sum of Squares total

$$RsqA := \frac{SSregA}{SStotA} \qquad RsqA = 0.703$$

Coefficient of determination, R^2 This is the fraction of the total squared error that is explained by the model. R^2 measures the relative predictive power of a model.

$$SSresA := \sum (rYA - rXA \cdot rbA)^2 \qquad SSresA = 0.477$$

Sum of Squares residual

$$s_e := \sqrt{\frac{SSresA}{rows(rXA) - cols(rXA)}} \qquad s_e = 0.345$$

Standard Error of Estimate This statistic measures the spread around the regression line.

Table II-2. Data for Acid-Side Regression Analysis

Constant	T(deg C)	O_2	pH	IT=1/(T+273.15)	DR	LDR	Adjusted LDR
1	27	0.2	2.02	3.3317E-03	50.20	1.70	5.5812
1	27	0.2	3.01	3.3317E-03	34.50	1.54	5.4183
1	24	0.2	3.25	3.3653E-03	109.00	2.04	5.9547
1	27	0.2	3.8	3.3317E-03	53.90	1.73	5.6121
1	26	0.2	5.07	3.3428E-03	7.18	0.86	4.7488
1	26	0.2	5.82	3.3428E-03	3.80	0.58	4.4725

DTN: MO0302PNLDUFTD.000 [DIRS 162385] (Run #66 Data); MO0304PNLLPHDD.000 [DIRS 163441]

NOTES: Adjusted LDR = LDR + 1093.826×IT - 0.338×$\log_{10}(O_2)$

APPENDIX III
FILE INFORMATION FOR ATTACHED CD-ROM

APPENDIX III - FILE INFORMATION FOR ATTACHED CD-ROM

III.1 FILE LISTING FOR APPENDIX I

Volume in drive D is 040831_1427
Volume Serial Number is 81DD-BB5A

Directory of D:\

```
08/06/2004  08:24a          101,376 CSNF-UO2.JNB
08/26/2004  03:31p          212,480 CSNF MR REV02_Attachment I.xls
          2 File(s)      313,856 bytes
          0 Dir(s)             0 bytes free
```

III.2 SPREADSHEET INFORMATION FOR APPENDIX I

The following spreadsheets are contained in Microsoft Excel file "CSNF MR REV2.XLS"

Spreadsheet A1: UO_2 Input Data and Derived Values for the Model Variables

Spreadsheet A2: CSNF Input Data and Derived Values for the Model Variables

Spreadsheet A3: Calculations Supporting the Development of the CSNF Model for Acidic Conditions.

Spreadsheet A4: Calculation of Average Release Rates for the High Drip Rate Tests.

Spreadsheet A5: Calculation of Average Release Rates for the Low Drip Rate Tests.

Spreadsheet A6: Calculation of Average Release Rates for the Rod Segment Tests.

Spreadsheet A7: Summary Fractional Release Rates of Sr-90, Tc-99, Mo-97 and Cs-137 @ 90°C (1/day)

Spreadsheet A8: Calculation of Effective Surface Area of Corroding CSNF

Spreadsheet A9: Comparison of Fractional Release Rate Model with Literature Data for Alkaline and Acidic Conditions

Spreadsheet A10: Comparison of Matrix Specific Dissolution Rate Model with Literature UO_2 Data for Alkaline Conditions

Spreadsheet A11: Comparison of Matrix Specific Dissolution Rate Model with Literature UO_2 Data for Alkaline Conditions

Spreadsheet A12: Comparison of Matrix Specific Dissolution Rate Model with Literature UO_2 Data for Acidic Conditions

Spreadsheet A13: Analysis of Gap- and Grain-Boundary Inventory Data

INTENTIONALLY LEFT BLANK

APPENDIX IV
DATA QUALIFICATION PLAN

INTENTIONALLY LEFT BLANK

APPENDIX IV - DATA QUALIFICATION PLAN

BSC	DATA QUALIFICATION PLAN	QA: QA Page 1 of 1

Section I. Organizational Information

Qualification Title

CSNF Surface Area Data to be used as input to the modeling report ANL-EBS-MD-000015 REV02

Requesting Organization

BSC Regulatory Integration Team

Section II. Process Planning Requirements

1. List of Unqualified Data to be Evaluated

The data to be qualified are geometric surface area data for spent fuel pellet fragments to be included in Section 4.1.3, Tables 4-5 and 4-6 of the CSNF modeling report ANL-EBS-MD-000015 REV 02. The data to be qualified also includes an estimate of the effective specific surface area of corroded CSNF that accounts for the effects of surface roughness and grain-boundary penetration. This specific surface area estimate 3.9×10^{-3} (m^2/g) is also included in Section 4.1.3 of the CSNF modeling report ANL-EBS-MD-000015 REV02. The source documents for these data are: Wilson 1990 [DIRS 100793], Appendix E; Barner 1985 [DIRS 109194], Tables 4.1 and 4.6; Gray and Wilson 1995 [DIRS 100758], Section 4.1.1, p 4.2.

2. Type of Data Qualification Method(s) [Including rationale for selection of method(s) (Attachment 3) and qualification attributes (Attachment 4)]

The qualification process to be used for these data involves a combination of the following methods (AP-SIII.2Q Rev. 1 ICN2, Attachment 3): Technical Assessment and Corroborating Data. The qualification process attributes (AP-SIII.2Q Rev. 1 ICN 2, Attachment 4) used were attributes 1 through 6 and 10 with most emphasis on attribute 10. The rational for selecting the technical assessment method is that it can be used to establish confidence in the data by evaluating and assessing the appropriateness the methodology used to plan, collect and analyze the data. The confirmation method was used also because appropriate data were available to compare to the unqualified data and enhance confidence in its accuracy.

3. Data Qualification Team and Additional Support Staff Required

Qualification Chairperson: James C. Cunnane - CSNF Modeling Report Originator
Data Qualification Team - Brady Hanson, PNNL

4. Data Evaluation Criteria

The qualification criteria are based on AP-SIII.2Q Rev. 1 ICN 2, Attachment 4 attributes 1 through 6 and 10 with most emphasis on attribute 10. The data qualification report will be documented in the model report.

5. Identification of Procedures Used

AP-SIII.10Q Rev 2 ICN2, AP-SIII.2Q Rev 1 ICN2

Section III. Approval

Qualification Chairperson Printed Name	Qualification Chairperson Signature	Date
James C. Cunnane		8/15/04
Responsible Manager Printed Name	**Responsible Manager Signature**	**Date**
Neil R. Brown		8/15/04

INTENTIONALLY LEFT BLANK

APPENDIX V
DATA QUALIFICATION REPORT

INTENTIONALLY LEFT BLANK

APPENDIX V - DATA QUALIFICATION REPORT

V.1 PURPOSE

The purpose of this data qualification report is to qualify the input data in Tables 4-5 and 4-6 for use in estimating the specific geometric surface area of commercial spent nuclear fuel (CSNF) pellet fragments within this modeling report. The purpose also includes qualifying the input value of 3.9×10^{-3} (m^2/g) for the specific surface area of corroded CSNF fragments based on single-pass flow-through test results (Section 4.1.3).

V.2 QUALIFICATION METHODS

The input surface area data (Wilson 1990 [DIRS 100793], Appendix E; Barner 1985 [DIRS 109194], Tables 4.1 and 4.6; Gray and Wilson 1995 [DIRS 100758], Section 4.1.1, p. 4.2)) are qualified in accordance with AP-SIII.2Q, *Qualification of Unqualified Data*. The qualification process used for these data involves a combination of the following methods (AP-SIII.2Q, Attachment 3):

- Technical Assessment
- Corroborating Data.

This qualification process is designed to provide the desired level of confidence and its intended use is only for this modeling report.

This report documents the data qualification task conducted in accordance with the approved data qualification plan (Appendix IV). For each of the qualification methods the qualification process attributes 1 through 6 and 10 (AP-SIII.2Q, Attachment 4) were used as appropriate. The rationale for selecting the technical assessment method is that it can be used to establish confidence in the correctness of the unqualified data by evaluating the methods used to plan, collect, and analyze the data. The corroboration method was also used because comparisons with other unqualified data provide additional confidence.

V.3 TECHNICAL ASSESSMENT

V.3.1 Table 4-5 Data

The pertinent sections of the source document from which the input data in Table 4-5 were obtained (i.e., Wilson 1990 [DIRS 100793], Appendix E) were reviewed. As described in the source document (Wilson 1990 [DIRS 100793], Acknowledgements) these data were developed by the Westinghouse Hanford Company and Pacific Northwest National Laboratory (PNNL) for the Yucca Mountain Project (YMP). The work was conducted under Contract No. W-7405-ENG-48 and the YMP-approved WHC/PNNL Quality Assurance Programs that met the contractual QA requirements. The laboratory activities were completed under the Westinghouse Hanford Company QA program, from Feb. 1986 to May 1987, and much of the data evaluation and the preparation of the report by Wilson (1990 [DIRS 100793]) were performed under the PNNL quality assurance program. This work was transferred from WHC to PNNL in June 1987 as part of the Hanford site contract consolidation effort. The WHC and PNNL quality assurance programs were reviewed and approved by LLNL, which managed the waste package task for YMP and treated WHC and PNNL as suppliers. Technical implementing documents, including

test plans, test procedures, and technical drawings were reviewed and approved by LLNL and WHC prior to their implementation, and determined to be technically adequate for the collection and analyses of the data. "Test Plan for Series 3 NNWSI Spent Fuel Leaching/Dissolution Tests," HEDL-7577, January 1986, C. N. Wilson, also included an appendix that identified all test instructions, technical procedures, and analytical procedures, including solution and solids analyses, and burnup and radiochemical analyses. The initial evaluation of the overall data quality has determined that the controls and methods used to plan, collect, and analyze the data in question were adequate when compared to generally accepted scientific and engineering practices at the time the data was generated.

V.3.2 Table 4-6 Data

The pertinent sections of the source document from which the input data in Table 4-5 were obtained (i.e., Barner 1985 [DIRS 109194], Section 4.5 and Table 4.1). [Note: Section 4.5 in the Barner report is MCC-generated data; the data in Table 4.1 of Barner's ATM-101 report was not generated by the MCC, but was taken from the fuel vendor data in the Carolina Power and Light Company, H.B. Robinson Unit 2 FSAR – Docket 50261-104]. As described in the source document (Barner 1985 [DIRS 109194]) these data were developed by the Pacific Northwest National Laboratory's Materials Characterization Center (MCC) under the U.S. Department of Energy Contract DE-AC06-76LO 1830. The MCC mission included development of characterization data for spent fuel to be designated as "Approved Testing Materials (ATMs), and the characterization data (including those used as input to Table 4-5) were developed using characterization plans and technical procedures that were consistent with this mission. The MCC data was generated under the controls of a PNL QA program that employed an NQA-1-based approach. The MCC QA program was scrutinized by several DOE repository programs (BWIP, SRPO, OCRD) as well as other clients. The MCC QA program implemented then was written to address contractual QA requirements from BWIP and SRPO, and was reviewed and approved by these DOE repository programs. The initial evaluation of the overall data quality has determined that the controls and methods used to plan, collect, and analyze the data in question were adequate when compared to generally accepted scientific and engineering practices at the time the data was generated.

V.3.3 Effective Specific Surface Area Data for CSNF in SPFTs

The pertinent sections of the source document (Gray and Wilson 1995 [DIRS 100758], Sections 4.1.1 and 4.1.6) from which the value of $3.9 \times 10^{-3}(m^2/g)$ for the specific surface area of corroded CSNF fragments was obtained. As described in the source document these data were developed by the Pacific Northwest National Laboratory (PNNL) for the Yucca Mountain Project (YMP). The work was conducted under Contract No. DE-AC06-76RLO 1830 and the YMP-approved WHC/PNNL quality assurance programs, which met the contractual QA requirements. The PNNL quality assurance program was reviewed and approved by LLNL, which managed the waste package task for YMP and treated PNNL as a supplier. Technical implementing documents, including test plans, test procedures, and technical drawings were reviewed and approved by LLNL and PNNL prior to their implementation, and determined to be technically adequate for the collection and analyses of the data. Evaluation of the overall data quality has determined that the controls and methods used to plan, collect, and analyze the data in question were adequate when compared to generally accepted scientific and engineering practices at the time the data was generated.

All three source documents clearly describe the technical approach used to determine the surface area data used as inputs in Tables 4-5 and 4-6 and Section 4.1.3 (Section 4.1.3). The technical approaches used to obtain the data in Tables 4-5 and 4-6 are consistent with the best available practices and are, therefore, acceptable. They involve estimating the geometric surface areas of the cracked fuel pellets using fragment weight and fragment or pellet crack dimensions based on photographic records. Because these are simple measurement processes conducted by technically competent individuals under an adequate and effective quality assurance program in effect at the MCC, the results are credible. The estimated value of 3.9×10^{-3} (m^2/g) for the specific surface area of corroding CSNF is based on comparison of BET and geometric-specific surface areas to estimate the surface roughness contribution to the specific surface area and comparison of the fractional dissolution rates measured on grain-sized powders and fuel pellet fragment samples of the same fuel to estimate the effects of grain boundary penetration (Gray and Wilson 1995 [DIRS 100758]). The result is reasonable and consistent with observation of surface roughness and grain-boundary penetration in corroded CSNF (Section 6.2.2.3). Because, as discussed in Section 6.4.1.4, the single-pass flow-through method is likely to maximize the effective specific surface area of the fragments, it is reasonable to use this value as an upper bound for the uncertainty range in the specific surface area parameter.

V.4 CORROBORATING DATA

V.4.1 Comparison of Results from Different Data Sources

As described in Section 4.1.3 two different approaches were used to obtain the data in Tables 4-5 and 4-6. The fact that similar geometric-specific surface areas were obtained for the ATM-101 fuel using the different methods employed by Wilson (1990 [DIRS 100793]) and Barner (1985 [DIRS 109194]) (Table 6-9) corroborates each data set.

Published data on geometric-specific surface areas of CSNF fragments have been reviewed and compiled by Jegou et al. (2001 [DIRS 162397], Table 38). When the CSNF fragment data are adjusted to remove the "shape factor" of 3, the specific surface area results are approximately 2 to 6 cm^2/g with most of the results being approximately 2 cm^2/g. The good agreement between these literature data and the input data in Tables 4-5 and 4-6 (Table 6-9 for conversion of these input data to specific geometric surface area estimates) corroborates these input data.

The subsection "Corroborating Data for Estimating CSNF Specific Surface Areas" (Section 6.4.1.5) shows that the effective surface area, estimated based on the results of long-term drip tests, are consistent with use of the value of 3.9×10^{-3}(m^2/g) for the specific surface area of corroded CSNF fragments of (Gray and Wilson 1995 [DIRS 100758], Sections 4.1.1 and 4.1.6) as an upper bound on the specific surface area of corroding CSNF.

V.4.2 Comparison with Fuel Pellet Cracking Data

As described in Section 6.2.1.1, literature data (Dehaudt 2001 [DIRS 164019], Section 5.2.7.1) show that the radial and transverse cracking of fuel pellets in irradiated CSNF results in creation of about 15 to 20 fragments per pellet. The specific surface area expected for such fragmented pellets can be estimated as described below.

Because the fuel fragments result from radial and transverse cracking of the fuel pellets, it is reasonable to approximate the fragment geometry for a cracked pellet to form 18 fragments as illustrated in Figure V-1.

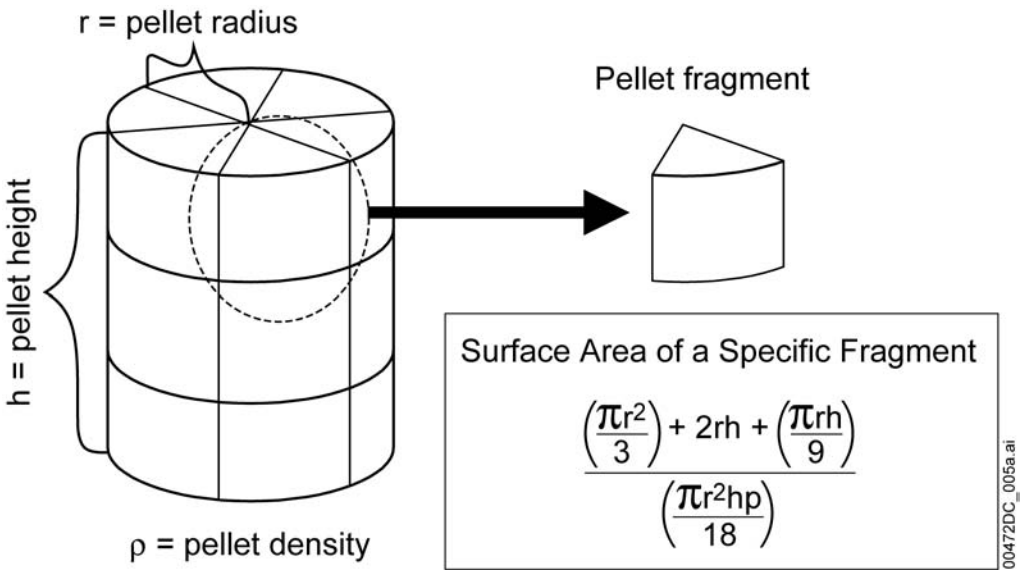

Figure V-1. CSNF Pellet with Eighteen "Pie-Shaped" Fragments Resulting From Radial and Transverse Cracking

Using the expression given above for the specific surface area of these idealized fragments, and the as-fabricated pellet dimensions and density data provided at the bottom of Table 4-5, the specific surface area of the fragments can be calculated to be about 1.6 cm^2/g.

To assess the sensitivity of the estimated geometric-specific surface area to the fragment shapes it is instructive to note that if the pellet were divided into 18 equally sized cubic fragments the specific surface area would be approximately 1.32 cm^2/g. If the 18 pellet fragments were in the form of spheres (which would minimize the specific surface area), the specific surface area would be approximately 1.27 cm^2/g. Although the literature data (Dehaudt 2001 [DIRS 164019], Section 5.2.7.1) do not show a very wide variation in the extent of CSNF cracking, it is worth noting the geometric-specific surface area is not very sensitive to the extent of cracking and, hence, the number of fuel fragments. Simple geometric arguments show that the specific geometric surface area will increase in proportion to the cubic root of the number of fragments (e.g., a factor of eight increase in the number of fragments would cause the specific geometric surface area to increase by about a factor of two). These estimates, based on the literature data for the number of pellet fragments expected in CSNF, and simple assumptions concerning the fragment shape, show that the specific geometric surface area is expected to be approximately 2 cm^2/g. This corroborates the data presented in Tables 4-5 and 4-6.

V.5 CONCLUSION

The conclusion from this report is that the qualification status of the input data considered here should be changed to show that it is qualified for the purposes of this report.